

Diss. ETH No. 14009

# **Molecular Dynamics Simulation of Aggregates of Lipids: Development of Force-Field Parameters and Application to Membranes and Micelles**

A dissertation submitted to the  
SWISS FEDERAL INSTITUTE OF TECHNOLOGY ZURICH

for the degree of  
Doctor of Natural Sciences

presented by  
Lukas Daniel Schuler  
Dipl. Naturwissenschaftler ETH

born June 6, 1969  
citizen of Schwyz, Switzerland

accepted on recommendation of  
Prof. Dr. Wilfred F. van Gunsteren, examiner  
Prof. Dr. P. Luigi Luisi, co-examiner  
Prof. Dr. Peter Walde, co-examiner

2000



*innigster Dank  
meinen lieben Eltern*



---

# Acknowledgements

More than a decade of my life has been spent at the ETH. Now, as I depart after ten years of study and research, it is time to acknowledge the few who have guided, and the many who have helped me to this Ph.D.

Three wise men appeared to lead me on my way.

Luigi Luisi gets heartfelt thanks. By allowing me to come to the group for “Informatikgestützte Chemie” he has let me tailor my work to a preference for computational simulation. He always made me feel comfortable and I enjoyed the special events together with his group very much as well as the “Instituts-tagung”, the meeting in Ascona and the 111th Faraday Discussion in Bristol – a unique forum that lets the audience profit the most.

Wilfred van Gunsteren – a boss receptive to my ideas, reasonable in his demands and patient in the wait for progress. He has always supported me in my work and for this I am very grateful. I would like to thank him also for the warm welcome extended to me on my arrival as a guest in the group for IGC. With biomas-supported tea, borrels, dinners, unforgettable farewell parties and ski-weekends, social life is unique. Thanks also to Jolande, his wife, who taught us present molecular dynamics more dynamic.

Peter Walde brought his knowledge and the experimentalists point of view to many discussions. With his advice I felt supported facing problems that arose. With his bibliographic collection of papers finding the relevant literature was always an easy task. Science aside, his amateur photography is much appreciated too.

Looking to the stars ...

Since my first steps into the world of GROMOS96 much has changed and many people have come and gone. Alexandre JJ Bonvin, is the only person I know able to answer questions while simultaneously chatting German/English/Dutch/French into a 'phone and programming shell scripts. My thanks speed northwards to Utrecht where he deservedly holds an assistant professorship.

Then there are Salomon Billeter and Christian Berweger – old hands at the UNIX game and ever ready with patient answers and advice. Above all else, the mountain holidays we shared will not be forgotten. Working together, walking together, we have become firm friends. Thanks also go to Renata, Salomon's wife. The many invitations helped to keep the group enjoying the SOLA – and summertime.

Unforgettable sysadmins: Walter Scott, Alexandre Bonvin, Salomon Billeter, Christian Berweger, Urs Stocker, Martin Borer, Xavier Daura, Jed Pitera, Dirk Bakowies, Christine Peter and Alice Glättli; thanks to all of these for making daily life with the various workstations less trouble than it would have been.

Heiko Schäfer and Roland Bürgi deserve special thanks. Without their painstaking efforts engineering the client/server network this thesis would have been more labour than it has been. And now, with their introduction of object-oriented analysis code it seems that the GROMOS star is once more rising. Also in praise, Tomas Hansson and Fred Hamprecht – shepherds of the PC flock. Again, the time they put in setting-up and keeping the cluster running are much appreciated.

Xavier Daura has given special help and for this I am truly grateful. Force field parametrisation seems at times a Sisyphean task, and it can be hard to see the way to progress. His advice, and his aid with free energy calculations, have helped me a great deal.

People of the chorus, less prominent, though no less appreciated, are many in number. I can mention now only a few.

Thanks to Prisca Cerutti for keeping Wilfred and his group so well organised and making us happy when submissions had to go quickly.

Thanks to Margrit Zeller for solving everyday problem of reaching members of the Luisi group.

Thanks to Cornelia Heiz, Nathalie Berclaz and Aline Fischer for the cordial invitations to excursions or parties for members of Luisi's group.

Thanks to Alan Mark for the various invitations and his sense of black humour – primarily at lunch time.

Thanks to Peter Gee who encouraged me again to go hiking more often.

Thanks to programmers of free and platform independent software.

With this host of people Christmas has come true and my thesis is born in December (2000).

# Contents

Acknowledgements .....	5
Zusammenfassung .....	9
Summary .....	11
Publications .....	13
<b>1. Introduction .....</b>	<b>16</b>
<b>1.1 Lipid Aggregates .....</b>	<b>16</b>
Interest in lipid aggregates .....	19
<b>1.2 Molecular Dynamics Simulation .....</b>	<b>20</b>
Force field .....	23
Atomic interactions .....	23
Bonded interactions .....	24
Cut-off.....	26
Energies, temperatures and different ensembles. ....	27
<b>1.3 Simulations in this work .....</b>	<b>29</b>
Chapter 2 – Dihedral angle potential energy functions of n-alkanes .....	30
Chapter 3 – MD Simulation of n-dodecylphosphate aggregates. ....	30
Chapter 4 – Improved liquid force-field for aliphatic hydrocarbons .....	30
Chapter 5 – Testing a well established DPPC bilayer membrane .....	31
<b>2. On the Choice of Dihedral Angle Potential Energy</b>	
<b>Functions for n-Alkanes .....</b>	<b>34</b>
2.1 Abstract .....	34
2.2 Introduction .....	34
2.3 Selection of target values .....	35
2.4 Model calculations and simulations .....	37
2.5 Results and Discussion .....	44
2.6 Conclusions .....	46
2.7 Acknowledgements .....	47
2.8 Appendix .....	47
Energy And Pressure Corrections For Finite Cut-Off .....	47
<b>3. Molecular Dynamics Simulation of n-Dodecylphosphate</b>	
<b>Aggregate Structures .....</b>	<b>54</b>
3.1 Abstract .....	54
3.2 Introduction .....	54
3.3 Methods .....	56
Molecular model and force field .....	56

---

System set-up .....	60
System equilibration .....	63
Calculation of NMR -SCD order parameters .....	66
Calculation of hydrogen bond lifetimes .....	66
Calculation of diffusion coefficients .....	66
<b>3.4 Results and Discussion .....</b>	<b>67</b>
bilayer structures bil-pK1-298, bil-pK1-348, bil-pK1-398 .....	68
bilayer structures bil-bas-298, bil-bas-348, bil-bas-398 .....	69
micelle structures, mic-C8-pK1-298, mic-pK1-298, mic-pK2-298 .....	70
micelle structures mic-pK2-298, mic-bas-298, mic-64-bas-298 .....	71
Hydrogen bond lifetimes .....	72
Percentage trans of torsion angles along the lipid chains .....	74
NMR -SCD order parameter .....	76
Distribution of atom types: cross section for bilayers .....	77
Distribution of atom types: radial distribution for micelles .....	80
Diffusion coefficients .....	80
Torsion angle dynamics .....	82
<b>3.5 Conclusions .....</b>	<b>84</b>
<b>3.6 Acknowledgement.....</b>	<b>85</b>
<b>4. An Improved GROMOS96 Force Field for Aliphatic   Hydrocarbons in the Condensed Phase .....</b>	<b>88</b>
4.1 Abstract .....	88
4.2 Introduction .....	88
4.3 Methods .....	90
4.4 Results and Discussion .....	93
4.5 Conclusions .....	105
4.6 Acknowledgement.....	106
<b>5. The GROMOS96 45A3 force field is benchmarked by   using DPPC, Dipalmitoylphosphatidylcholine .....</b>	<b>108</b>
5.1 Introduction .....	108
5.2 Methods .....	110
5.3 Results and Discussion .....	111
5.4 Conclusions .....	116
<b>Cumulative References.....</b>	<b>120</b>
<b>Curriculum Vitae .....</b>	<b>131</b>
Personal Information .....	131
Education .....	131
<b>The Final Point.....</b>	<b>132</b>



---

# Zusammenfassung

Die Anwendung der klassischen Molekulardynamik-Simulation im Bereich von biomolekularen Systemen hat sich im Verlauf der letzten Jahre auf Lipide, Membranen und gemischte Membran-Protein-Systeme ausgeweitet. In Zürich in der Gruppe von Prof. van Gunsteren, wo die Molekulardynamik-Simulation in dieser Zeit vor allem auf Peptide und Proteine mit Erfolg angewandt wurde, ergab sich mit der vorliegenden Arbeit die Gelegenheit, diesen Schritt hin zu den Lipiden ebenfalls zu wagen. In der Forschungsgruppe von Prof. Luigi Luisi wurden vor allem Liposomen oder grosse Vesikel experimentell untersucht. Diese Arbeiten bildeten die Grundlage zu den Simulationen über *n*-Dodecylphosphate, die im Kapitel 3 vorgestellt werden. Gerne hätte man weitere und grössere Lipidsysteme simuliert und auf ihre molekularen Eigenschaften hin untersucht. Doch sobald die ersten Untersuchungen dieser Doktorarbeit unternommen wurden, tauchten Probleme auf, die auf eine unzureichende Beschreibung der real existierenden Eigenschaften von Lipid-Schwänzen hindeuteten: Eine Doppelschichtmembran von *n*-Dodecylphosphorsäure und -phosphat sollte bei etwa 3 °C schmelzen. Selbst beim starken Erhitzen auf über 50 °C wurden die meisten Lipid-Schwänze in einer durchgestreckten *trans*-Konformation gefunden. Daher wurden die experimentell bekannten Daten über *n*-Alkane genutzt, um eine gültige Parametrisierung der Torsionen dieser Kohlenwasserstoffketten in Flüssigkeiten zu erreichen. Kapitel 2 beschreibt das gewählte Vorgehen im Detail. Die Abweichung der Flüssigkeitskonformere von den experimentellen Werten war beträchtlich zuvor und gering danach. Die Parameter dieser erfolgreichen Kraftfeldoptimierung wurden verwendet, um das System von *n*-Dodecylphosphat in Kapitel 3 eingehend zu untersuchen. Vergleiche zwischen Mizellen und Doppelschichtmembranen wurden durchgeführt. Bemerkenswerte Ergebnisse hierbei sind die Bestätigung zur pH-Abhängigkeit der Lipid-Aggregate und der Unterschiede in der Beweglichkeit der Moleküle innerhalb von Membranen und Mizellen.

Unglücklicherweise behielten die vielversprechenden Resultate ihre Gültigkeit nur für kurzkettige Lipide wie eben diese Dodecylketten. Eine Anwendung auf langkettige Dipalmitoylphosphatidylcholine (DPPC) oder langkettige Alkane wie Pentadecan, die testweise erfolgten, förderten ein gravierendes Dichteproblem dieses Flüssigkeitskraftfeldes zu Tage. Fehler von über 5% in der Dichte dieser Systeme können nicht einfach hingenommen werden. Eine systematische Untersuchung tat Not: In Kapitel 4 werden *n*-Alkane, Cyclo-

alkane, Isoalkane, Neoalkane und einige weitere verzweigte aliphatische Moleküle auf ihre Dichte, Verdampfungswärme und ihr Lösungsvermögen in Wasser hin untersucht. Die Dichte und Verdampfungswärme werden als die Schlüsseleigenschaften für die Abstimmung unseres empirischen Modells angesehen und dienen als experimentelle Orientierungspunkte. Das Kraftfeld, das die nicht-bindenden Wechselwirkungen beschreibt, wurde in seinen van der Waals Parametern optimiert. Die sehr gründliche Neuausrichtung brachte eine erfolgreiche Tendenz in den Kettenlängen-abhängigen Eigenschaften zu Stande, inklusive der anschliessend überprüften Löslichkeiten. Für zyklische Alkane war allerdings ein eigenes implizit repräsentiertes Atom für die Methylengruppen ( $\text{CH}_2$ ) nötig. Wir konnten zufrieden feststellen, dass die Simulation von langkettigen Lipiden oder Polymeren keine Probleme ergeben sollten.

Das letzte Kapitel 5 testet die Optimierungen und hält fest, dass die Beschreibungen der Kopfgruppenladungen mehr zu einer exakten Membranstruktur beizutragen scheinen, als dies erwartet wurde. Wir müssen den Schluss zulassen, dass das Kraftfeld von GROMOS96 vielleicht weniger geeignet ist, mit den bisher vorgesehenen reduzierten Ladungen insgesamt neutrale Moleküle mit einer hohen internen Polarität genau zu beschreiben. Ein Test mit atomaren Ladungen, wie sie für DPPC-Doppelschichtmembranen in Groningen (NL) eingesetzt wurden, scheint dies zu bestätigen.

Nichtsdestotrotz war der Aufwand, der in Kapitel 4 betrieben wurde, alles andere als „für die Katz“ und das nun vorliegende Kraftfeld wird weiterhin für die gemischten aliphatischen und wässrigen Systeme eingesetzt werden können bis hin zu Polymeren oder beliebigen Lipidstrukturen. Offen geblieben ist die Frage, inwiefern das neue Kraftfeld für Proteinstrukturen und gemischte biomolekulare Systeme geeignet ist. Wir sind diesbezüglich optimistisch.

---

# Summary

In the last few years lipids, membranes and mixed membrane protein systems have been explored by application of classical Molecular Dynamics simulation of biomolecules. At the same time Molecular Dynamics (MD) was applied successfully in the group of Prof. Wilfred van Gunsteren in Zurich, but mainly to peptides and proteins. The opportunity of this thesis, therefore, was to make a step towards application to lipid systems. In the research group of Prof. Luigi Luisi liposomes and giant vesicles have been investigated intensively by many experimentalists. Their achievements are the experimental foundation of our simulations of *n*-dodecylphosphoric acid and -phosphates, which will be discussed in Chapter 3. It would have been interesting to investigate molecular properties of more and larger lipid systems, but problems appearing in the beginning of this PhD research, which brought about the insufficient description of lipid tails in the model used, made it necessary to investigate these systems further in detail: A lipid bilayer membrane of *n*-dodecylphosphate should melt at about 3 °C. Even at above 50 °C most of the lipid tails showed an all-*trans* conformation in the simulations. Therefore, it was necessary to reparametrise the torsional angle potentials of hydrocarbon chains of *n*-alkanes, for which experimental data is available. Chapter 2 describes this approach in detail. The conformational equilibrium in liquid simulations deviated from the actual experimental one, but very little after the reparametrisation. With this successful optimisation of the force field, the *n*-dodecylphosphate aggregates have been investigated in Chapter 3. Comparison between micelles and bilayer membranes has been made. The observed pH-dependence of these lipid aggregates and the difference in mobility of these molecules within their membranes or micelles are remarkable results.

Unfortunately, the force field could only be validated for short lipid systems as the described dodecyl chains. The application to long-chain dipalmitoylphosphatidylcholines or long-chain alkanes such as *n*-pentadecane showed a serious density increase. Deviations from experimental values by more than 5% in the density are too large for these systems. A systematic parametrisation approach was unavoidable: In Chapter 4 *n*-alkanes, cycloalkanes, isoalkanes, neoalkanes and some other aliphatic molecules are investigated with respect to their density, heat of vaporisation and free energy of hydration. The density and heat of vaporisation are considered to be key quantities for the parametrisation of the empirical model used. The van der

Waals parameters of the force field describing non-bonded interactions have been reconsidered. This modification resulted correct trends in density, heat of vaporisation and free energy of hydration as a function of chain-length. For cyclic alkanes a new united-atom type for methylenes ( $\text{CH}_2$ ) was to be introduced. We are confident that simulation of long-chain lipids or polymers should now be possible without problems.

The final Chapter 5 describes tests of the optimised force field and shows the importance of head-group charges for an exact description of membrane structures. A test with a DPPC-bilayer membrane, seems to demonstrate that the head-group charges as inferred from the GROMOS96 force field parameters for similar moieties are too small to reproduce the correct density.

Nevertheless, the reparametrisation that is described in Chapter 4 is very useful since the resulting force field will still be useful for mixed aliphatic and water systems up to polymers or lipid aggregates. The question that remains open is, whether the new force field parameter set is also reliable for protein structures and mixed biomolecular systems. In regards to the answer we are optimistic.

---

# Publications

This thesis has led to the following publications:

*On the Choice of Dihedral Angle Potential Energy Functions for n-Alkanes*

Lukas D. Schuler and Wilfred F. van Gunsteren

Molecular Simulation, 2000, Vol. 25, pp. 301-319

*Molecular Dynamics Simulation of n-Dodecylphosphate Aggregate Structures*

Lukas D. Schuler, Peter Walde, P. Luigi Luisi and Wilfred F. van Gunsteren

European Biophysical Journal, 2001, Vol. 30, pp. 330-343

*An Improved GROMOS96 Force Field for Aliphatic Hydrocarbons in the Condensed Phase*

Lukas D. Schuler, Xavier Daura and Wilfred F. van Gunsteren

Journal of Computational Chemistry, 2001, Vol. 22, pp. 1205-1218

This thesis has contributed to the following publications:

*Molecular Dynamics Simulation of Biomolecular Systems*

W. F. van Gunsteren, D. Bakowies, R. Bürgi, I. Chandrasekhar, M. Christen, X. Daura, P. Gee, A. Glättli, T. Hansson, C. Oostenbrink, C. Peter, J. Pitera, L. Schuler, T. Soares and H. Yu

CHIMIA, 2001, Vol. 55, pp. 856-860

*A Molecular-Dynamics Simulation Study of the Conformational Preferences of Oligo-(3-hydroxy-alkanoic acids) in Chloroform Solution*

P. J. Gee, F. A. Hamprecht, L. D. Schuler, W. F. van Gunsteren, E. Duchardt, H. Schwalbe, M. Albert and D. Seebach

Helvetica Chimica Acta, 2002, Vol. 85, pp. 618-632

*A consistent potential energy parameter set for lipids: Dipalmitoylphosphatidylcholine as a benchmark of the GROMOS96 45A3 force field*

I. Chandrasekhar, M. Kastholz, R. D. Lins, C. Oostenbrink, L. D. Schuler, D. P. Tieleman and W. F. van Gunsteren

European Biophysical Journal, 2003, Vol. 32 pp. 67-77



# **Chapter 1**

---

## **Introduction**

# 1. Introduction

## 1.1 Lipid Aggregates

Molecules that are known to be attracted simultaneously by both polar (e.g. water) and apolar (e.g. *n*-hexane) solvents often belong to substances that are classified as amphiphiles. These molecules consist in general of a polar part and an apolar part and are widely used in nature as building blocks of cellular membranes in all kinds of organisms from bacteriae to humans. The typical amphiphiles found therein are called lipids.

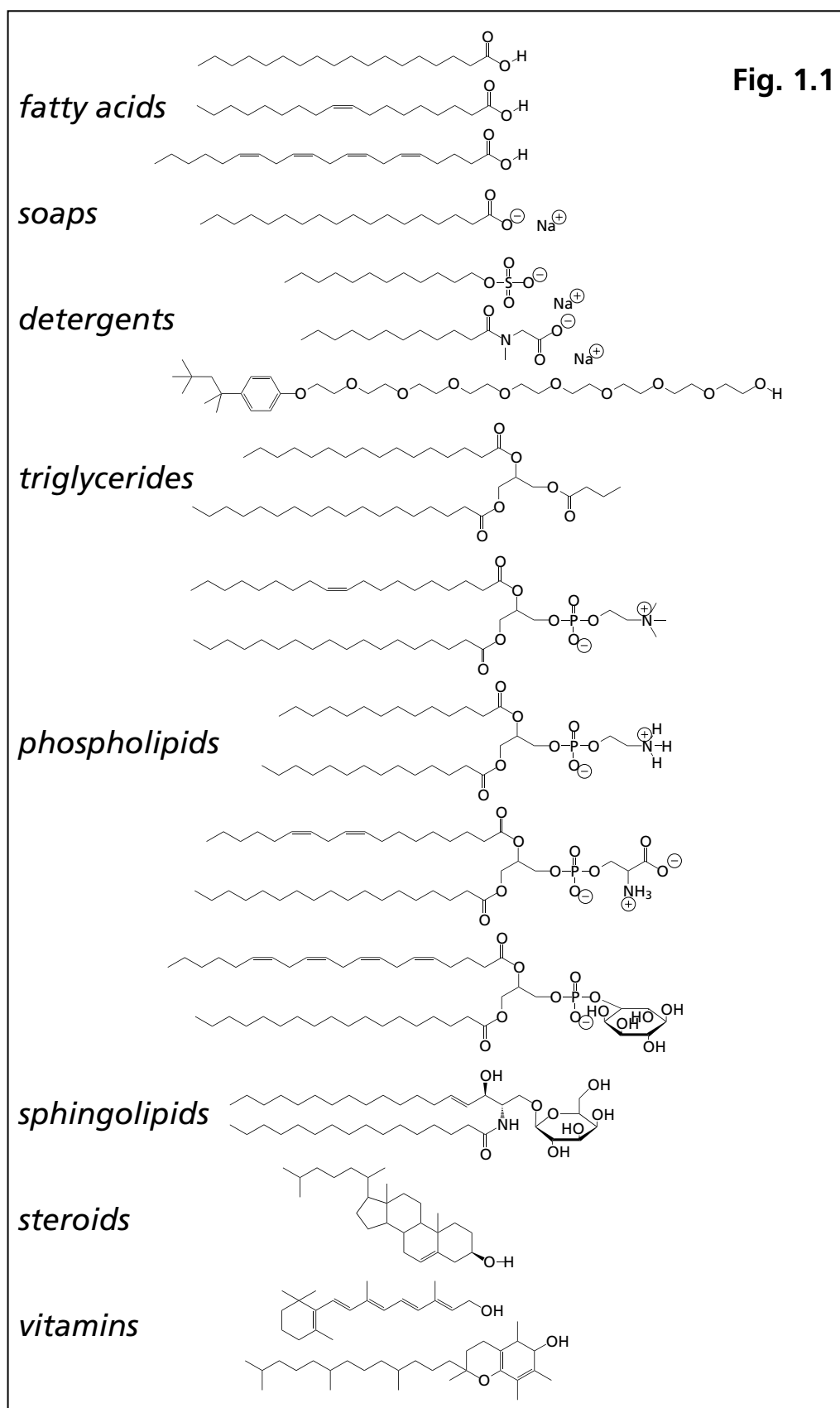
Humans instead have learned to seethe soaps, amphiphiles that act as powerful washing agents (not as TV shows). Since the chemical industry synthesized many different artificial amphiphiles for similar purposes, they are commonly named tensides or detergents. In this research also artificial lipids have been introduced and studied.

Figure 1.1 exemplifies some molecular structures of different amphiphiles, that help explain the variety that sails under the term or can act as a lipid. We note that the tails of amphiphiles usually only consist of hydrocarbons, whereas the polar heads may contain different heteroatoms. This often leads to bulky head groups that are charged (e.g. deprotonated). Therefore, many amphiphiles are actually salts and include counterions when crystallised.

Whereas the lipids occurring in nature are supplying living cells with a boundary by aggregating to a supramolecular structure commonly described as lipid-bilayer membrane, not all of the manmade detergents or lipids may be able to form this supramolecular structure. Since the seventies it has been discussed how lipid-bilayer membranes can be described accurately starting with the fluid mosaic model of Singer and Nicolson [1]. Soon it was evident, that the properties of the lipid heads and tails must balance the forces that govern the supramolecular structure [2-4], besides the fact that an actual biological membrane may consist of many different lipid molecules and include supporting protein structures.

Amphiphiles used for washing purposes usually aggregate into micelles in dilute aqueous solutions, which makes them dissolve easily in large amounts in water. Most of those amphiphiles consist of a single chain for the tail, whereas natural lipids may have two chains as tail group. It is not only the lipid or tenside itself that determines the favoured aggregate structure. Depending on environmental conditions such as the media in which the substance is dissolved,





the amphiphile concentration, the temperature or other parameters, the amphiphile may adopt different aggregate structures. A simple example for this is just a childrens experiment: The dish washing tensides often used, like sodium dodecylsulphate (SDS), are most likely to form spherical micelles if dissolved in water. That means they adopt a nearly spherical structure containing dozens of tenside molecules which all point with their polar groups surfacewise into the water, whereas most of the tail groups are hidden inside the aggregate. If a child blows a film dragged off the surface of the solution, which is covered by tenside molecules, a big bubble is produced that may contain billions of amphiphilic molecules. Now the apolar tails are all pointing towards the air both inside and outside the bubble. Water enclosed in between the head groups of these two layers will evaporate and the bubble will burst, since the large bubble sphere does not accomplish a stable structure for the tenside at high concentrations. Evidence of tails pointing off the surface can be seen from the fancy oil colours that are produced by scattered light. Since the same detergents or lipids are able to show very different aggregate structures depending on conditions applied, it is common to investigate their different appearances systematically and plot them in a so called phase diagram. This way, experimentalists have found many different phases of pure or mixed lipid systems.

The phases of dipalmitoylphosphatidylcholine lipids (DPPC) upon melting and hydration are shown in the phase diagram of Figure 1.2, adapted from Small [5], which also contains sketches of how the lipids might arrange within these phases.

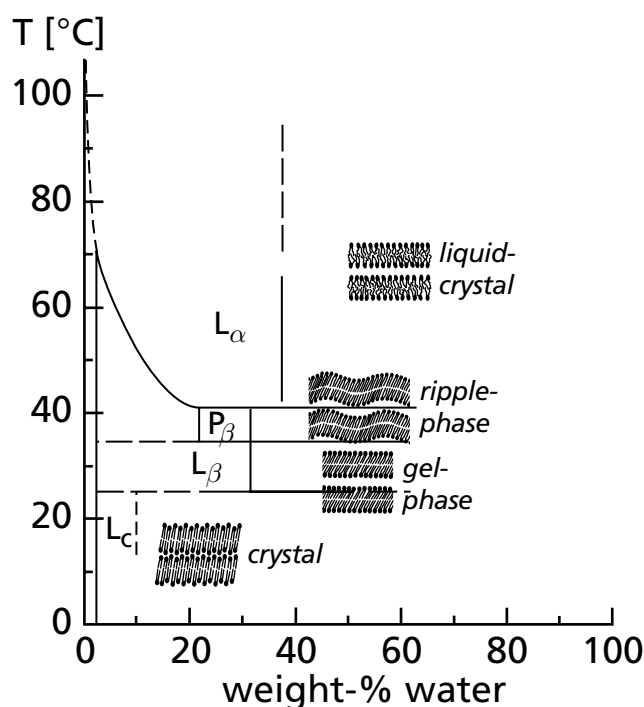


Fig. 1.2

## Interest in lipid aggregates

Amongst the structures intensively investigated in the laboratory of Luisi et al., the large spherical bilayer membranes became familiar as giant vesicles or liposomes. To evoke growth of large unilamellar vesicles (in which the membrane consists of exactly one bilayer) the method of electroformation [6] is often used, but its mechanism is not completely understood. Liposomes are of interest for the cosmetics industry which has used them since many years, while their application in drug delivery has considerable potential to be increased in the future, see e.g. [7].

In research of the group of Luisi et al. liposomes are more of interest as containers for chemical reactions, even as catalysts [8,9] and they are seen as simplest models for cellular membranes. The hypothesis that prebiotic chemical evolution on Earth took place in containers of amphiphilic structures has been supported by several authors [10,11,12].

That simple amphiphilic substances have a potential for building up large vesicular membranes has been demonstrated already [13,14] mainly by choosing appropriate pH-conditions.

Whether specially designed lipids could be grown to liposomes and then be applied as targets for fusion experiments between different liposomes was the initial question that led to the following investigations [15]. Since the experimental approach needs a lot of effort to synthesize, purify and apply specially designed lipids, a collaboration was initiated that could investigate similar systems using theoretical molecular models. It was asked, if it is possible to use molecular dynamics simulation to study liposomal fusion processes. The answer is clear: No, not even today in the year 2000. The reasoning is simple and a technical one: The computational power currently available does not allow simulation of such systems in atomic detail, they are still too big in terms of number of particles or interactions.

Nevertheless, a study of much simpler systems was started. With these, the applicability of molecular dynamics simulation to lipid aggregate structures using the GROMOS96 software package [16] could be shown and some of the smaller lipids investigated earlier, for which the adopted aggregates are known experimentally [14], could be studied providing insight in atomic detail.

Before presenting these investigations, the basics of molecular dynamics application for simulation of biomolecular systems should be described.

## 1.2 Molecular Dynamics Simulation

When Molecular Dynamics is new to the reader, it was so to the author before he started his PhD too. Therefore, I think it should be explained in an easy manner for those who would like to know how they should judge the method by which results have been obtained, but who are not familiar with it.

Computer simulations are nowadays widely used for many different applications. Amongst the more popular ones such as simulation of aircraft aerodynamics and ship hydrodynamics before these are actually built, simulation of virtual sceneries and motions for movies or architects may come to one's mind when thinking about this topic. This usually misleads the non-expert public when computational chemists speak about their work, since our purpose is not primarily to obtain nice colour pictures and movies of molecules we are interested in. Most of the time computational chemists deal with statistical averages they want to calculate, they obtain via computations and they judge. In that respect they act more as bookkeepers of their simulations than as directors of art. The advantage in using computers is obvious: machines are fast and precise when cleverly used. On the other hand they are of no intelligence. Every single task you want a computer to do you have to instruct. Fortunately the instructions that have been proven to work well you can keep over the years and reuse. Therefore it is not always necessary to invent new program code, but one relies on software packages that have grown over time as is the case for GRO-MOS96 which will be used throughout the work presented here.

To understand how molecular dynamics simulations are modelled, let's imagine you'd play billiard on the floor of a squash court. Squash courts usually are enclosed transparent boxes, so an outside observer can watch the moving billiard balls. What does determine the movements of the billiard balls after they have been placed? First there is the initial hit by the cue. It makes the first ball move and spin in a given direction, with a given kinetic energy. As soon as it hits another ball or an obstacle like the wall, it will change direction and transfer some of its kinetic energy to the object hit. In the natural squash environment there is friction from the floor while gravitation keeps the balls to your feet. They will slow down and stop. Gravitation is an outside force to our system from the mass called Earth attracting the masses of the billiard balls and vice versa. Sir Isaac Newton is famous for formulating the laws of gravitation and mechanics in his book called "Principia" and Newton's equations of motion are applied also in classical molecular dynamics simulation.

$$\frac{d\mathbf{r}_i(t)}{dt} = \mathbf{v}_i(t) \quad \text{Eq. 1.1}$$

$$\frac{d\mathbf{v}_i(t)}{dt} = m_i^{-1} \mathbf{f}_i(t) \quad \text{Eq. 1.2}$$

Newton realised that any moving object, that is not disturbed by any force, will move on in a straight line. Let's imagine we could switch off gravitation for our squash billiard game. Then the billiard balls would bounce also on the floor and the ceiling and float through the whole squash box. They would eventually stop, since the air (and the wall) has exerted some friction to them. The air itself consists of smaller particles, mainly two-atomic nitrogen and oxygen molecules and those rush too. When they are hit by the billiard ball some of its kinetic energy is transferred to them. The gaseous air will get slightly warmer, its molecules move faster, whereas the billiard ball will slow down. To keep the billiard balls running, they must be in vacuum within the squash court. Then the balls will behave similar as the gaseous air itself. It is just that we can see the billiard "gas" in the squash court, but not such lightweights as single atoms or molecules. So the difference between the two is mainly a scaling factor of about nine to ten orders of magnitude. Billiard balls are hard spheres, whereas real atoms are usually described softer than that. So we could exchange the hard balls by using foam rubber balls. To get a simple description of molecules, several atoms could be connected via elastic springs between their ball centers. This way, the foam rubber balls would oscillate within the molecules along their bonds (springs) depending on hits they have to absorb and the entire molecules would rotate and float the same time before hitting the next obstacle. This model we imagine can even get more detailed if we include attractive non-bonded forces by putting some magnets inside their foam rubber bodies. If they bounce into each other at high speed, they will lose contact again, at low speed they might reorient in their preferred direction and stick together.

Molecular dynamics simulation formulates similar boxes filled with atoms or molecules as we finally got into our squash court. Gravitation usually is neglected, the atoms and molecules are just that lightweight in nature that we need not to take it into account, since they keep their fast motion at simulated temperatures anyway. The walls are avoided in simulations, since they would disturb the motions of the particles involved. If a vacuum simulation is not ap-

appropriate, the systems are made periodic. It's just as if the walls would not be visible, but still exist. As soon as a particle hits a wall on one side of the box, it is transferred to the opposite wall of the box and reenters the box at that position with the same speed and direction it had before. Particles close to any wall will interact with periodic images of the particles close to the opposite wall.

The aim of molecular dynamics is to get a realistic model for molecular motions and molecular structures achieved in thermodynamically equilibrated systems. This helps explaining phenomena that can not be seen, measured or observed because the time or the size scale is too small to observe or because there is no instrumentation for measurements. Although Molecular Dynamics (MD) could be used to simulate systems that never have been observed before, this is not always wise to do. Without the comparison with reality known through experiment, judgement of the accuracy and validity of results from the simulation is impossible. One should realise, that MD simulation needs two things. On one hand, the motion of particles has to be described. For all molecular motions that do not include low temperatures or light particles, it can be done by application of Eq. 1.1 and 1.2. This excludes quantum-mechanical phenomena such as chemical reactions and is therefore also called classical MD. The typical MD calculation uses a propagator that calculates the moves of the particles involved in time, knowing their velocities, by applying small timesteps of typically 1 or 2 femtoseconds in order not to lose information about the fastest motions involved. On the other hand, a huge effort has to be undertaken to describe the particles as simple as possible but as precise as necessary to get realistic results for the biomolecular systems involved. This is important for the force calculator, that derives the forces from the actual particle conformations and the potentials with which they are described (Eq. 1.3).

$$\mathbf{f}_i(t) = -\frac{\partial}{\partial \mathbf{r}_i} V(\mathbf{r}_1, \mathbf{r}_2, \dots, \mathbf{r}_N) \quad \text{Eq. 1.3}$$

How a liquid system may be simulated using Molecular Dynamics has been described in detail in [17].

If we consider our squash court “simulation”, the laws of physics apply simply because they are known to exist in this universe. So particles move as they are supposed to move. Their actual potentials consist of elastic soft foam rubber, springs and magnets and will determine the interparticle forces.

## Force field

To describe real particles for MD simulation, a so called force field has to be developed. How strong atoms are bound to each other, how big and how soft their bodies are, and how charged and heavy do they look like for their environments. Although this can be done in many different ways, the functional forms used for potentials do not deviate that much between the different MD software packages that exist. Only GROMOS96 [16] has been used for the molecular dynamics simulations within this work. Therefore only the functional forms used within GROMOS96 will be explained.

## Atomic interactions

Every atom that is described explicitly in the simulations, has its own geometrical position, velocity, atomic mass and partial charge. When an atom  $i$  approaches another atom  $j$ , its van der Waals potential energy is described via a Lennard-Jones type of interaction using the product of  $C_{12}^{1/2}$  and  $C_6^{1/2}$  parameters for each of the atoms involved (Eq. 1.4).

$$V^{LJ} = \left[ \frac{C_{12}(i, j)}{r_{ij}^6} - C_6(i, j) \right] \frac{1}{r_{ij}^6} \quad \text{Eq. 1.4}$$

with  $C_{12}(i, j) = C_{12}^{1/2}(i)C_{12}^{1/2}(j)$  and likewise for  $C_6(i, j)$ . To not disturb the molecular structures by strong forces, the first and second covalently bound neighbours of an atom within any molecule are always excluded from this interaction. The third neighbours have separate parameters called  $CS_6^{1/2}$  and  $CS_{12}^{1/2}$  that yield smaller interactions of the same type as in Eq. 1.4. In some cases they are excluded as well, like hydrogens in a phosphate group or for atoms attached to aromatic rings. From the fourth neighbour on, the potential of Equation 1.4 is considered fully, as if the atoms would not belong to the same molecule. It is therefore considered as part of the non-bonded interaction.

Some of the computational effort involved in this non-bonded force evaluation has been reduced by using so-called united atoms. United atoms are hydrocarbon functional groups such as methyl ( $-\text{CH}_3$ ), methylene ( $-\text{CH}_2-$ ) and methyne ( $>\text{CH}_1-$ ), which help to reduce the number of particles by representing the involved hydrogen atoms only implicitly. Also methane ( $\text{CH}_4$ ) has

been represented as a united atom, but is unique. Since hydrogen atoms are not present in hydrocarbons using united-atom models, the parametrisation is different from that for carbon atoms with attached hydrogen atoms. There are no charges introduced in hydrocarbons, except for united atoms bound to atoms with big charges where it may be desirable due to polarisation. Not many force fields nowadays rely on united atoms, but the advantage of computation for bigger systems of many hydrocarbons is obvious, and there is no evidence that they fail where an all-atom model doesn't.

### Bonded interactions

To connect atoms to molecules, their bonds must be described for the connectivity, their angles for the geometry, improper dihedrals for structural invariance such as chirality and torsions for the conformation. All these belong to the bonded interactions.

Bonds are treated using squared harmonic potentials. Their deviation from an ideal equilibrium bond length  $b_0$  is taken into account by multiplication with a constant  $K_{b_n}$  for the strength of the elastic bond, if bond vibrations are considered to be necessary for the simulation. In most simulations bond lengths are constrained to fixed equilibrium distance  $b_0$  by SHAKE [18] and bond interactions are not calculated.

$$\sum_{n=1}^{N_b} \frac{1}{4} K_{b_n} \left[ b_n^2 - b_{0_n}^2 \right]^2 \quad \text{Eq. 1.5}$$

Bond-angles are treated using harmonic potentials of their cosines by assuming an ideal angle  $\theta_0$  for each geometry  $n$  and a constant  $K_{\theta_n}$  for the stiffness of the angular bending properties.

$$\sum_{n=1}^{N_\theta} \frac{1}{2} K_{\theta_n} \left[ \cos \theta_n - \cos \theta_{0_n} \right]^2 \quad \text{Eq. 1.6}$$

To keep chiral tetrahedral groups or planar groups in correct shape, the additional improper dihedral-angle potentials are used. They run over four connected atoms and use a harmonic potential for bending of the angle  $\xi$  between two planes each defined by three different of the four atoms involved. Its potential involves a big force constant to keep deviations from ideal geometries small.



$$\sum_{n=1}^{N_{\xi}} \frac{1}{2} K_{\xi_n} \left[ \xi_n - \xi_{0_n} \right]^2 \quad \text{Eq. 1.7}$$

Dihedral angle torsional potentials are superimposed upon the third-neighbour special van der Waals type of interactions similar to Equation 1.4. They consist of one or several cosine functions showing a certain multiplicity to enhance barriers between the given conformers in different molecules. Since barriers and energy differences between different conformers are defined, these terms can be of more importance for an overall structure in a liquid than one might think, as we will see in Chapter 2.

$$\sum_{n=1}^{N_{\varphi}} K_{\varphi_n} \left[ 1 \pm \cos(m_n \varphi_n) \right] \quad \text{Eq. 1.8}$$

The actual potential is the sum over all bonded and non-bonded potentials involved.

$$V^{physical}(\mathbf{r}; \mathbf{s}) = V^{bonded}(\mathbf{r}; \mathbf{s}) + V^{nonbonded}(\mathbf{r}; \mathbf{s}) \quad \text{Eq. 1.9}$$

The van der Waals potential (Eq. 1.4) belongs to the non-bonded part of the total interaction potential. Since atoms may be charged, also electrostatic interactions have to be considered. This is also the case for intramolecular interactions where atoms are not excluded as close neighbours. Electrostatic interactions are treated according to Coulomb's law including a reaction-field correction.

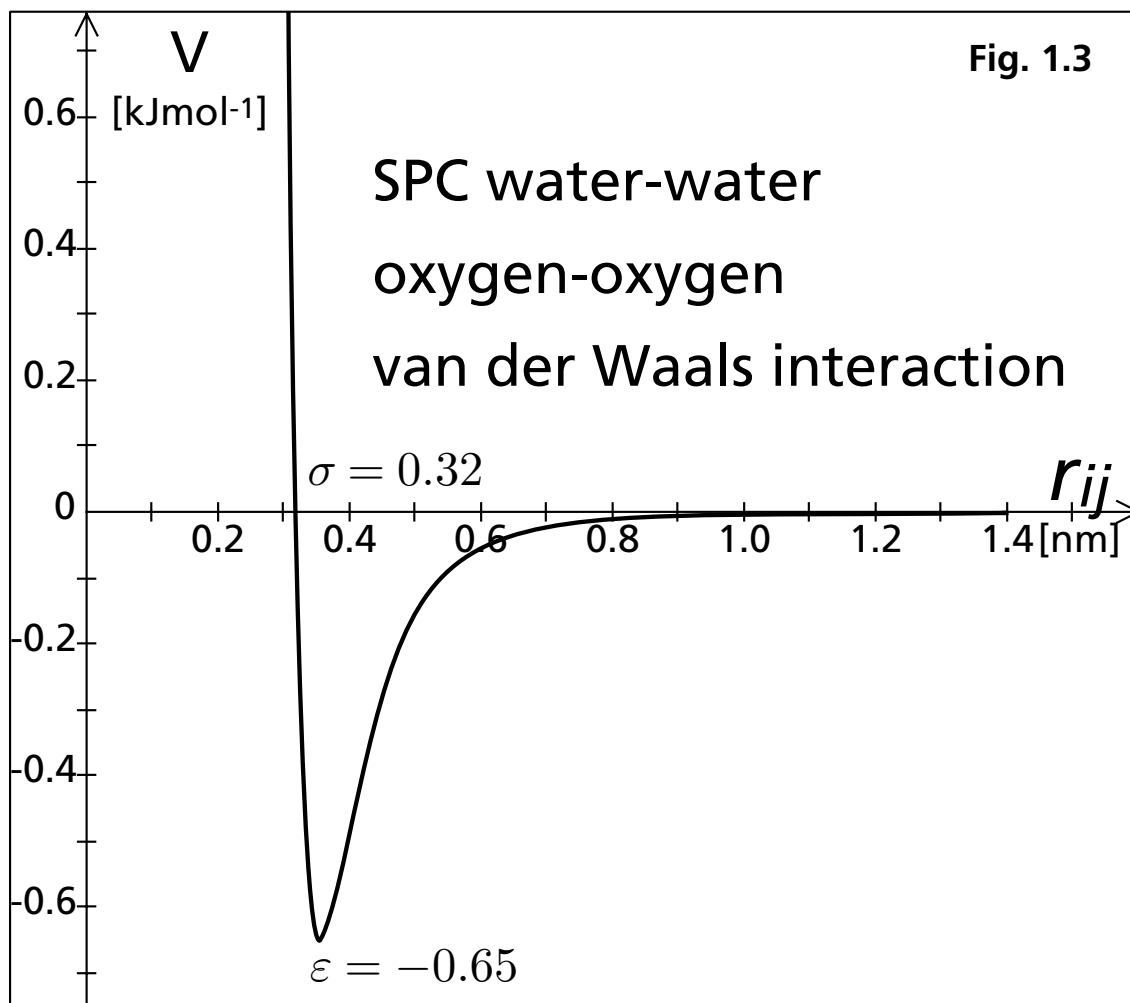
$$V^{CRF} = \frac{q_i q_j}{4\pi\epsilon_0\epsilon_1} \left[ \frac{1}{r_{ij}} - \frac{\frac{1}{2} C_{rf} r_{ij}^2}{R_{rf}^3} - \frac{1 - \frac{1}{2} C_{rf}}{R_{rf}} \right] \quad \text{Eq. 1.10}$$

## Cut-off

In principle the total potential of the system (Eq. 1.9) should be considered for all particles involved. This is usually not affordable since the number of interacting particles grows with the 3rd power of the interaction radius. GROMOS96 uses a twin-range cut-off [19] that reduces the calculation in two ways. Within the smaller cut-off, interacting particles are evaluated every simulation step, in between the smaller and larger cut-off, usually only every 5th time step the interaction pairlist is updated, assuming that pairlist fluctuations are rare in between. Non-bonded interactions are considered within the smaller cut-off. The remaining non-bonded interaction is only applied between charge groups, that is a group of atoms within a molecule defined such that their total charge is neutral or equals an electrostatic unit. This leads to dipolar interactions between charge groups, reducing the distance dependence of electrostatic interactions to one over the 3rd power of the interaction radius and allowing for a smaller long-range cut-off. As a byproduct, charge groups are also used in the molecular virial and pressure calculation of interacting molecules, which will be important in Chapter 4.

In most simulations using GROMOS96 the twin-range cut-off is chosen as 0.8 nm for the smaller and 1.4 nm for the larger radius. This requires the smallest wall-to-wall distance in a periodic system to be larger than twice the cut-off, so always bigger than 2.8 nm. Otherwise it would be possible, that a simulated particle sees its own image and this would lead to artifacts within the system, reducing it to a crystal. A cut-off of 1.4 nm still leaves ample room for speculations about the tolerance of the system for this truncation as we will discuss in Chapter 5 and therefore at least a cut-off correction might be useful. To a first approximation, it is common to apply a Poisson-Boltzmann reaction-field force correction beyond the long-range cut-off, which smoothens the interaction potential.

A typical functional form for the non-bonded van der Waals interaction is displayed in Figure 3 for the interaction between two water oxygens of the single point charge (SPC) model [20] often used. If the sum of non-bonded interaction is considered, the repulsive character in the Coulombic part due to the equal charges dominates completely such that the two oxygen atoms would never seek contact. Instead in the water model the opposite charged hydrogen atoms get attracted by the oxygens and without additional intermolecular potentials, hydrogen bonds are modelled.



### Energies, temperatures and different ensembles.

The total energy in a classical simulated system consists of the sum of kinetic and potential energy.

$$H(\mathbf{p}, \mathbf{r}; m, s) = K(\mathbf{p}; m) + V(\mathbf{r}; s) \quad \text{Eq. 1.11}$$

The kinetic energy may be derived directly from the masses and velocities of the given particles, not using their positions. Velocities along constrained bonds must always be zero to not affect the bond lengths.

$$K(\mathbf{p}; m) = \sum_{i=1}^N \frac{1}{2} m_i \mathbf{v}_i^2 \quad \text{Eq. 1.12}$$

The potential energy may be derived from the positions of the particles by applying the force field involved.

In principle, the total energy of the system (Eq. 1.11) should be conserved, since the system does not communicate with the world outside the system. This is in practice not the case for two major reasons. First, the cut-off introduces fluctuations in the potentials of the system, that make particles move slightly more randomised and let them gain kinetic energy such that the total energy and temperature would increase over time. Second, if constraints are applied, which is usually the case for bonds, certain degrees of freedom of the system are frozen. Both approximations will affect how particles move and therefore their temperature and kinetic energies will change. To hinder this drift of the energy of the system, the temperature is usually controlled by coupling it to a thermostat. The thermostat applied in GROMOS96 uses the weak coupling method introduced by Berendsen et al. [21]. The temperature is coupled to a bath with a relaxation time of typically 0.1 ps. The weak coupling method has the advantage of its simplicity, where only the velocities of particles involved have to be scaled to relax towards the kinetic energy corresponding to the preferred temperature. This method will keep the temperature, kinetic energy and therefore also the total system energy nearly constant. One disadvantage should not be close-mouthed. Systems containing less particles of high frequency motions (e.g. only big particles in a crystal), will easily transfer kinetic energy of high frequency motions (e.g. bond angle vibrations and conformational changes) into low frequency motions (e.g. translational velocity). This phenomenon is familiar under the name of the flying ice cube and has been observed several times, but luckily not within this work. The whole system is moving across the periodic box at high velocity, whereas all internal vibrational and rotational motions are frozen close to absolute zero. To avoid this anormal und unwanted behaviour the centre of mass motion that might build up during longer simulation time is periodically removed. As soon as the total translational motion is removed, an eventually lowered temperature of internal degrees of freedom will be scaled up again. This has to be done as often as the temperature fluctuations are kept in the usual range. For systems within this work, every 50 or 100 ps was frequent enough to remove the centre of mass motion.

In MD simulations, the number of particles is usually kept constant and chosen big enough to fulfill the cut-off criteria for periodic boxes. Besides that, most often the temperature is chosen to be constant as well. There are exceptions when protocols such as simulated annealing are applied. For simulating

under realistic conditions, usually the situation of the laboratory experiments is chosen. Therefore the pressure of the system is kept constant at about one atmosphere. This is done in the same way as the temperature is controlled. Instead of the velocities, the positions and the volume are scaled, such that the pressure relaxes to the desired value using a coupling time of typically 0.5 ps. A specialty in the pressure scaling is that it may either be chosen isotropic as for homogeneous systems or anisotropic for systems that are not similar along different axes of the system. When the density of a system is accurately known, it might be convenient to use constant volume simulations where the box size will not change.

Both ensembles are used very often and they are commonly abbreviated as NPT and NVT ensembles, N for number of particles, P for pressure, V for volume, T for temperature that are kept constant. The main advantage of NPT ensembles over NVT ensembles is that they find accommodative structures for the desired pressure themselves, whereas under constant volume simulations a reasonable model of correct density should exist beforehand to gain realistic simulation results.

## 1.3 Simulations in this work

It was decided not to start with simulations of very large systems, since first I was a newcomer to the field of Molecular Dynamics (MD) simulation, second GROMOS96 had not been applied to other biomolecular systems than sugars, peptides, proteins and DNA. Therefore the first system we concentrated on was the simulation of bilayer membranes of *n*-dodecylphosphoric acid and its phosphates. This system could be simulated containing about seven thousand atoms only. First results using the GROMOS96 force-field set 43A1 for condensed phase simulations were disappointing insofar as the bilayer membrane underwent hardly any change upon increasing the temperature. This crystalline stability which was considered unnatural, could only occur from artifacts that had been introduced by the simulation technique or the force field used. Structural evidence was given that most of the alkyl chains involved stayed in an all-*trans* conformation during the simulations, also at higher temperatures. This could not be the case in a real system, since it is known that membranes undergo a phase transition when melted which increases the *gauche* conformers in their chains.

## Chapter 2 – Dihedral angle potential energy functions of *n*-alkanes

When alkyl-chains were not showing the correct amount of different conformers within a membrane, this certainly must have been also the case for *n*-alkanes. Therefore to study the dihedral angle potential energy functions involved, small *n*-alkanes were investigated intensively. Force-field parameters were improved to achieve the *trans/gauche* ratio in these liquid *n*-alkanes by adjusting the potential energy function to known experimental and ab initio data. Comparison with an all-atom force field showed that the latter does not necessarily yield an improved description of molecular behaviour. The new parameter set could then be intensively used for further simulations.

## Chapter 3 – MD Simulation of *n*-dodecylphosphate aggregates.

The improved force field showed the phase transition upon melting of bilayer membranes and therefore a detailed investigation of bilayers and micelles of *n*-dodecylphosphoric acid and -phosphates was undertaken.

Speculative, experimentally non-existent conditions were imposed in order to study the reliability of the force field and the structures involved. One of the conclusions of interest for experimentalists was that these lipids might have more freedom to diffuse within lipid bilayers than within micelles.

## Chapter 4 – Improved liquid force-field for aliphatic hydrocarbons

Although the condensed phase force field was applied with success to the systems consisting of *n*-dodecylphosphates in Chapter 3, it was shown that for longer aliphatic chains aliphatic systems tend to get too dense and therefore too crystalline. The force field improvement made in Chapter 2 couldn't avoid these tendencies. A detailed investigation of *n*-alkanes, cycloalkanes, and branched alkanes such as iso- or neoalkanes was undertaken to judge the applicability of the existing GROMOS96 condensed phase force fields and improve upon these by introducing new force-field parameters for various kinds of aliphatic systems. Several important properties have changed dramatically: the dependence of density and heat of vaporisation and free energy of hydration upon chain length of *n*-alkanes have been corrected. A new CH<sub>2</sub> united-atom type for aliphatic rings was introduced, since the "CH2" for chains and "CH2r" for rings seem to be incompatible when the correct density should be reproduced. And

finally most of the branched alkanes show more realistic properties when combining the new van der Waals parameters (including the new tetrahedral bare carbon atom type 45 “CH0”) and the modified torsional dihedral parameters of Chapter 2.

### Chapter 5 – Testing a well established DPPC bilayer membrane

One of the bilayer systems most accurately known in the experimental and the simulation world has been DiPalmitoylPhosphatidylCholine (DPPC). It is therefore also used as a benchmarking lipid. Testing the new force field of Chapter 4 with a well equilibrated DPPC-bilayer structure should not change the basic properties of the membrane. To our displeasure, a change towards a gel phase crystal at a temperature above the phase transition temperature was observed. This was considered to be wrong and some investigations on the dependence of the lipid bilayer structure on the choice of electrostatic interactions were made.

There was not more time to invest for a detailed description of the systems considered here, but the final results showed already that the choice of partial atomic charges is not trivial for lipid bilayer systems. The reason for not having observed these difficulties before might lie in the fact that counterions shield the head group charges in a reasonable way for the systems of Chapter 3. After the most promising set of partial charges and charge groups was chosen, the carbonyl van der Waals parameters were successfully reconsidered.

Several projects could be undertaken next: it might be worth to test the force field of Chapter 4 more extensively but also consider to improve it further by starting over with alkenes and alkynes before considering heteroatomic groups. Some hints where problems might still be are also given in Chapter 4. The question might be investigated whether one should reconsider different united-atoms types for different bonds, respective hybridisations. I cannot exclude this step to be necessary at some point.

One should make sure that the new force field could be used as well for proteins and check that the new atom type 44 for aliphatic rings models proline residues well. If it is shown that protein simulations yield reliable results with the improved liquid force field, this is promising for treatment of mixed lipid protein systems. Transmembrane proteins might become within reach and the computational advantage of an united-atom force field will still pay off.

The author wishes good luck to any of his successors  
Lukas D. Schuler, December 2000



## Chapter 2

---

# On the Choice of Dihedral Angle Potential Energy Functions for $n$ -Alkanes

# 2. On the Choice of Dihedral Angle Potential Energy Functions for *n*-Alkanes

## 2.1 Abstract

The parameters of the GROMOS96 force field governing dihedral angle transitions in aliphatic chains have been reconsidered, since these parameters do produce a too large ratio of *trans* to *gauche* conformations in such chains. A refined set of parameters for dihedral angle interactions and third-neighbour interactions involving CH<sub>2</sub> and CH<sub>3</sub> atoms is proposed. They were obtained by fitting to the heat of vaporisation, pressure and *trans-gauche* ratio for liquids of three *n*-alkanes, *n*-butane, *n*-pentane and *n*-hexane. The new parameter set does reproduce better these quantities and should therefore be more appropriate for use in simulations of polymers and membranes. A comparison of the mentioned properties obtained from simulations with united-atom models and from simulations with an all-atom model shows that the latter does not necessarily yield an improved description of molecular behaviour.

## 2.2 Introduction

The practical value of computer simulation of molecular systems relies very much on the accuracy of the potential energy function or force field that is used. For biomolecular systems a number of force fields have been developed and refined during the past decades, and are widely used [16, 22-34]. The potential energy functions of different force fields have slightly different forms, and the force field parameters are generally obtained by fitting of a range of molecular properties against different sets of quantum-mechanical and experimental data regarding small molecules. A force field can be tested by application to biomolecular systems for which structural, energetic and dynamic data are available.

When using the most recent version of the GROMOS (Groningen Molecular Simulation) force field [16,35,36] in simulations of membranes, which involve – in contrast to proteins, sugars and nucleotides – long aliphatic carbon chains, we observed that the GROMOS96 43A1 force field [16] favours too

strongly *trans* over *gauche* conformations in aliphatic chains. In the parametrisation of the GROMOS 43A1 force field, the CH<sub>1</sub>, CH<sub>2</sub> and CH<sub>3</sub> united-atom van der Waals interaction parameters had been determined such that the energy (heat of vaporisation) and density of a number of *n*-alkanes in the liquid phase was reproduced [35]. The parameters of the torsional angle term in the force field had not been changed from the previous force field version [37]. Thus, these could be varied to obtain values for which a correct *trans-gauche* ratio is obtained, while still maintaining the correct energy and density of the *n*-alkane liquids.

We report a refinement of the parameters for aliphatic chains in the GROMOS 43A1 force field. The experimental and quantum-mechanically calculated data used in the parametrisation are considered, and a comparison of the properties of the *n*-alkanes butane, pentane and hexane obtained using various parameter sets and also using OPLS parameters [32,33] is presented. The effects of using different cut-off radii for the intermolecular non-bonded interactions is considered in an appendix.

## 2.3 Selection of target values

First, the target values to be used in the parametrisation have to be chosen. As target values for the heat of vaporisation  $\Delta H_{\text{vap}}$  and the pressure  $p$  (for a given density) for *n*-butane, *n*-pentane and *n*-hexane were taken experimental values for these quantities [38], as in [35]. To select a target value for the ratio of *trans* to *gauche* conformations or for the *gauche-trans* energy difference, values obtained by spectroscopic measurements or by quantum-theoretical model calculations were considered. Over several decades, a range of experimental and theoretical values has been published, as is illustrated for *n*-butane in Figure 2.1. The most recent data seem to converge around 2.7 kJ·mol<sup>-1</sup>. We have chosen the average of the encircled data points as target value for the *n*-butane *gauche-trans* energy difference: 2.66 ± 0.16 kJ·mol<sup>-1</sup>. A similar procedure was followed to select the target *gauche-trans* difference  $E_g - E_t$  for *n*-pentane and *n*-hexane, see Table 2.1. Literature values from high-level *ab-initio* quantum calculations were used to obtain target values for the energy difference  $E_{tg} - E_t$  between the *trans/gauche* barrier and the *trans* conformation, and for the energy difference  $E_{gg} - E_t$  between the *gauche/gauche* or *cis* barrier and the *trans* conformation, see Table 2.1.



<i>Molecule</i>	$E_{pot}$	<i>References</i>	<i>Target value [kJ/mol]</i>
<i>n</i> -Butane	$E_g-E_t$	[50, 52, 53, 54, 56, 57]	2.66±0.16 <sup>a</sup>
	$E_{vg}-E_t$	[56]	13.85±0.42 <sup>b</sup>
	$E_{gg}-E_t$	[56]	22.93±2.09 <sup>b</sup>
<i>n</i> -Pentane	$E_g-E_t$	[40, 45, 50, 53, 58, 59, 60, 61]	2.26±0.25 <sup>c</sup>
	$E_{vg}-E_t$	—	—
	$E_{gg}-E_t$	—	—
<i>n</i> -Hexane	$E_g-E_t$	[56, 62]	2.14±0.16 <sup>d</sup>
	$E_{vg}-E_t$	[56]	11.76±0.42 <sup>b</sup>
	$E_{gg}-E_t$	[56]	21.67±0.42 <sup>b</sup>

<sup>a</sup> average over several methods,

<sup>b</sup> best available ab-initio level result,

<sup>c</sup> average over all data and

<sup>d</sup> average over larger molecules.

## 2.4 Model calculations and simulations

The functional form of the GROMOS96 force field has been given in references [16, 35, 36, 63]. The terms representing torsional interactions and non-bonded interactions are

$$V^{trig}(\vec{r}) = \sum_{n=1}^{N_\varphi} K_{\varphi_n} \left[ 1 + \cos(\delta_n) \cos(m_n \varphi_n(\vec{r})) \right] \quad \text{Eq. 2.1}$$

and

$$V^{nonb}(\vec{r}) = \sum_{\substack{\text{non-bonded} \\ \text{pairs } (i,j)}} \left[ \frac{C_{12}(i,j)}{r_{ij}^6} - C_6(i,j) \right] \frac{1}{r_{ij}^6} \\ + \sum_{\substack{\text{non-bonded} \\ \text{pairs } (i,j)}} \frac{q_i q_j}{4\pi\epsilon_0\epsilon_1} \left[ \frac{1}{r_{ij}} - \frac{C_{rf} r_{ij}^2}{2R_{rf}^3} - \frac{1 - \frac{1}{2} C_{rf}}{R_{rf}} \right] \quad \text{Eq. 2.2}$$

The summation in Eq. 2.1 runs over the  $N_\varphi$  dihedral or torsional angles  $\varphi_n(\vec{r})$  in the molecules, which depend on the Cartesian coordinates  $\vec{r}$  of the atoms in the system. The parameters of the torsional interaction term for dihedral angle  $\varphi_n$  are the force constant  $K_{\varphi_n}$ , phase shift  $\delta_n$  and multiplicity  $m_n$ .

dihedral-angle potential energy functions  
[kJ/molecule]

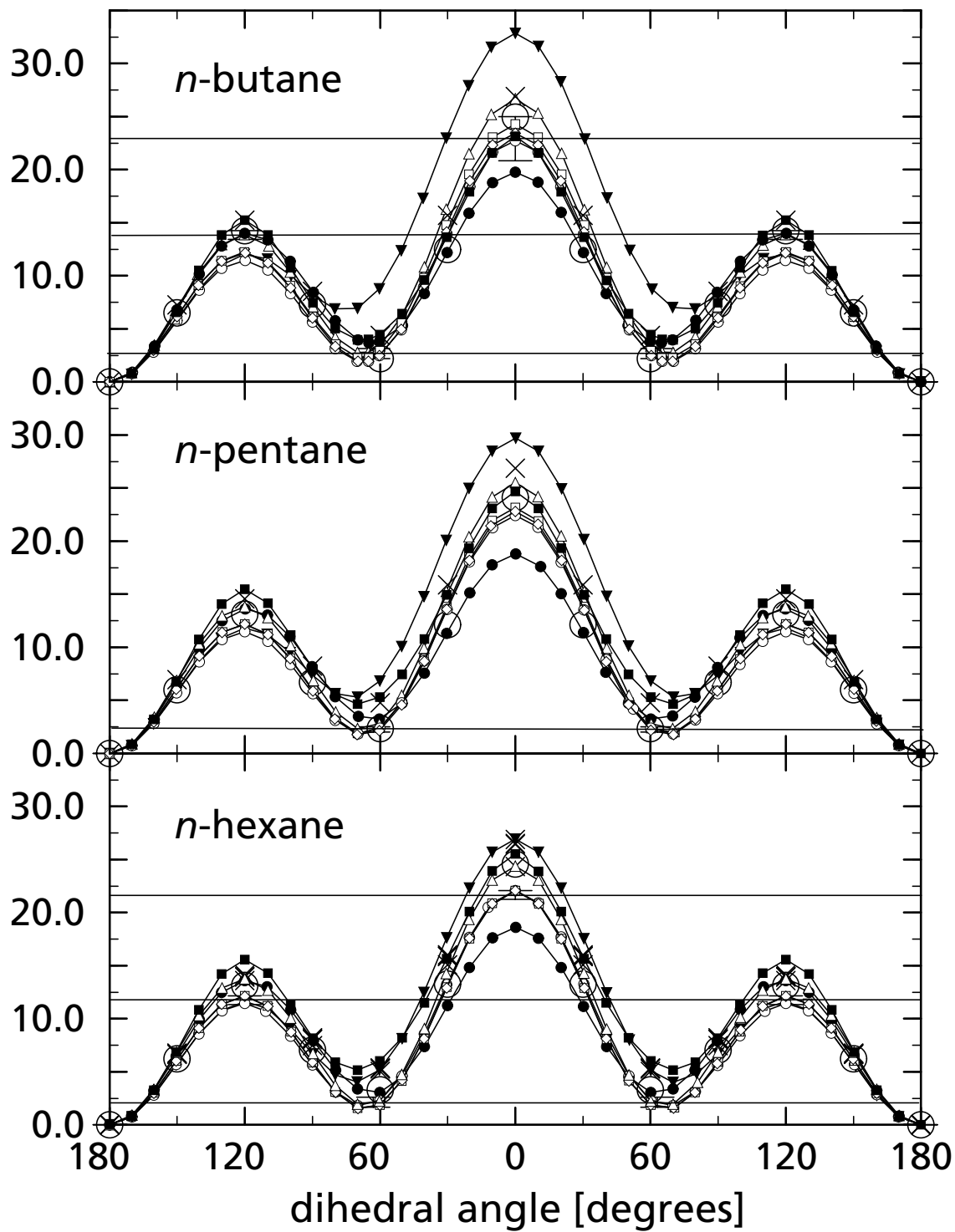


**Figure 2.2** The original GROMOS96 potential energy as function of dihedral angle value for *n*-butane, *n*-pentane and *n*-hexane is shown as eyeguiding line with filled triangles. Target energy values derived from experimental or theoretical work (Table 2.1) are indicated with horizontal lines.

The modifications of the GROMOS96 force field, in which the third-neighbour van der Waals repulsive ( $CS_{12}$ ) parameter was reduced and the force constant ( $K_{\varphi_n}$ ) for alkane dihedral angle potentials was increased (Table 2.2), are shown as eyeguiding lines with open white triangles (a), squares (b), circles (c) or diamonds (d).

The result for the OPLS united- and all-atom force fields were obtained using a modified version of the GROMOS96 software (for all-atom electrostatic 1–4 scaling). The results are shown as filled circles (united-atom) or filled squares (all-atom) including an eyeguiding line.

Additional values illustrated are: Hartree Fock for several basis sets (up to 6-31G\*\*, large crosses) and MP2 6-31G\*\* (large circles).

The summation over the non-bonded pairs ( $i, j$ ) requires some clarification. No non-bonded interaction is calculated for atom pairs that are connected by one or two bonds (or in special cases not considered here, three bonds) and slightly weaker van der Waals interactions are used for certain atom types, *e.g.*, the aliphatic  $CH_1$ ,  $CH_2$ , and  $CH_3$  united atoms considered here, separated by three bonds. These are called third-neighbour or 1–4 van der Waals interactions and parameters ( $CS_{12}(i, j)$  and  $CS_6(i, j)$ ) replacing  $C_{12}(i, j)$  and  $C_6(i, j)$  in Eq. 2.2). The distance between atoms  $i$  and  $j$  is indicated by  $r_{ij}$ . The second term in Eq. 2.2, Coulomb plus reaction field, only applies when the atoms carry non-zero partial charges  $q_i$ . For aliphatic carbons in the GROMOS and OPLS *united-atom* force fields these charges are zero. In the calculations using the OPLS all-atom force field, we used a dielectric permittivity of 1 ( $\epsilon_1 = \epsilon_2 = 1.0$ ) both inside ( $\epsilon_1$ ) and outside ( $\epsilon_2$ ) the long-range cut-off radius  $R_{rf} = 1.4$  nm. Since the ionic strength of the *n*-alkane liquids is zero, the inverse Debye screening length  $\kappa$  is also zero, which means that  $C_{rf} = 0$  in Eq. 2.2.

Within the GROMOS96 force field, the general van der Waals parameters  $C_{12}(i, j)$  and  $C_6(i, j)$  and the third-neighbour van der Waals parameters  $CS_{12}(i, j)$  and  $CS_6(i, j)$  are defined separately for each pair of atom types. It is possible within the GROMOS force field to parametrise self-interactions (between pairs of identical atoms) separately from crossed interactions (between different atom types). The force field doesn't depend on a given set of combination rules, which adds considerable flexibility to the parametrisation. By default, however, the parameters for crossed interactions are generated by taking a geometric mean of the self-interaction values:  $C_{12}(i, j) = [C_{12}(i, i)C_{12}(j, j)]^{1/2}$

and  $C_6(i,j) = [C_6(i,i)C_6(j,j)]^{1/2}$ , and likewise for the third-neighbour van der Waals parameters  $CS_{12}(i,j)$  and  $CS_6(i,j)$ . Improvement of the *trans-gauche* ratio for aliphatic carbon chains or  $n$ -alkanes only involves a refitting of the torsional angle interaction parameter  $K_{\varphi_n}$  for dihedrals of type  $\square\text{---CH}_n\text{---CH}_n\text{---}\square$  and of the third-neighbour van der Waals parameters  $CS_{12}(\text{CH}_2,\text{CH}_2)$ ,  $CS_{12}(\text{CH}_3,\text{CH}_3)$ ,  $CS_6(\text{CH}_2,\text{CH}_2)$  and  $CS_6(\text{CH}_3,\text{CH}_3)$ . It turned out that the latter two parameters could be kept at their GROMOS96 43A1 values while varying the other three parameters to fit the calculated liquid energy, pressure and *trans-gauche* ratio for the three  $n$ -alkanes to the target values given in Table 2.2.

The GROMOS96 software [16] was used in all simulations. For the investigation of liquid alkane properties, 512 molecules ( $= N_{molecule}$ ) have been used within a cubic box under periodic boundary conditions. The box length  $\ell_{box}$  chosen corresponds to the experimental density at 298.15 K of the liquid ( $\rho_{liquid}$ ) and is calculated through equation 2.3 leading to 4.41814 nm for  $n$ -butane, 4.62264 nm for  $n$ -pentane and 4.80535 nm for  $n$ -hexane.

$$\ell_{box} = \left( \frac{N_{molecule} \cdot M_{molecule}}{\rho_{liquid}} \right)^{1/3}, \quad \text{Eq. 2.3}$$

where  $M_{molecule}$  is the mass of an  $n$ -alkane molecule. Starting from a regular array of molecules, a molecular dynamics simulation at constant volume and temperature (NVT) of 500 ps was carried out. Initial velocities were taken from a Maxwellian distribution at 298.15 K and the initial centre of mass motion was removed. The time coupling constant for coupling to the temperature bath was set to  $\tau_T = 0.1$  ps [21]. The time step used in the leap-frog integration scheme was 0.002 ps. Except for bond constraints maintained at a relative geometrical tolerance of  $10^{-4}$  by the SHAKE algorithm [18] all internal interactions were treated explicitly. A twin range cut-off of 0.8/1.4 nm was applied to the non-bonded interactions and the non-bonded pairlist and the long-range forces were updated every 5 time steps.

The trajectories of configurations were used after 100 ps of equilibration time to calculate the average energy, the average pressure, the geometric *trans-gauche* ratio (Eq. 2.4), and the number of transitions of dihedral angles, from which both the frequency of transition and the transition-derived *trans-gauche* ratio (Eq. 2.5) can be calculated. The geometric definition of the percentage of *trans* conformations depends on the number of *trans* configurations  $n_{\varphi_t}$  and the number of *gauche* configurations  $n_{\varphi_g}$  in the trajectory:



**Table 2.2** GROMOS96 third-neighbour non-bonded and dihedral angle potential parameters were tested using  $n$ -alkane simulations. New parameter sets (a to d) were used to improve the dihedral angle potential energy profiles (Figure 2.2). Results have been compared to OPLS united-atom and all-atom approaches. Reference values for experimental heat of vaporisation and pressure are found in [38], those for the percentages of *trans* configuration are interpolated from [45, 50, 52, 64] for  $n$ -butane, from [45, 50] for  $n$ -pentane and from [50] for  $n$ -hexane, where the value in parentheses is an average measured for longer  $n$ -alkanes also from [50].

<i>Forcefield</i>		<i>Parameters</i>					<i>Properties</i>				
<i>Name, interaction</i>	<i>Dihedral potential</i>	$\delta_n$	$m_n$	<i>1-4 van der Waals parameters</i>	$\Delta H_{vap}$	$p$	$r_{geom}$	<i>Number of transitions</i>			
<i><math>n</math>-Butane, <math>CH_3-CH_3</math></i>	$K\varphi_n$			$CS_{12}(CH_3, CH_3)$	$CS_6(CH_3, CH_3)$	[atm]	[%]	[per dihedral per 100 ps]			
Experimental target						<b>21.62</b>	<b>2.43</b>	<b>60</b>	-		
GROMOS96 43A1	5.86	+1	3	0.1206173E-04	0.6852528E-02	20.76	130.13	91	1.72		
GROMOS96a	7.08	+1	3	0.6793766E-05	0.6852528E-02	20.87	124.87	66	1.79		
GROMOS96b	6.28	+1	3	0.6412316E-05	0.6852528E-02	20.74	121.64	63	3.08		
GROMOS96c 43A2	5.92	+1	3	0.6030865E-05	0.6852528E-02	21.00	121.77	60	3.79		
GROMOS96d	6.28	+1	3	0.6030865E-05	0.6852528E-02	20.84	108.80	59	3.00		
OPLS ua	$\left\{ \begin{array}{l} 3.18402 \\ -0.65898 \\ 6.70904 \end{array} \right.$	$\left\{ \begin{array}{l} +1 \\ -1 \\ +1 \end{array} \right.$	$\left. \begin{array}{l} 1 \\ 2 \\ 3 \end{array} \right\}$	0.0	0.0	21.05	130.11	68	2.56		
OPLS aa	$\left\{ \begin{array}{l} 3.640080 \\ -0.328444 \\ 0.583668 \end{array} \right.$	$\left\{ \begin{array}{l} +1 \\ -1 \\ +1 \end{array} \right.$	$\left. \begin{array}{l} 1 \\ 2 \\ 3 \end{array} \right\}$	0.1866303E-05	0.1015252E-02	21.20	131.27	74	2.00		

$$\langle r_{geom} \rangle = \frac{\sum n_{\varphi_t} \cdot 100}{\sum n_{\varphi_t} + \sum n_{\varphi_g}}, \quad \begin{array}{l} \varphi = \{-180^\circ \dots + 180^\circ\} \\ \text{for } \varphi_t = |\varphi| > 120^\circ \\ \varphi_g = |\varphi| < 120^\circ \end{array} \quad \text{Eq. 2.4}$$

The geometric *trans-gauche* ratio is obtained by defining the top of the *trans-gauche* torsional energy barrier ( $\varphi = \pm 120^\circ$ ) as the separation line. In the same vein, one could define a dihedral angle transition to occur if the dihedral angle passes this barrier. However, if the dihedral angle immediately returns backwards over the barrier, one would not consider such crossing events as two transitions. Therefore, for the dihedral transitions, the definition used in the GROMOS package was applied [16]. A dihedral transition is only considered to be completed if the dihedral angle passes the bottom of an adjacent well in the dihedral energy term (Eq. 2.1). Then the time difference  $\Delta t_{\varphi_t}$  between two subsequent transitions from and to the *trans* configuration and the corresponding time difference  $\Delta t_{\varphi_g}$  can be used to define a transition-derived percentage of *trans* conformations:

$$\langle r_{trans} \rangle = \frac{\sum \Delta t_{\varphi_t} \cdot 100}{\sum \Delta t_{\varphi_t} + \sum \Delta t_{\varphi_g}}, \quad \begin{array}{l} \Delta t_{\varphi_t} = t_{\varphi_t} \rightarrow t_{\varphi_g} \\ \Delta t_{\varphi_g} = t_{\varphi_g} \rightarrow t_{\varphi_t} \end{array} \quad \text{Eq. 2.5}$$

Time differences in equation 2.5 have been taken from the registered transitions of the dihedral angles of the same type. In all cases, the transition-derived average *trans-gauche* ratios are within 10% of the average geometrical *trans-gauche* ratios. For the parametrisation, only the geometrical *trans-gauche* ratios have been taken into account and only this data is shown in Table 2.2.

To calculate the heat of vaporisation simulations in vacuum are required. The final coordinates and velocity vectors of the liquid simulation trajectory have been used to initialise simulations in vacuum. The 512 molecules were re-distributed into a much larger box of 400 nm side length to avoid intermolecular interactions. With this large cubic box and a single cutoff of 1.0 nm, a vacuum trajectory of 100 ps was produced (50 ps equilibration time). From the potential energies  $E_{pot}$  of the liquid and vacuum simulations the heat of vaporisation for the pure substance was calculated using Eq. 2.6 which simply cor-

Table 2.2 (Continued)

Forcefield		Parameters				Properties					
Name, interaction	Dihedral potential	$\delta_n$	$m_n$	1-4 van der Waals parameters	$\Delta H_{\text{vap}}$	$p$	$r_{\text{geom}}$	Number of transitions			
<i>n</i> -Pentane, $\text{CH}_3\text{---CH}_2\text{---CH}_2\text{---CH}_2\text{---CH}_3$	$K\varphi_n$	$\delta_n$	$m_n$	$\text{CS}_{12}(\text{CH}_2, \text{CH}_3)$	$\text{CS}_6(\text{CH}_2, \text{CH}_3)$	[kJ/mol]	[atm]	[%]	[per dihedral per 100 ps]		
Experimental target						<b>26.43</b>	<b>0.68</b>	<b>64</b>	–		
GROMOS96 43A1	5.86	+1	3	0.9262491E-05	0.5689469E-02	26.30	40.92	86	2.41, 2.42		
GROMOS96a	7.08	+1	3	0.5675873E-05	0.5689469E-02	26.12	31.39	69	1.92, 2.03		
GROMOS96b	6.28	+1	3	0.5347702E-05	0.5689469E-02	26.47	35.76	66	3.15, 3.10		
GROMOS96c 43A2	5.92	+1	3	0.5347702E-05	0.5689469E-02	26.09	24.64	66	3.74, 3.84		
GROMOS96d	6.28	+1	3	0.5186203E-05	0.5689469E-02	25.96	25.93	65	3.11, 3.16		
OPLS ua	$\left\{ \begin{array}{l} 2.95181 \\ -0.56693 \\ 6.57934 \end{array} \right\}$	$\left\{ \begin{array}{l} +1 \\ -1 \\ +1 \end{array} \right\}$	$\left\{ \begin{array}{l} 1 \\ 2 \\ 3 \end{array} \right\}$	0.0	0.0	26.25	39.90	72	2.71, 2.72		
									–		
									–		
OPLS aa	$\left\{ \begin{array}{l} 3.640080 \\ -0.328444 \\ 0.583668 \end{array} \right\}$	$\left\{ \begin{array}{l} +1 \\ -1 \\ +1 \end{array} \right\}$	$\left\{ \begin{array}{l} 1 \\ 2 \\ 3 \end{array} \right\}$	0.1866303E-05	0.1015252E-02	26.37	117.74	80	1.64, 1.64		
									–		
									–		
Experimental target						<b>31.55</b>	<b>0.20</b>	<b>65 (66)</b>	–		
GROMOS96 43A1	5.86	+1	3	0.7112889E-05	0.4723813E-02	31.87	31.12	86, 80, 86	2.33, 3.38, 2.37		
GROMOS96a	7.08	+1	3	0.4741926E-05	0.4723813E-02	31.80	-3.72	67, 71, 67	2.36, 1.94, 2.30		
GROMOS96b	6.28	+1	3	0.4459842E-05	0.4723813E-02	31.78	9.35	65, 68, 65	3.64, 3.05, 3.59		
GROMOS96c 43A2	5.92	+1	3	0.4741926E-05	0.4723813E-02	31.63	0.44	63, 71, 63	4.39, 3.60, 4.39		
GROMOS96d	6.28	+1	3	0.4459842E-05	0.4723813E-02	31.70	2.10	63, 69, 63	3.58, 3.06, 3.56		
OPLS ua	$\left\{ \begin{array}{l} 2.95181 \\ -0.56693 \\ 6.57934 \end{array} \right\}$	$\left\{ \begin{array}{l} +1 \\ -1 \\ +1 \end{array} \right\}$	$\left\{ \begin{array}{l} 1 \\ 2 \\ 3 \end{array} \right\}$	0.0	0.0	32.07	4.08	70, 77, 70	3.05, 2.55, 3.07		
									–		
									–		
OPLS aa	$\left\{ \begin{array}{l} 3.640080 \\ -0.328444 \\ 0.583668 \end{array} \right\}$	$\left\{ \begin{array}{l} +1 \\ -1 \\ +1 \end{array} \right\}$	$\left\{ \begin{array}{l} 1 \\ 2 \\ 3 \end{array} \right\}$	0.1866303E-05	0.1015252E-02	32.07	166.02	80, 84, 80	1.51, 1.27, 1.41		
									–		
									–		

responds to the enthalpy difference  $H_{gas} - H_{liquid}$ . The average total potential molecular energy of the liquid phase is subtracted from the average total potential molecular energy lacking the intermolecular contacts in the gas phase under the assumption of ideality in the gas using  $RT$  replacing  $pV$ ,

$$\Delta H_{vap} = E_{pot}(g) - E_{pot}(\ell) + RT \quad \text{Eq. 2.6.}$$

## 2.5 Results and Discussion

The van der Waals repulsive parameter  $CS_{12}$  of the GROMOS96 43A1 force field shows a too large repulsion between third neighbours in the energy as function of dihedral angle for aliphatic chains. *n*-Butane shows the largest deviation in energy levels using the original GROMOS96 parameters.

As can be seen in Table 2.2, the simulated percentage of *trans* conformers is too large, 91, 86 and (86,80,86) percent for the three *n*-alkane liquids as compared to the target values of 60, 64 and 65 percent, respectively. The *trans-gauche* ratio can be reduced by decreasing the third-neighbour repulsive van der Waals parameters  $CS_{12}$ . This decrease will also reduce the *trans/gauche* energy barriers which can be counteracted by increasing the force constant of the torsional angle energy term  $K_{\varphi_n}$ . These parameter changes will also affect the heat of vaporisation and the pressure of the liquids. A large number of parameter value combinations was tested. The results for a few of these are shown in Table 2.2. The amplitude of the dihedral potential energy term was either set to fit the barrier height of *n*-hexane (models b, c and d) or *n*-butane (model a). This affects the kinetics of dihedral transitions and in the case of *n*-hexane changed the molecular kinetics completely: the central dihedral is less mobile than the end dihedral angles. Large deviations in the heat of vaporisation were not observed using the new models a to d, but the sampling of dihedral space is indeed different compared to GROMOS96 43A1 and also the pressure was positively affected. The modification indicated by the symbol GROMOS96c yields the best agreement with the nine target values. Compared to the GROMOS96 43A1 results these parameters yield a significant improvement of the *trans-gauche* ratio, while agreeing even slightly better with the target values for the heat of vaporisation and pressure.

Table 2.2 also contains values for the OPLS united-atom [32, 66] and all-atom [33,65,67] force fields. The OPLS united-atom parameters which are relatively old, yield surprisingly good agreement with the target values, which were partially not yet available in 1984. The much newer OPLS all-atom model produces too high pressures and too large *trans-gauche* ratios.

The OPLS parameters originate from (N,P,T) Monte Carlo simulations using a 1.1 nm intermolecular non-bonded cut-off in the all-atom case [65] and values in the range of 0.95 to 1.5 nm in the united-atom case [66]. When fitting the OPLS force field parameters, a correction was made that approximately accounts for the non-bonded interactions between atom pairs at a distance larger than the cut-off distance ( $R_c$ ). We have analysed the size of these long-range contributions to the energy and pressure as a function of cut-off radius in the appendix. The results for the three *n*-alkanes using GROMOS96 and OPLS force fields with a cut-off radius of 1.4 nm are shown in Table 2.3. The

**Table 2.3** 1.4 nm cut-off contribution correction to heat of vaporisation and pressure for *n*-alkanes. Heat of vaporisation and pressure from MD simulations using a non-bonded cut-off radius  $R_c=1.4$  nm and the corresponding contributions  $E_{R_c}$  and  $p_{R_c}$  calculated using Eqs. A.2.8 and A.2.9. All simulation results have been obtained with the GROMOS96 program [16]. For further explanation see captions of Tables 2.2, 2.4–2.6 and the methods section.

	<i>n</i> -Butane		<i>n</i> -Pentane		<i>n</i> -Hexane	
	$\Delta H_{vap}$	$p$	$\Delta H_{vap}$	$p$	$\Delta H_{vap}$	$p$
	$kJmol^{-1}$	$atm$	$kJmol^{-1}$	$atm$	$kJmol^{-1}$	$atm$
<i>Experiment</i>	21.62	2.4	26.43	0.68	31.55	0.20
GROMOS96 (43A1)						
MD	20.76	130	26.30	41	31.87	31
$-E_{R_c}, p_{R_c}$	0.61	-119	0.81	-137	1.01	-153
sum	21.37	11	27.11	-96	32.88	-122
GROMOS96 (43A2)						
MD	21.00	122	26.09	25	31.63	0
$-E_{R_c}, p_{R_c}$	0.61	-119	0.81	-137	1.01	-153
sum	21.61	3	26.90	-112	32.64	-153
OPLS-UA						
MD	21.05	130	26.25	40	32.07	4
$-E_{R_c}, p_{R_c}$	0.62	-121	0.82	-139	1.02	-154
sum	21.67	9	27.07	-99	33.09	-150
OPLS-AA						
MD	21.20	131	26.37	118	32.07	166
$-E_{R_c}, p_{R_c}$	0.38	-75	0.51	-86	0.64	-96
sum	21.58	56	26.88	32	32.71	70

contribution of forces beyond  $R_c = 1.4$  nm enlarges the heat of vaporisation by at most  $1 \text{ kJmol}^{-1}$  and reduces the pressure by maximally 150 atm. Inclusion of the long-range contribution improves the agreement with experiment for *n*-butane, while for *n*-pentane and *n*-hexane the heat of vaporisation becomes too large. For the latter two liquids the pressure becomes too low for the united-atom models and it is still a bit too high for the OPLS all-atom model.

We note that the evaluation of the long-range contributions from pairs beyond the cut-off distance using Eqs. (A.2.8–9) is only possible for systems with an isotropic and homogeneous distribution in space of the different types of atom pairs, such as pure liquids or simple mixtures. For proteins and DNA in aqueous solution or membranes, such contributions cannot be estimated using equations (A.2.8–9), but should be explicitly calculated. The GROMOS96 force field has therefore been parametrised using a relatively long cut-off of 1.4 nm and without any corrections of the type of equations (A.2.8–9). This 1.4 nm cut-off radius is thus a parameter of the GROMOS96 force field. When comparing results in Table 2.3, the pure MD-simulation results should be used for GROMOS96, whereas the long-range contributions  $-E_{R_c}$  and  $p_{R_c}$  should be included for OPLS. For *n*-butane the OPLS results agree better than the GROMOS96 ones with experiment, whereas for *n*-pentane and *n*-hexane the GROMOS96 results are better than both OPLS united-atom and all-atom results. This illustrates the observation that a more complex model need not necessarily give better results than a simple model. One should note that for proteins an all-atom model almost quadruples the number of non-bonded interactions to be calculated compared to a united-atom model. For membrane simulations the computational effort will be increased by an even larger factor.

## 2.6 Conclusions

The dihedral angle energy parameter  $K_{\varphi_n}$  for dihedral angles of type  $\square-\text{CH}_n-\text{CH}_n-\square$  and the third-neighbour van der Waals repulsive parameters for atom types  $\text{CH}_2$  and  $\text{CH}_3$  of the GROMOS 43A1 set of force field parameters have been modified to better fit the heat of vaporisation, pressure and *trans-gauche* ratio for liquid *n*-butane, *n*-pentane and *n*-hexane. The new parameter set, denoted GROMOS 43A2 yields significantly better results than the 43A1 set.

When comparing the mentioned properties calculated using OPLS united-atom force field parameters and OPLS all-atom force field parameters with the GROMOS 43A2 parameters, the OPLS force fields perform better for *n*-butane, whereas the GROMOS96 force field does better for *n*-pentane and *n*-hexane. This illustrates that a more complex and time consuming (all-atom) model need not necessarily yield better results than a simple (united-atom) one. This finding suggests that the efficiency of biomolecular simulation will benefit from the use and development of united-atom models.

## 2.7 Acknowledgements

We would like to thank Pier L. Luisi for this scientific collaboration and financial support, Alexandre Bonvin, Wolfgang Damm, Xavier Daura and Alan Mark for their help and advice, and Peter Walde for stimulating discussions.

## 2.8 Appendix

### Energy And Pressure Corrections For Finite Cut-Off

The use of a cut-off radius ( $R_c$ ) for non-bonded interactions in a molecular simulation is only allowed if the contribution of the forces between atoms at a distance larger than  $R_c$  is negligible, or if a good approximation of these forces can be formulated. For a homogeneous atomic liquid the contribution of atom pairs at a distance beyond  $R_c$  to the potential energy is [17].

$$E_{R_c} = 2\pi N_{at}^2 V^{-1} \int_{R_c}^{\infty} r^2 V^{nonb}(r) g(r) dr, \quad \text{Eq. A.2.1}$$

and to the pressure it is

$$p_{R_c} = -\frac{1}{3} 2\pi N_{at}^2 V^{-2} \int_{R_c}^{\infty} r^2 \left( r \frac{dV^{nonb}}{dr} \right) g(r) dr. \quad \text{Eq. A.2.2}$$

The number of atoms in the volume  $V$  is  $N_{at}$ ,  $V^{nonb}(r)$  is the non-bonded atom–atom interaction, and  $g(r)$  is the atom–atom radial distribution function. The integrals in (Eq. A.2.1) and (Eq. A.2.2) can be calculated when  $V^{nonb}(r)$  and  $g(r)$  are known. For a non-bonded interaction of Lennard-Jones type,

$$V^{nonb}(r) = \frac{C_{12}}{r_{12}} - \frac{C_6}{r_6} \quad \text{Eq. A.2.3}$$

and for large values of  $R_c$  one may use the approximations

$$V^{nonb}(r) = -C_6 r^{-6} \quad \text{Eq. A.2.4}$$

and

$$g(r)=1. \quad \text{Eq. A.2.5}$$

Then one obtains for a system of  $N_{at}$  atoms

$$E_{R_c} = -\frac{2\pi}{3} \frac{N_{at}^2}{V} \frac{C_6}{R_c^3} \quad \text{Eq. A.2.6}$$

and

$$p_{R_c} = -\frac{4\pi}{3} \left( \frac{N_{at}}{V} \right)^2 \frac{C_6}{R_c^3} = 2E_{R_c} V^{-1}. \quad \text{Eq. A.2.7}$$

**Table 2.4** Lennard-Jones  $C_6$  attractive parameters for intermolecular non-bonded interactions (see Eq. 2.2), in  $\text{kJmol}^{-1}\text{nm}^6$ , for alkanes or aliphatic chains in the GROMOS96 (43A1, 43A2) [16], OPLS united atom (UA) [66] and OPLS all-atom (AA) [65] force fields.

<i>Pairtype</i>	<i>Force field</i>		<i>Pair type</i>	<i>Force field</i>
	<i>GROMOS96</i>	<i>OPLS-UA</i>		<i>OPLS-AA</i>
CH <sub>2</sub> —CH <sub>2</sub>	0.007105	0.007003	C—C	0.00203050
CH <sub>2</sub> —CH <sub>3</sub>	0.008394	0.008528	C—H	0.00049889
CH <sub>3</sub> —CH <sub>3</sub>	0.009916	0.010385	H—H	0.00012258



For a system of  $N_{molecule}$  molecules, each consisting of  $N_{am}$  atoms per molecule, the value of  $E_{R_c}$  per molecule is

$$E_{R_c}^{mol} = -\frac{2\pi}{3} \frac{N_{at}}{V} \frac{C_6}{R_c^3} N_{am} \quad \text{Eq. A.2.8}$$

and

$$p_{R_c} = 2E_{R_c}^{mol} V^{-1} N_{molecule}. \quad \text{Eq. A.2.9}$$

The expressions  $E_{R_c}^{mol}$  and  $p_{R_c}$  were evaluated for the homogeneous systems of *n*-butane, *n*-pentane and *n*-hexane using cut-off radii  $R_c$  ranging from 0.8 to 1.8 nm and  $C_6$  parameters from the GROMOS96 and OPLS force fields. The  $C_6$  parameters are listed in Table 2.4. Since the *n*-alkanes contain two types of atoms, CH<sub>2</sub> and CH<sub>3</sub> in the united-atom representation, and C and H in the all-atom representation, the  $C_6$  value used in equations A.2.8–9 is a weighted sum of the  $C_6$  values of each type of atom pair with the fraction of each pair type given in Table 2.5 as weight factor. Table 2.6 contains the heat of vapori-

**Table 2.5** Densities of molecules, atoms and pairs of atoms of different types. For further explanation see text of methods section and the appendix.

	<i>n</i> -Butane	<i>n</i> -Pentane	<i>n</i> -Hexane
Box volume [nm <sup>3</sup> ]	86.2419	98.7803	110.9620
Number of molecules in box [ $N_{molecule}$ ]	512	512	512
Number of atoms			
per molecule [ $N_{am}$ ]:			
united-atom models (CH <sub>2</sub> , CH <sub>3</sub> )	4 (2, 2)	5 (3, 2)	6 (4, 2)
all-atom models (C, H)	14 (4, 10)	17 (5, 12)	20 (6, 14)
in box [ $N_{at}$ ]:			
united-atom models	2048	2560	3072
all-atom models	7168	8704	10240
Fraction of atom pairs of types			
for united-atom models:			
CH <sub>2</sub> —CH <sub>2</sub>	4/16	9/25	16/36
CH <sub>2</sub> —CH <sub>3</sub>	8/16	12/25	16/36
CH <sub>3</sub> —CH <sub>3</sub>	4/16	4/25	4/36
for all-atom models:			
C—C	16/196	25/289	36/400
C—H	80/196	120/289	168/400
H—H	100/196	144/289	196/400

sation and pressure as obtained from MD simulations, and the values of expressions A.2.8 and A.2.9 for different cut-off radii  $R_c$ . Beyond  $R_c = 1.4$  nm the long-range contributions become rather small compared to other approximations inherent to the force fields. Below  $R_c = 1.0$  nm, the assumptions of homogeneity (generally a charge-group or molecular cut-off is used in biomolecular force fields), and Eq. A.2.5) become incorrect, especially for the larger *n*-hexane.

The OPLS parameters have been obtained by fitting of the heat of vaporisation and the density of *n*-alkanes in (N,P,T) Monte Carlo simulations of the liquids [65, 66]. It is explicitly stated in [65, 66] that the contribution  $E_{R_c}$  to the energy was included in the fitting of the heat of vaporisation. However, nothing is stated in [65, 66] about inclusion of the corresponding contribution  $p_{R_c}$  to the pressure when fitting to the experimental density.

When deriving the force field parameters of the GROMOS96 force field, the contributions  $E_{R_c}$  and  $p_{R_c}$  were not considered [35], since a relatively long cut-off radius  $R_c = 1.4$  nm was used for both the electrostatic and van der Waals interactions, which makes these contributions rather small.

**Table 2.6** Effect of the intermolecular non-bonded interaction cut-off radius  $R_c$  on the simulated heat of vaporisation and pressure, and the corresponding contributions  $E_{R_c}$  and  $p_{R_c}$  calculated using Eqs. A.2.8 and A.2.9. For further explanation see captions of Tables 2.2–2.5.

$R_c$ [nm]	exp.	GROMOS96 (4342)																	
		OPLS-UA					OPLS-AA												
<i>n</i> -Butane																			
$\Delta H_{vap}$ [kJmol <sup>-1</sup> ]																			
MD	-	17.43	19.38	20.26	21.00	20.92	21.05	17.76	19.85	20.66	21.05	21.29	21.48	20.52	21.09	21.25	21.20	21.27	21.15
$-E_{R_c}$	-	3.28	1.68	0.97	0.61	0.41	0.29	3.35	1.71	0.99	0.62	0.42	0.29	2.06	1.05	0.61	0.38	0.26	0.18
sum		21.62	20.71	21.06	21.23	21.61	21.34	21.11	21.56	21.65	21.67	21.71	21.77	22.58	22.14	21.86	21.58	21.53	21.33
$p$ [atm]																			
MD	-	786	392	191	122	63	51	810	402	202	130	79	59	438	292	171	131	108	100
$p_{R_c}$	-	-639	-327	-189	-119	-80	-56	-651	-333	-193	-121	-81	-57	-400	-205	-119	-75	-50	-35
sum		2.43	147	65	2	3	-17	159	69	9	9	-2	2	38	87	52	56	58	65
<i>n</i> -Pentane																			
$\Delta H_{vap}$ [kJmol <sup>-1</sup> ]																			
MD	-	21.19	24.22	25.60	26.09	26.55	26.72	20.92	24.24	25.64	26.25	26.63	26.67	24.98	26.02	26.42	26.37	26.61	26.31
$-E_{R_c}$	-	4.33	2.22	1.28	0.81	0.54	0.38	4.39	2.25	1.30	0.82	0.55	0.39	2.72	1.39	0.81	0.51	0.34	0.24
sum		26.43	25.52	26.44	26.88	26.90	27.09	25.31	26.49	26.94	27.07	27.18	27.06	27.70	27.41	27.23	26.88	26.95	26.55
$p$ [atm]																			
MD	-	969	380	147	25	-31	-42	966	382	147	40	-20	-38	506	275	175	118	74	53
$p_{R_c}$	-	-736	-377	-218	-137	-92	-64	-745	-382	-221	-139	-93	-65	-462	-237	-137	-86	-58	-41
sum		2.43	233	3	-71	-112	-106	221	0	-74	-99	-113	-103	44	38	38	32	16	12
<i>n</i> -Hexane																			
$\Delta H_{vap}$ [kJmol <sup>-1</sup> ]																			
MD	-	28.94	30.83	31.63	31.63	32.14	32.33	29.18	31.10	32.07	32.41	32.72			31.49	32.16	32.07	32.01	32.12
$-E_{R_c}$	-	2.78	1.61	1.01	1.01	0.68	0.48	2.80	1.62	1.02	0.68	0.48			1.75	1.01	0.64	0.43	0.30
sum		31.55	31.72	32.44	32.64	32.82	32.81	31.98	32.72	33.09	33.09	33.20			33.24	33.17	32.71	32.44	32.42
$p$ [atm]																			
MD	-	452	158	0	-56	-116		466	140	4	-55	-100			313	228	166	134	134
$p_{R_c}$	-	-420	-243	-153	-103	-72		-424	-245	-154	-103	-73			-264	-153	-96	-65	-45
sum		2.43	32	-85	-153	-159	-188	42	-105	-150	-158	-173			49	75	70	69	89



# Chapter 3

---

## Molecular Dynamics Simulation of *n*-Dodecylphosphate Aggregate Structures

# 3. Molecular Dynamics Simulation of *n*-Dodecylphosphate Aggregate Structures

## 3.1 Abstract

Aggregates of *n*-dodecylphosphate present an attractive model system of simple phospholipid amphiphile supramolecular structures for study by molecular dynamics simulation since these systems have been studied experimentally earlier under various conditions. A detailed molecular dynamics description of the properties of planar bilayer membranes (as a model for unilamellar vesicular membranes) and spherical micelles under various simulated conditions is presented. It is shown that the united-atom model of GROMOS96 applying the force-field parameter set 43A2 for biomolecular systems yields properties in agreement with experimental ones in most cases. Hydrogen-bonding plays a role in stabilising the bilayer aggregates at low pH, but not for the micelles, which are energetically favoured at high pH. NMR  $-S_{CD}$  order parameters for a lipid bilayer system, the diffusion of amphiphiles within aggregates and of counterions, and lifetimes of hydrogen bonds between amphiphiles and to water are estimated from the MD simulations.

## 3.2 Introduction

It has been suggested that simple phospholipids may have played an essential role in the prebiological, chemical evolution on earth [10-12,68,69]. Single-tail fatty acids [13,70-72] and also alkyl-phosphates or -phosphonates were shown to vesiculate under conditions at which about one half of the molecules is negatively charged and the other half is uncharged. Between about pH 7 to 9 this is the case for fatty acids, around pH 2 it is the case for alkylphosphates or -phosphonates [14]. Somewhat more complex phospholipids such as double tail [73,74] and cyclic [74] dialkyl- or branched [75] monoalkyl-phosphates have also been studied experimentally in this respect. A particular single-tail

phospholipid, *n*-dodecylphosphate, has been studied experimentally to some extent and was found to form both vesicles (at low pH) and micelles (at high pH) depending on the pH-conditions of the aqueous solution [14,76,77]. If only unilamellar vesicles, which vary in diameter after spontaneous vesiculation, are considered, one roughly finds diameters in the range of 25 to 250 nm. For the larger vesicles, a small patch of bilayer vesicular-membrane shows negligible curvature. Undulations of membranes allow for locally convex or concave curvature [78]. It is therefore reasonable to assume that a patch of vesicular membrane could be modelled to a good approximation as a planar bilayer patch. Experimentalists have indicated that hydrogen bonding may increase the stability of bilayers which could explain vesicle formation at  $\text{pH} \approx \text{p}K_1 = 2$  [11,70]. For intermediate pH values of e.g. 7.5 Walde et al. [14] observed large insoluble aggregates for *n*-dodecylphosphates. At  $\text{pH} = 11.2$  the aggregates have completely disappeared as inferred from light and electron microscopy, and micelles are assumed to exist in the case of single-tail lipids [14]. Under salty conditions (0.5 M NaCl) the formation of micelles at high pH has been noted as well [76,77]. Apart from the sketched dependence of the aggregation state on pH, not much is known about *n*-dodecylphosphate aggregates. No NMR-order-parameters of pure *n*-dodecylphosphoric acid or its salts have been measured to our knowledge. The only X-ray examination we are aware of suggests that solubility and crystalline appearance are similar to fatty acids, and alkyl dihydrogen phosphates would show a tilting angle of  $37^\circ$  in the crystal form [79] which could also be relevant for a bilayer structure.

Molecular dynamics (MD) simulation offers the possibility to study the structural, dynamical and energetic properties of complex systems in atomic detail, provided a reliable force field is available and the conformational space of the system is sufficiently sampled [80]. Molecular systems containing lipids in various forms, liquid crystals, monolayers, bilayers and micelles have been studied with MD simulation [31,81-92]. Here we have used MD simulation on a nanosecond timescale to investigate systems built up from mixtures of *n*-dodecylphosphates and *n*-dodecylphosphoric acid under various conditions of pH and temperature, starting from bilayer and micellar structures. Although the simulation time scale is too short to observe transitions between the different types of lipid aggregates, analysis and comparison of the structural, dynamical and energetic differences between various simulations should give insight into the interactions that govern association and structure of assemblies of single-chain phospholipids.

## 3.3 Methods

### Molecular model and force field

The molecular systems were modelled using the GROMOS96 force field which uses a united-atom representation for aliphatic hydrocarbons [16,35,36, 93]. Figure 3.1 shows the molecular topology and partial atomic charges of *n*-dodecylphosphoric acid and the two *n*-dodecylphosphates in the three charge states (neutral,  $-e$ ,  $-2e$ ) that were used in the simulations. To mimic the various pH-conditions, we combined the acidic, monoanionic or dianionic forms with each other in various ratios. At  $\text{pK}_1 \approx \text{pH} = 2$  we combine the acidic and monoanionic forms in a 1:1 ratio. At  $\text{pK}_2 \approx \text{pH} = 7$  we have approximately a 1:1 ratio of the monoanionic and the dianionic forms. At basic  $\text{pH} = 11.2$  we have only the dianionic forms. We assume that these compositions of the system reflect the pH-dependent differences for a real system, since standard classical molecular dynamics simulation does not include transfer of protons. Water was modelled using the simple point charge (SPC) model [20]. The quality of the results of classical molecular dynamics simulation is determined largely by the empirical force field that is used. To provide detailed information on this, the structural elements of the phospholipids and their respective force-field parameters are listed in Table 3.1. The functional forms of the various bonded and non-bonded interaction terms have been given in [16,63]. The 1–4 interaction for aliphatic hydrocarbons has recently been modified to improve the *trans* to *gauche* ratio for liquid *n*-alkanes [93]. This improved parameter set is indicated as GROMOS96 set 43A2.

In simulations of mixed *n*-dodecylphosphoric acid, *n*-dodecylphosphate bilayers based on parameter set 43A1, no transition of the bilayers from the starting all-*trans* conformations to a liquid-crystalline phase were observed (unpublished results). With the newer parameter set 43A2 [93] a complete melting of the membrane is observed if the temperature is raised sufficiently.





**Table 3.1** Structural elements of phospholipids and their respective force field parameters (continued)

<i>bond types</i>	<i>type code</i>	$K_{b_n}$ 10 <sup>6</sup> [kJmol <sup>-1</sup> nm <sup>-4</sup> ]	<i>ideal bondlength</i> [nm]		
-O—H	1	15.70	0.100		
-CH <sub>2</sub> —O—	17	8.18	0.143		
-P—O	23	8.60	0.148		
~CH <sub>2</sub> —CH <sub>2</sub> —	26	7.15	0.153		
-P—O—	27	4.84	0.161		
<i>bond-angle types</i>	<i>type code</i>	$K_{\theta_n}$ [kJmol <sup>-1</sup> ]	<i>ideal bondangle</i> [°]		
-CH <sub>2</sub> —O—P—O—H	4	420	103.0		
-P—O—H	11	450	109.5		
-CH <sub>2</sub> —O—P—O	13	450	109.6		
~CH <sub>n</sub> —CH <sub>2</sub> —CH <sub>2</sub> —	14	530	111.0		
-CH <sub>2</sub> —CH <sub>2</sub> —O—	14	530	111.0		
-CH <sub>2</sub> —O—P—	25	530	120.0		
O—P—O	28	780	120.0		
<i>torsional angle types</i>	<i>type code</i>	$K_{\varphi_n}$ [kJmol <sup>-1</sup> ]	<i>phase</i>	<i>multiplicity</i>	
-CH <sub>2</sub> —O—P—O~	9	3.14	+1.0	2	
-CH <sub>2</sub> —O—P—O~	11	1.05	+1.0	3	
~O—P—O—H	9	3.14	+1.0	2	
~O—P—O—H	11	1.05	+1.0	3	
-CH <sub>2</sub> —CH <sub>2</sub> —O—P—	14	3.77	+1.0	3	
-CH <sub>2</sub> —CH <sub>2</sub> —CH <sub>2</sub> —O—	17	5.92	+1.0	3	
~CH <sub>n</sub> —CH <sub>2</sub> —CH <sub>2</sub> —CH <sub>2</sub> —	17	5.92	+1.0	3	

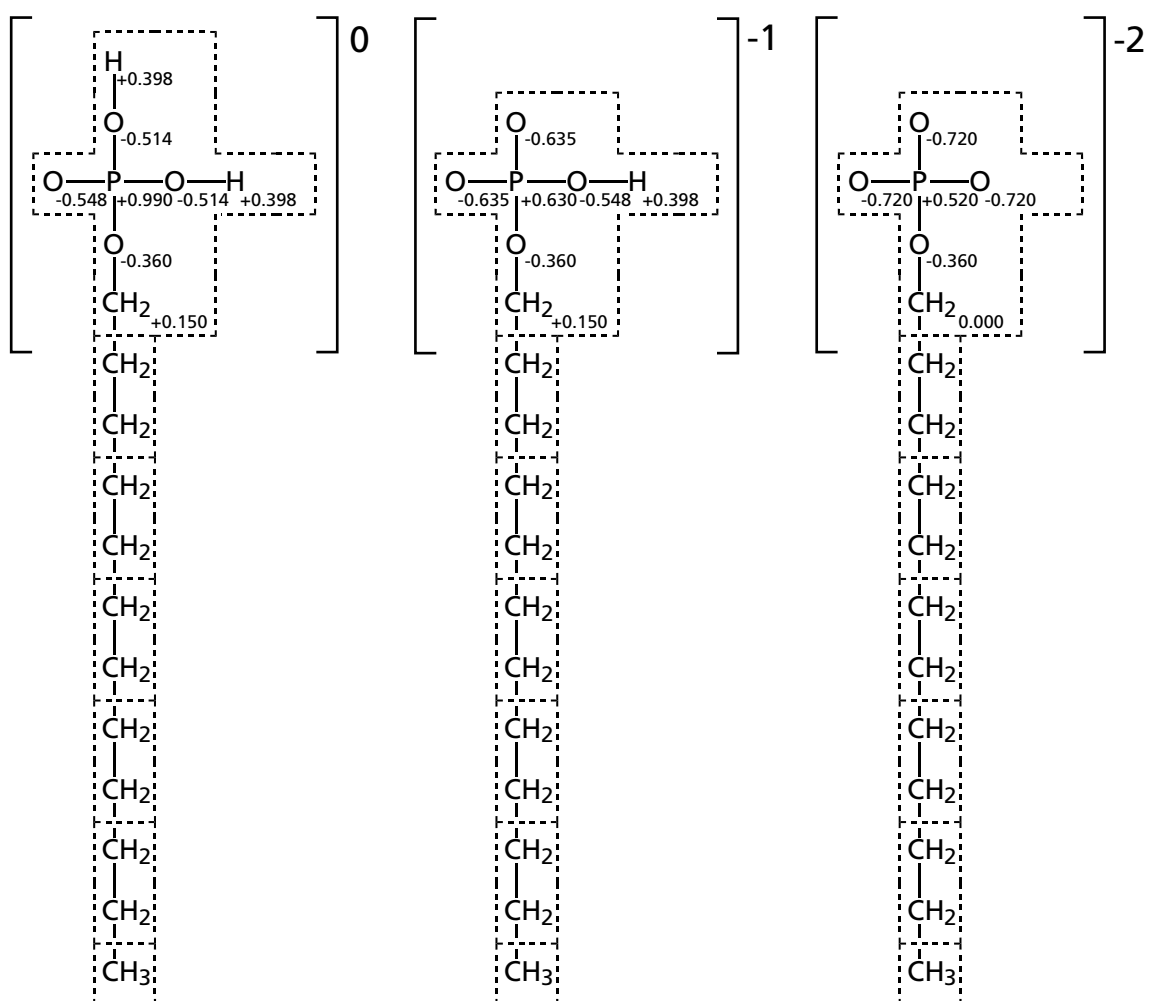


**Figure 3.1** Acidic, monoanionic and basic forms of *n*-dodecylphosphate.

The phosphate-monoanion head group has been defined in [16] (see page IV-228), for use in 3-Phospho-D-Glycerate (PDG). GROMOS96 building block definitions include charge groups (indicated by dashed boxes) and partial charges (indicated by real numbers). Charges are given in  $e$  and have been chosen analogous to those of other phosphates. For aliphatic hydrocarbons ( $\text{CH}_n$ ) united atoms are used. Note that they are not charged and therefore no charge has been displayed. For the definition of atom types, bond, bond-angle and dihedral-angle potential energy terms see Table 3.1.

### System set-up

Table 3.2 shows the different systems that were studied. A bilayer patch of twice  $8 \times 8$  lipids (32 neutral ones and 32 with charge  $-e$ ) was simulated with 64  $\text{Na}^+$  ions at  $\text{pK}_1 \approx 2$  for three different temperatures, 298 K, 348 K and 398 K. At basic pH the bilayer patch consists of twice  $8 \times 8$  lipids with charge  $-2e$ , 256  $\text{Na}^+$  ions and much more water molecules. Three types of micellar systems were simulated. At  $\text{pK}_1 \approx 2$  the system consists of 90 lipids with different tail lengths (45 neutral ones and 45 with charge  $-e$ ) and 45  $\text{Na}^+$  ions and water. The one with the longer tails was simulated at  $\text{pK}_2 \approx 7$  (45 lipids with charge  $-e$  and 45 lipids with charge  $-2e$ ) and at basic pH (90 lipids with charge  $-2e$ ). Finally a smaller micelle (64 lipids with charge  $-2e$ ) was simulated at this pH. The number of 90 lipids was chosen as the average of the experimentally determined aggregation numbers [76]. We note that for the shorter tail length ( $\text{C}_8$ ) we would expect an aggregation number of  $43 \pm 5$  at comparable conditions of  $\text{pH}=4.5$  and  $T=303$  K [94].

For bilayers we used rectangular periodic boundary conditions, for micelles truncated octahedral ones. To obtain an initial structure for the bilayer patches an estimate of the head-group area of the lipids is useful. For *n*-dodecylphosphate this quantity is actually not known experimentally. A rough estimate was obtained as follows. Aggregates of lipids may be characterized using a geometric packing parameter  $P$  [4]. For example, a spherical micelle is characterized by  $P < 1/3$ , and a planar bilayer by  $P=1$ . The area  $a_0$  occupied by one head group is approximately given as a function of the carbon tail length  $\ell_c$  and the volume  $v$  of the carbon tail by

$$a_0 = \frac{v}{\ell_c P}. \quad \text{Eq. 3.1}$$

For an elongated all-*trans* *n*-alkyl single-chain with 12 carbons we assume that  $\ell_c=1.672$  nm and that  $v=0.3502$  nm<sup>3</sup> [4]. For our bilayer patch ( $P=1$ ) assuming all-*trans* conformations this leads to a value of  $a_0=0.21$  nm<sup>2</sup>.

At  $\text{pK}_1$  the uncharged acid and the monoanion lipids are present in a 1:1 ratio positioned in a chess board like geometry. This leads to a lipid-lipid neighbour to neighbour distance of 0.46 nm. For bilayers, the initial assembly of translated molecules was randomized with rotations of individual lipids around their body axis. Micelles were constructed by modifications of head groups and subsequently simulating the assembly of lipids while restraining

**Table 3.2** Simulated systems and their simulation conditions. The system labels are used throughout this work and this table is meant as a reference for the various simulation conditions. Five different groups of simulations can be distinguished: bilayers at low ( $pK_1=2$ ) or high pH ( $=11.2$ ) and micelles at low ( $pK_1$ ) or neutral ( $pK_2$ ) and basic pH. Experiments [14] indicate the existence of bilayers at low and micelles at high pH.

<i>parameters</i>	<i>bilayers</i>					
	bil-pK <sub>1</sub> -298	bil-pK <sub>1</sub> -348	bil-pK <sub>1</sub> -398	bil-bas-298	bil-bas-348	bil-bas-398
number of lipids	128	128	128	128	128	128
number of tail carbons	12	12	12	12	12	12
number of Na <sup>+</sup> -ions	64	64	64	256	256	256
number of water molecules	1420	1420	1420	7351	7351	7351
atoms in total	6692	6692	6692	24485	24485	24485
pH	pK <sub>1</sub> ≈2	pK <sub>1</sub> ≈2	pK <sub>1</sub> ≈2	basic	basic	basic
T [K]	298	348	398	298	348	398
box shape	rectangular	rectangular	rectangular	rectangular	rectangular	rectangular
pressure-coupling	anisotropic	anisotropic	anisotropic	anisotropic	anisotropic	anisotropic
initial box lengths						
x [nm]	3.68	3.68	3.68	3.80	3.80	3.80
y [nm]	3.68	3.68	3.68	3.50	3.50	3.50
z [nm]	7.60	7.60	7.60	20.0	20.0	20.00
simulated time [ns]	3.0	5.0	4.0	3.0	3.0	3.0
equilibration period [ns]	1.5	3.5	2.5	1.5	1.5	1.5

Table 3.2 Simulated systems and their simulation conditions (continued).

parameters	micelles			
labels	mic-C8-pK <sub>1</sub> -298	mic-pK <sub>1</sub> -298	mic-pK <sub>2</sub> -298	mic-bas-298 mic-64-bas-298
number of lipids	90	90	90	90 64
number of tail carbons	8	12	12	12 12
number of Na <sup>+</sup> -ions	45	45	135	180 128
number of water-molecules	6208	6161	6071	6102 6102
atoms in total	19974	20193	19923	20016 19522
pH	pK <sub>1</sub> ≈2	pK <sub>1</sub> ≈2	pK <sub>2</sub> ≈7	basic basic
T [K]	298	298	298	298 298
box shape	trunc. octah.	trunc. octah.	trunc. octah.	trunc. octah. trunc. octah.
pressure-coupling	isotropic	isotropic	isotropic	isotropic isotropic
initial box length				
x [nm]	7.60	7.60	7.60	7.60 7.60
y [nm]	7.60	7.60	7.60	7.60 7.60
z [nm]	7.60	7.60	7.60	7.60 7.60
simulated time [ns]	3.0	3.0	3.0	8.0 3.0
equilibration period [ns]	1.5	1.5	1.5	1.5 1.5

their CH<sub>3</sub>-tail atoms to a fixed position until the structure became spherical. Then the restraints were removed and solvent molecules as well as ions were added. Energy minimisation was carried out followed by short (50 ps) MD simulation while restraining the positions of the lipid atoms.

### System equilibration

Initial velocities were taken from a Maxwell-Boltzmann distribution at the required temperature. Various properties were monitored as function of time to investigate equilibration and convergence. Equilibration could take as long as a few nanoseconds because of the slow diffusion of the charged particles under the influence of long-range Coulomb interactions. This is illustrated in Figure 3.2.

All simulations have been carried out under the following identical conditions. Covalent bonds have been constrained using the SHAKE algorithm [18] with a relative accuracy of  $10^{-4}$ . For non-bonded interactions a twin-range cut-off scheme using 0.8 and 1.4 nm distance criteria was applied. Short-range forces were calculated at every time step of 2 fs, while intermediate-range forces were calculated every 5th step. A dielectric continuum with dielectric permittivity  $\epsilon_2$  equal to 54 (corresponding to SPC water) was assumed beyond the larger cut-off distance. Solute and solvent degrees of freedom were separately coupled to a temperature bath using the Berendsen thermostat [21] with a coupling time of 0.1 ps. The centre of mass motion was removed every 50 ps. The pressure was correspondingly coupled to one atmosphere with a coupling time of 0.5 ps and an isothermal compressibility  $\kappa_T = 4.575 \times 10^{-6} \text{ [kJmol}^{-1}\text{nm}^{-3}]^{-1}$  was used as for mixed protein/water systems [16]. System configurations were saved every picosecond for analysis.

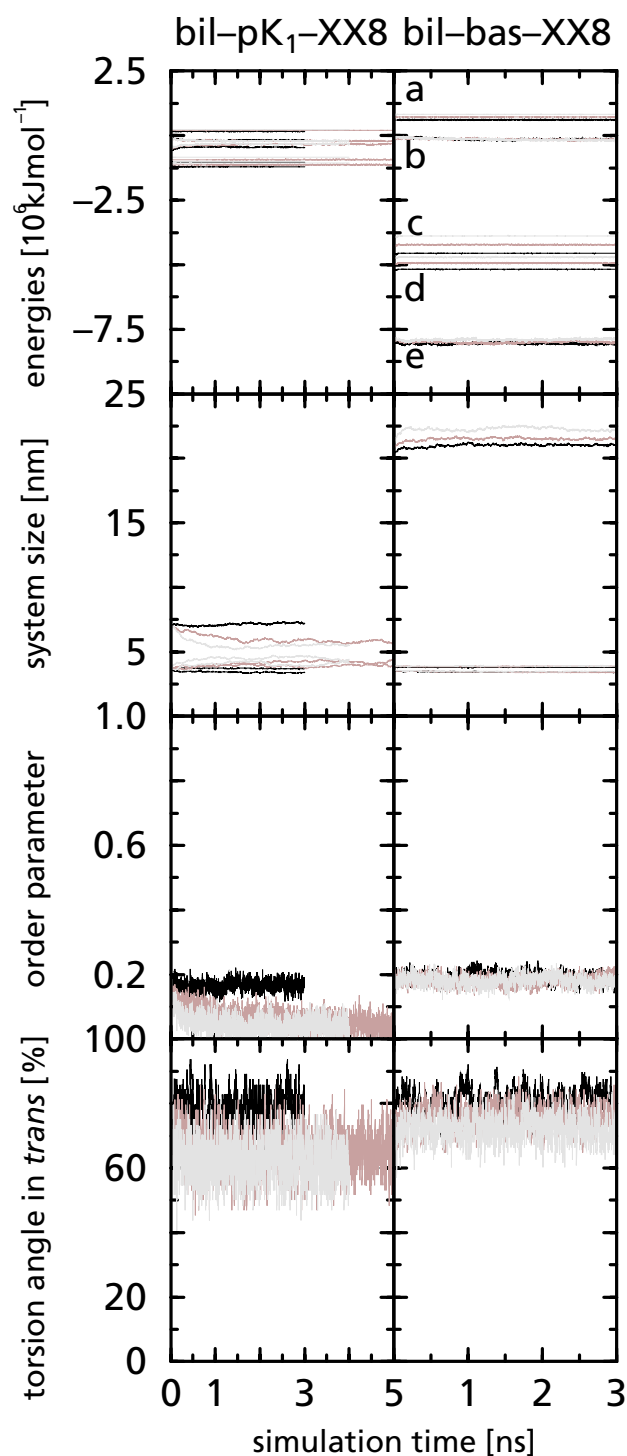
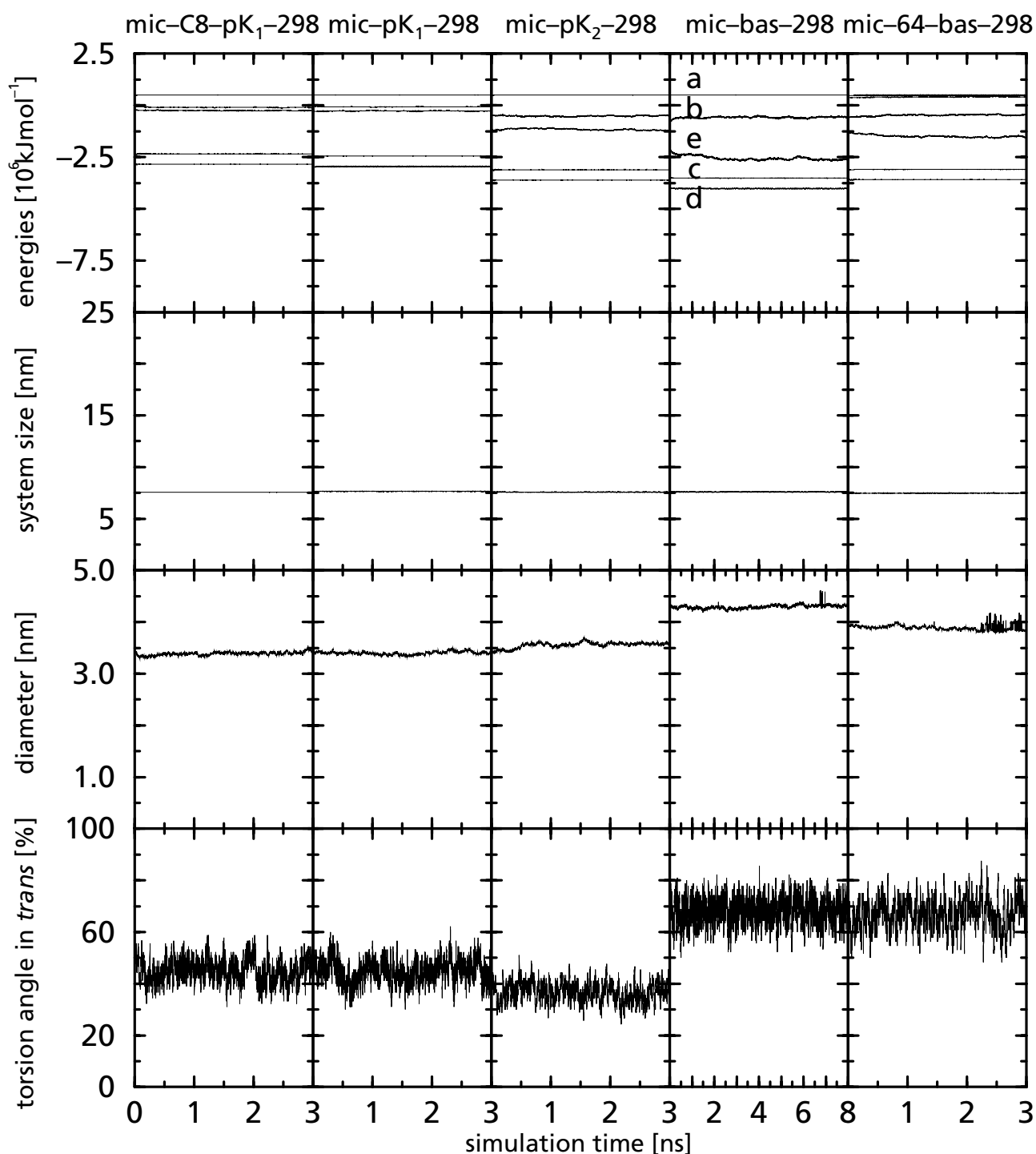


**Figure 3.2** Various system properties as function of time.

The various systems are indicated with the abbreviations defined in Table 3.2. The total (c), kinetic (a) and potential energies (d) of the systems and electrostatic interaction energies between lipids and ions (e) and lipids and water interaction energies (b) are shown in the top panels. Room temperature (298 K) results are given as solid black lines, higher temperatures as dark (348 K) and light (398 K) gray lines.





The second panels show the lengths of the axes of the computational boxes.

The third panels show  $-S_{CD}$  NMR order parameter values for the last CH<sub>2</sub> group in the lipid tails for the bilayer systems. For micelles, the average diameter of the micelle (in nanometers) is shown.

The lowest panels show the average percentage of *trans* conformation seen in the terminal torsion angles of the lipid chains in the systems.

### Calculation of NMR $-S_{CD}$ order parameters

In NMR measurements aimed at obtaining order parameters, deuterated lipids are used and the measured directions are the CD-bonds of the hydrocarbon tails. Since we use a united-atom model, the CD-bond vectors are not directly available from the trajectory. Instead, other vectors were used. Considering the  $-CD_2-$  group at position  $n$  in the hydrocarbon tail, vectors orthogonal to the vector connecting the carbons at position  $n-1$  and  $n+1$  were considered, assuming that these would reflect the time motion of the CD-bonds at carbon position  $n$  along the hydrocarbon tail. This technique has been introduced by Egberts and Berendsen [81]. For the  $n$ th  $-CH_2-$  united atom ( $C_n$ ) we define  $\hat{z}$  as the unit vector from  $C_{n-1}$  to  $C_{n+1}$ ,  $\hat{y}$  as the vector orthogonal to  $\hat{z}$  in the plane through atoms  $C_{n-1}$ ,  $C_n$  and  $C_{n+1}$ , and  $\hat{x}$  as the vector orthogonal to  $\hat{y}$  and  $\hat{z}$ . The calculation of the  $-S_{CD}$  order parameter is done through equation 3.2 which takes into account the possible rotation of the tail, where  $\theta_x$  and  $\theta_y$  represent the angles between the orthogonal vectors  $\hat{x}$  and  $\hat{y}$  and the aggregate or bilayer normal.

$$-S_{CD} = \left( \langle \cos^2 \theta_x \rangle + \frac{1}{2} \left( \langle \cos^2 \theta_y \rangle - 1 \right) \right) \quad \text{Eq. 3.2}$$

### Calculation of hydrogen bond lifetimes

Hydrogen bonds were defined by a hydrogen-acceptor distance smaller than 0.25 nm and an acceptor-hydrogen-donor angle larger than 135 degrees [16]. The hydrogen bond lifetimes were calculated using a 2 ps time resolution.

### Calculation of diffusion coefficients

Diffusion coefficients were calculated from the mean-square displacement of an atom using the Einstein relation.

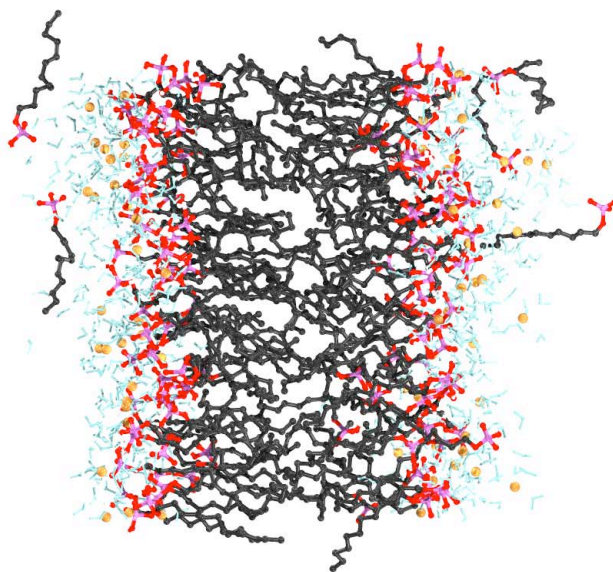
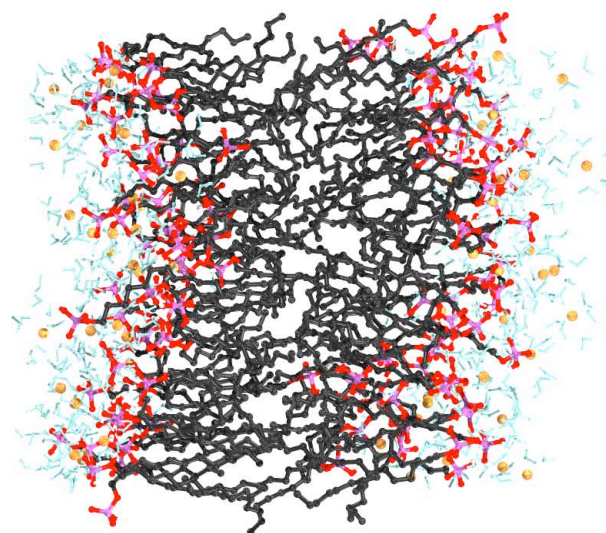
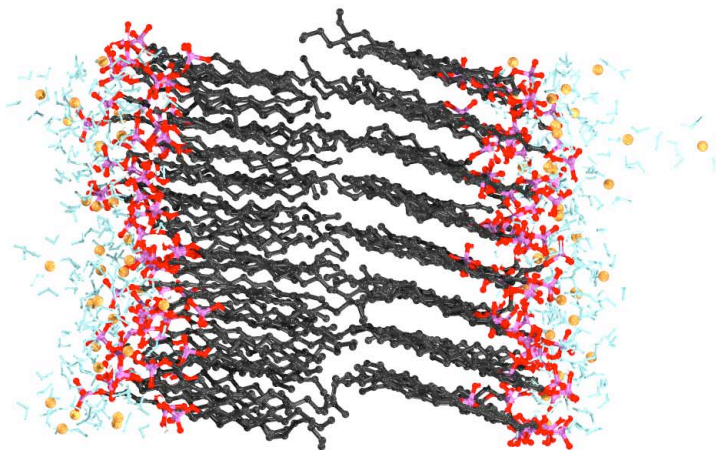
## 3.4 Results and Discussion

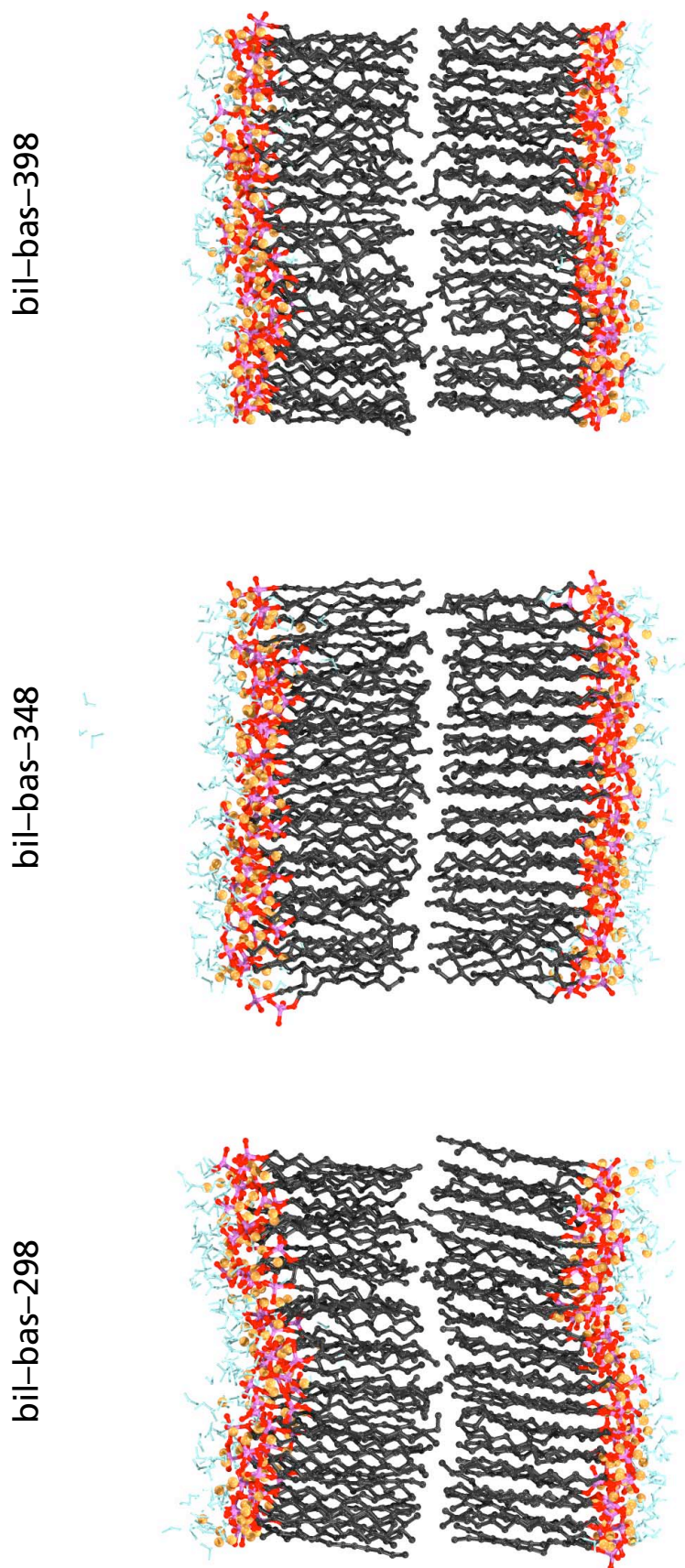
Figure 3.3 shows snapshots of simulated aggregates at the ends of the simulations (see next four pages). Under acidic conditions ( $\text{pH} \approx 2$ ) the bilayers show increased disorder with increasing temperature. This is not observed under basic conditions ( $\text{pH} \geq 11$ ). Under acidic conditions the micelles look rather spherical, under basic conditions more elongated (same pH as for bilayer systems). In some simulations, e.g. bil- $\text{pK}_1$ -398 or mic-C8- $\text{pK}_1$ -298, individual lipids escape from the bilayer or micelle into solution. Our nanosecond simulations are too short to obtain meaningful statistics regarding these processes.

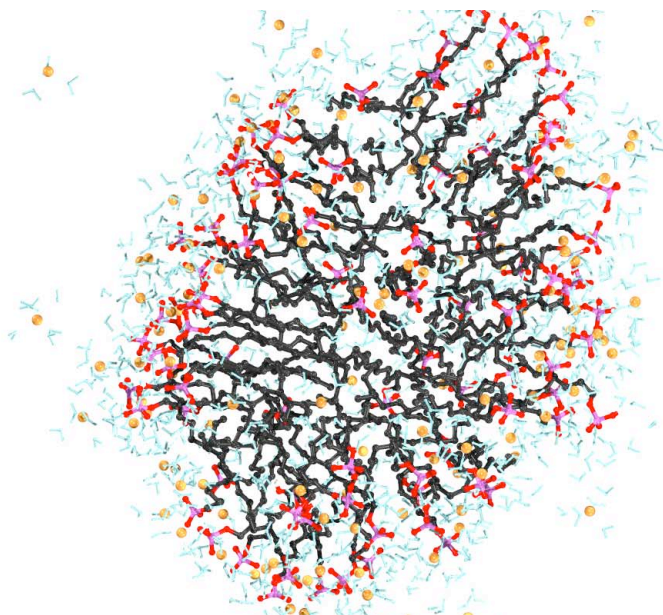
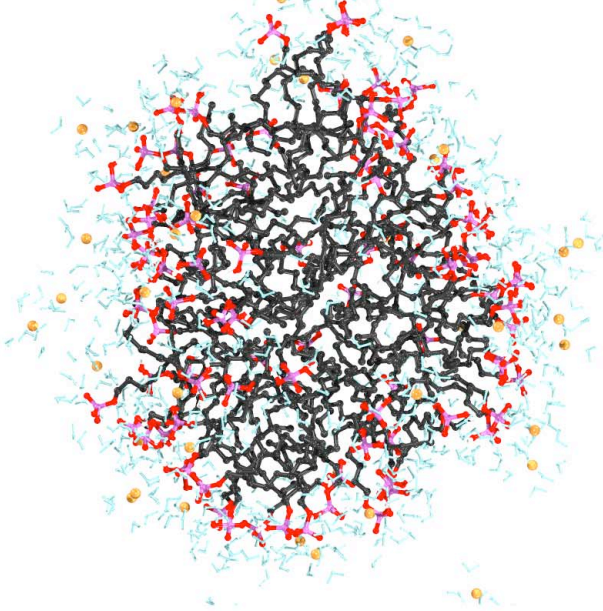
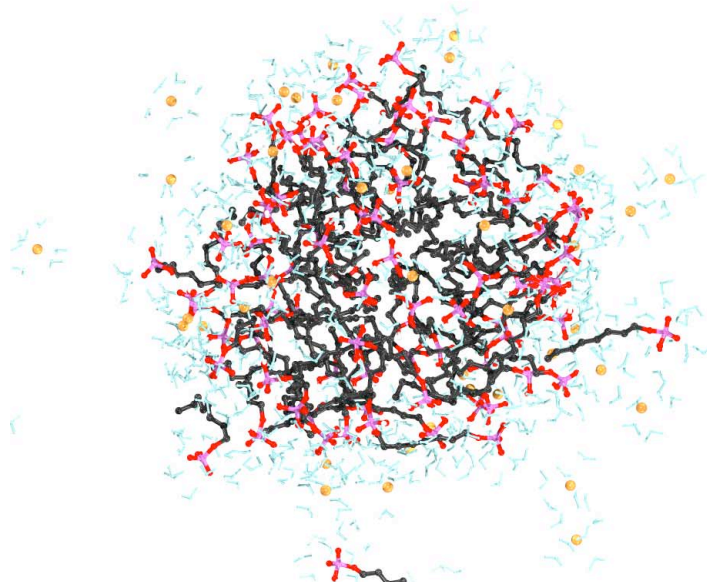
Experimentally it has been found that the concentration of non-associated lipids in equilibrium with the vesicles, is about 20 mM, or about one lipid within water for the acidic 128 lipid bilayer system at room temperature (the abbreviation bil- $\text{pK}_1$ -298 stands for bilayer system at  $\text{pH} = \text{pK}_1$  at  $T = 298$  K). At 298 K and at 348 K no diffusion of an individual lipid from the aggregate to the bulk water is observed within a few nanoseconds. At 398 K diffusion of 4 to 6 lipids into and from the solvent is observed. At room temperature in bil- $\text{pK}_1$ -298 the lipids show an ordering with respect to the surface. This is obvious for the lower layer in Figure 3.3 (angle of about  $25^\circ$  from bilayer normal). The upper layer shows a similar ordering, but in a different direction, which is not obvious from the picture. This behaviour has been observed for many single tail lipid crystals [79,95-99]. The tilted ordering is not observed at high pH within bilayers (Figure 3.3). Instead, a surface undulation is seen through the periodic box at room temperature, which disappears at higher temperatures.

**Figure 3.3** *n*-dodecylphosphate structures obtained at the end of the lipid simulations. Lipid hydrocarbon tails appear in black, head groups in intermediate gray shades. Ions and solvent molecules close to them and to the lipids are shown in light greys.

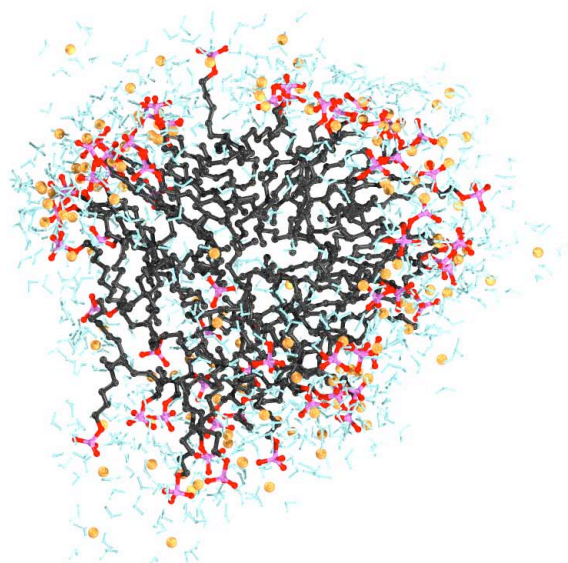
The display is layed out on four pages. First double page: bilayer simulations at  $\text{pK}_1 \approx 2$  and at 298 K, 348 K or 398 K on the left page (bottom to top, best view from right hand side of the book). On the right page: bilayer simulations at basic  $\text{pH} = 11.2$  and at 298 K, 348 K or 398 K. Second double page: unstable micelles (90 lipids) at  $\text{pK}_1$  and at 298 K with different carbon chain lengths (8 and 12 units) and at  $\text{pK}_2$  (neutral pH). The same micelle is also shown on the last page together with micelles (90 and 64 lipids) at basic pH and at 298 K. Thus, e.g. mic-C8- $\text{pK}_1$ -298 means, the micellar system of 90 lipids with chain lengths of 8 carbons per lipid (default is always  $\text{C}_{12}$  = dodecylphosphate) was built as the structure that reflects  $\text{pH} = \text{pK}_1$  and has been simulated at  $T = 298$  K. Any bilayer system of 128 lipids is abbreviated by (bil) correspondingly, and for micellar systems different from 90 lipids the label contains the aggregation number.

bil-pK<sub>1</sub>-398bil-pK<sub>1</sub>-348bil-pK<sub>1</sub>-298

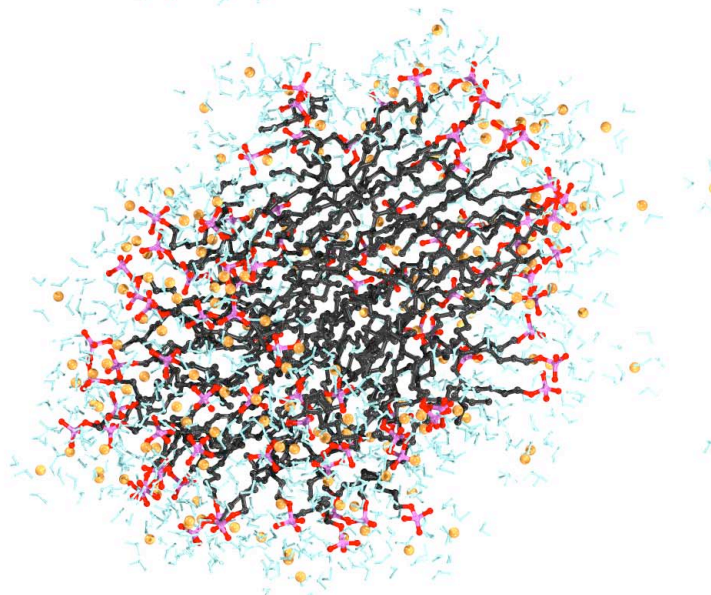


mic-pK<sub>2</sub>-298mic-pK<sub>1</sub>-298mic-C8-pK<sub>1</sub>-298

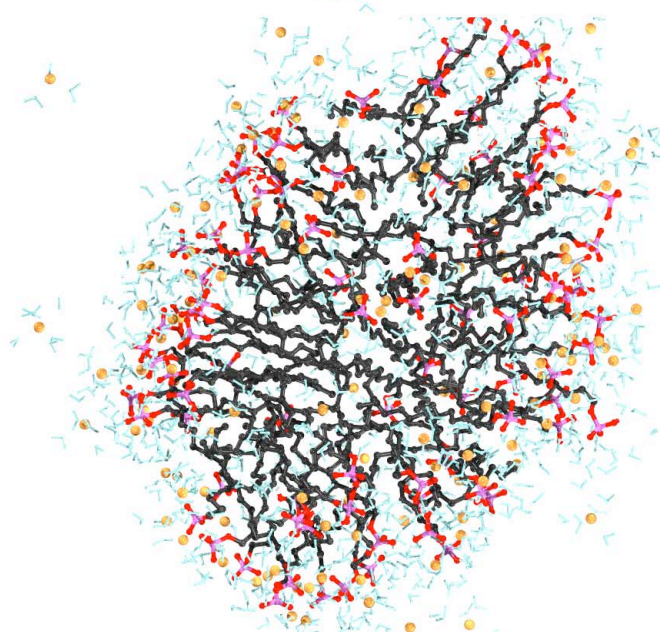
mic-64-bas-298



mic-bas-298



mic-pK<sub>2</sub>-298



### Hydrogen bond lifetimes

Between lipid head groups of monoalkyl-phosphoric acid and -phosphate in the neutral and monoanionic protonation state there are more potential hydrogen bonds than from these lipids to water molecules for systems at  $pK_1$ . For the bilayer bil- $pK_1$ -298 at room temperature and acidic pH (Table 3.3), intermolecular hydrogen bonds of lipid head groups occur during 18% of the simulation time whereas hydrogen bonds of head groups to water molecules are formed during 2% of the simulation time. For the same system the lifetime of hydrogen bonds to water, is longer than the lifetime of the hydrogen bonds between the lipids, 13 ps compared to 9 ps on average. The bilayer bil-bas-298 at high pH shows shorter lifetimes for hydrogen bonds to water of about 4 ps. Between lipids in the basic systems no hydrogen bonds exist.

For micelles at acidic pH (mic-C8- $pK_1$ -298 and mic- $pK_1$ -298) the occurrence of hydrogen bonds is comparable for both systems, about 13% for hydrogen bonds between head-groups and about 2% for hydrogen bonds of head groups to water. The lifetime of these hydrogen bonds is shorter (16 and 9 ps) between head groups than between head group and water (26 and 24 ps). The difference in tail lengths is, therefore, particularly reflected in the difference of lipid-lipid hydrogen-bonding lifetimes. Lipid to water hydrogen bonding has the same lifetime for the smaller *n*-octyl- and the larger *n*-dodecyl-phosphates. With increasing pH, the micelle at  $pK_2 \approx pH=7$  [76,77], mic- $pK_2$ -298, shows similar hydrogen bonding characteristics as the simulated acidic micelle mic- $pK_1$ -298 at  $pK_1=2$  does for the intermolecular head-group hydrogen-bonding, but hydrogen-bonding of lipids to water (occurrence 1% and lifetime 12 ps) is reduced by a factor of 2. For micelles at basic pH (mic-bas-298 and mic-64-bas-298) almost no hydrogen bonds to water are observed (less than 1%) and their lifetime is shorter by a factor of 3. All this indicates that the lifetimes of hydrogen bonds to water in aggregates of *n*-dodecylphosphoric acid and -phosphates are clearly pH-dependent.

The assumption that hydrogen bonding between lipid head groups is important to stabilise the lipid vesicles of *n*-dodecylphosphoric acid and -phosphates (bilayer patch in our model) as stated by Walde et al. [14] is supported by these data. It seems that the mixing with water in the head-group region is low and contacts to water molecules are few. This intramembrane hydrogen-bonding network reflects a major effect of the acidic pH-conditions and is not lost by the curvature in the micellar structure (comparing the bilayer and mi-



celle at  $pK_1$ ). On the other hand the micelle structures at basic pH are purely stabilised through polar electrostatic interactions. Hydrogen bonding to water in the experimentally known micellar aggregates at basic pH lasts half as long as in bilayer membranes at acidic pH.

In the bilayer system *bil-pK<sub>1</sub>-298* the bulk water hydrogen bonds have a lifetime of 1.4 ps, which is shorter than for lipid to water (2 ps) and lipid-lipid (9 ps) hydrogen bonds.

**Table 3.3** Occurrence of hydrogen bonds [%] and average hydrogen bond lifetimes [ps]. For both the bilayer and the micellar systems, lipid-lipid hydrogen bonds between the phosphate head groups and lipid-water hydrogen bonds between the phosphate head groups and solvent molecules are given. Note that for structures simulated at basic pH, hydrogen bonds between lipid head-groups can not exist.

<i>bilayer simulations</i>	<i>bil-pK<sub>1</sub>-298</i>	<i>bil-pK<sub>1</sub>-348</i>	<i>bil-pK<sub>1</sub>-398</i>	<i>bil-bas-298</i>	<i>bil-bas-348</i>	<i>bil-bas-398</i>
type of hydrogen-bond						
lipid-lipid						
occurrence	17.6	5.7	1.3	—	—	—
lifetime	8.6	5.0	3.3	—	—	—
lipid-water						
occurrence	2.0	0.8	0.4	5.1	1.2	0.6
lifetime	13.3	7.5	4.2	4.4	1.2	0.7
<i>micelle simulations</i>	<i>mic-C8-pK<sub>1</sub>-298</i>	<i>mic-pK<sub>1</sub>-298</i>	<i>mic-pK<sub>2</sub>-298</i>	<i>mic-bas-298</i>	<i>mic-64-bas-298</i>	
type of hydrogen-bond						
lipid-lipid						
occurrence	12.3	13.7	12.8	—	—	
lifetime	16.3	8.8	14.4	—	—	
lipid-water						
occurrence	2.2	2.0	1.3	0.6	1.0	
lifetime	25.6	24.1	12.1	4.6	4.7	

### Percentage *trans* of torsion angles along the lipid chains

For every carbohydrate tail the torsion angles  $\theta$  along the lipid chain (starting at the head group) were calculated and the percentage *trans* population of the total population was determined. *Trans* was defined as  $|\theta| > 120^\circ$  and *gauche* as  $|\theta| \leq 120^\circ$  (compare to page 38, Figure 2.2). Figure 3.4 shows the averages for the different simulations.

The picture of the simulated structures for bilayers at different temperatures in Figure 3.3 and the percentage *trans* in Figure 3.4 show temperature dependence along the tails. The *trans* percentages can be compared to values measured for liquid *n*-alkanes for which about  $\frac{2}{3}$  of the corresponding torsion angles would be in the *trans* conformation at room temperature [93]. Within the membrane only the tail torsion angle might have the freedom to rotate as in a liquid. We note for acidic pH (bil-pK<sub>1</sub>-298) this freedom is not given in the bilayer; at room temperature we find 7 out of 9 torsion angles to be over 90% in the *trans* conformation. At high pH and room temperature the structure (bil-bas-298) is less rigid than at low pH. Higher temperature simulations show a decreasing amount of *trans* conformations at acid pH (bil-pK<sub>1</sub>-348, bil-pK<sub>1</sub>-398), the membrane obviously melts and dissolves as seen in Figure 3.3. At basic pH, there is instead only little liquefaction.

Micellar aggregates of 90 or 64 lipids at high pH conditions (mic-bas-298 and mic-64-bas-298) show less torsion angles in *trans* conformation than bilayer membranes. The trend for tail torsion angles to adopt more *gauche* conformations is observed both in the micelles and in the bilayers. The smaller micellar aggregate shows less *trans* conformations. The experimentally non-existent micelles (mic-pK<sub>1</sub>-298, mic-pK<sub>2</sub>-298) behave very differently. At pK<sub>2</sub> two distinct torsion angles seem to adopt the *gauche* conformation more strongly than the *trans*: A kind of screwed lipid structure with two *gauche* conformations is favored. In the micellar aggregates at pK<sub>1</sub> the distribution of *trans* versus *gauche* conformations along the chain starting from the tail end is remarkable: both the pK<sub>1</sub>-micelles with 90 lipids and different tail-lengths (mic-C8-pK<sub>1</sub>-298 and mic-pK<sub>1</sub>-298), show the same trend for different torsion angles in sequence along the tails.

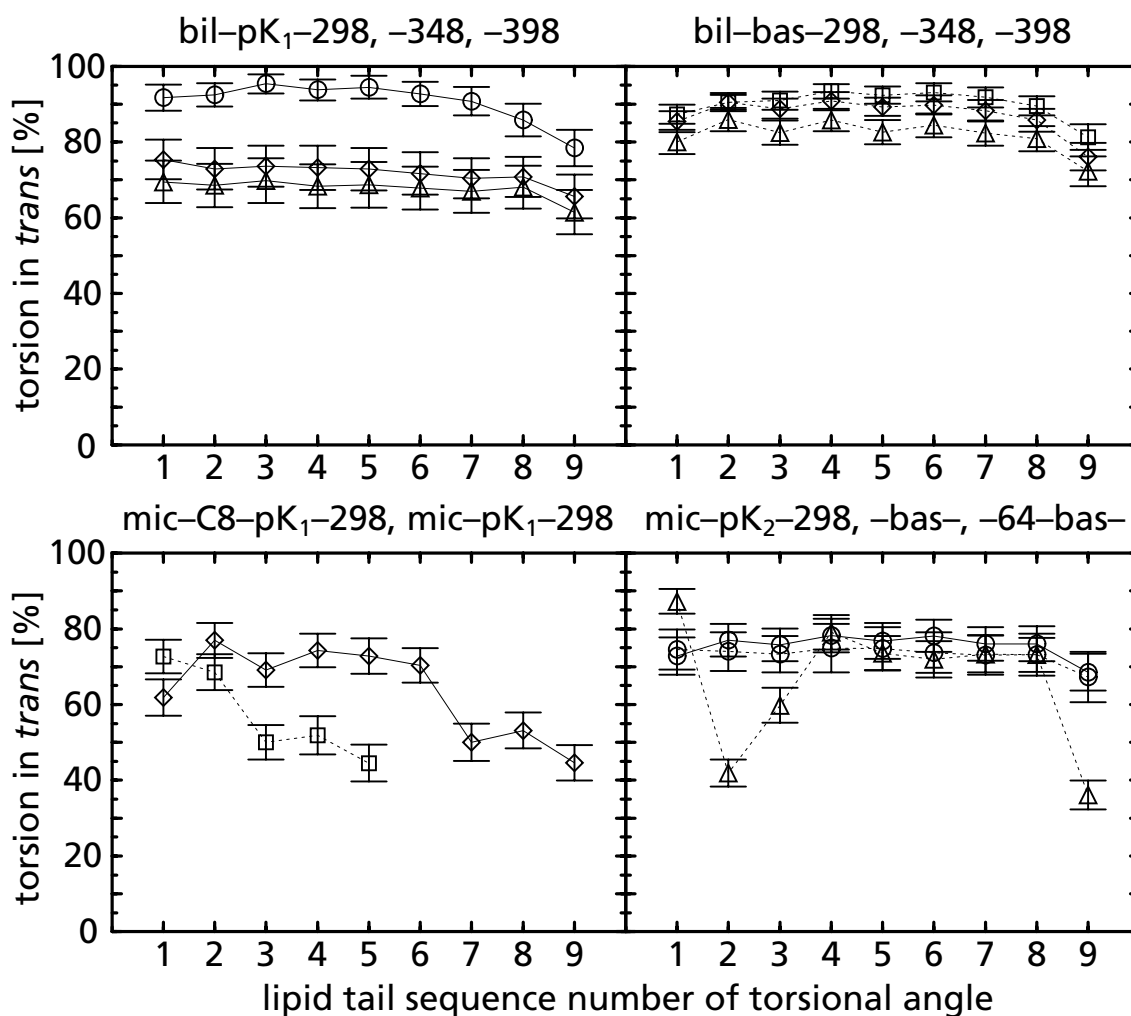


**Figure 3.4** Percentage of torsion angles in the *trans* conformation as a function of their positions in the lipid chains.

Upper left: pK<sub>1</sub>-bilayer, 3 temperatures, bil-298 (○), bil-348 (◇), bil-398 (△)

Upper right: pH>11-bilayer, 3 temperatures, bas-298 (○), bas-348 (◇), bas-398 (△)

Lower left: pK<sub>1</sub>-micelles at 298 K, mic-C8-pK<sub>1</sub>-298 (□, dotted line), mic-pK<sub>1</sub>-298 (◇)

Lower right: pK<sub>2</sub>- and pH>11-micelles at 298 K, mic-pK<sub>2</sub>-298 (△),

mic-bas-298 (○, solid line), mic-64-bas-298 (○, dotted line)

NMR  $-S_{CD}$  order parameter

NMR-measurements of  $-S_{CD}$  order parameters provide a measure of the lipid tail ordering in bilayer membranes that are immobilised like in a planar Langmuir-Blodgett film (e.g. MacRitchie [100]). Deuterated hydrocarbons are synthesized for tail groups that are pure with respect to the unique deuterium (D) position along the tail. If the directions of the CD-bonds, like they would occur in a frozen crystal, are parallel, the order parameter value  $-S_{CD}$  is one. If the distribution of directions is homogeneous,  $-S_{CD}$  drops to zero. The order parameter  $-S_{CD}$  in our simulations was calculated from the ensemble average of (Eq. 3.2) over time for the bilayers.

In Figure 3.5, a comparison of bilayers at acidic  $pK_1$  and basic pH shows that in the basic case only slightly more order is seen at room temperature. A temperature increase melts the acidic bilayer but not the basic one, which may be trapped in a metastable state. Since NMR order parameter measurements of *n*-dodecylphosphate are not available, a comparison with experimental data for a *n*-dodecyl-double-tail lipid, dilaurylphosphatidylcholine, obtained at room temperature from  $L_\alpha$ -phase powder spectra [101] is given in Figure 3.5. It seems that the atoms near the end of the lipid tail in a double-tail lipid have more motional freedom than those of a single-tail lipid of the same length. Experiments for small deuterated *n*-alkyl chains that have been inserted or belong to lipid aggregates [102-104] show a range of 0.18 to 0.24 for the NMR  $-S_{CD}$  order parameter at position 1 next to the head group. A similar value of 0.20 is found in our simulation of a *n*-dodecylphosphate bilayer.

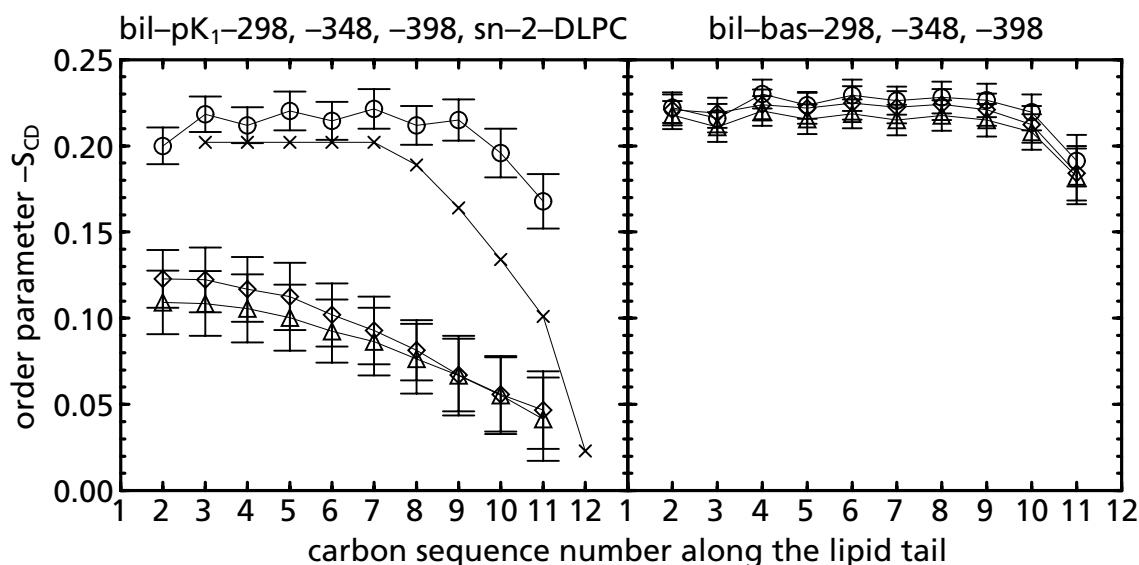


**Figure 3.5** NMR  $-S_{CD}$  order parameter versus carbon numbers along the lipid chains. The  $-S_{CD}$  NMR order parameters are displayed for all simulated bilayer systems of *n*-dodecylphosphate. Both panels show the structures simulated at three different temperatures 298 K (○), 348 K (◇) or 398 K (△), at  $pK_1 \approx 2$  on the left (experimental condition for vesicles of *n*-dodecylphosphoric acid and *n*-dodecylphosphate), at basic pH on the right (experimental condition for micelles of *n*-dodecylphosphate). The experimental values for the deuterated sn2-chain of dilaurylphosphatidylcholine [101] are shown for comparison (×).

### Distribution of atom types: cross section for bilayers

The average distribution of particles (here distinguished by atom types) within the simulated system shows how close the different atoms come to each other. Figure 3.6 contains the atom distributions along the z-axis of the system (orthogonal to the bilayer plane) through the membrane, and shows all atom types present in the simulated system. Upon increasing the temperature of the acidic bilayer membrane (bil- $pK_1$ -298, -348, -398) the peaks representing head group atoms (OM, OA, P) move closer to each other, indicating that the membrane is getting thinner. In addition, the intermingling of tails increases, because the distribution histograms of the  $CH_2$ -groups of the two layers which meet each other in the inner section of the bilayer, start merging. No water atom types (OW, H) appear within the membrane, the water density is flat outside the bilayer and drops where head-group atoms appear. Statistically water exchange through such a small system of 64 lipids in cross-section is only a rare event. The simulation at high temperature, bil- $pK_1$ -398, shows that few lipids are able to diffuse into the water within a simulation time of nanoseconds (Figure 3.3). In a test simulation a water molecule at 398 K, was only once observed crossing the *n*-dodecylphosphate lipid bilayer. For longer simulations and larger systems such events may also be observed at lower temperature.

The basic bilayer (bil-bas-298, -348, -398) shows a gap between the two layers, the  $CH_3$ -atom density is reduced (Figure 3.6). The  $CH_2$ -group distribution is more flat than at acidic pH and much closer contacts of ions ( $Na^+$  atom type) to the head-group atoms (P, OM, OA atom types) are found. No water is found within the membrane. No significant change with temperature occurs in the distributions.

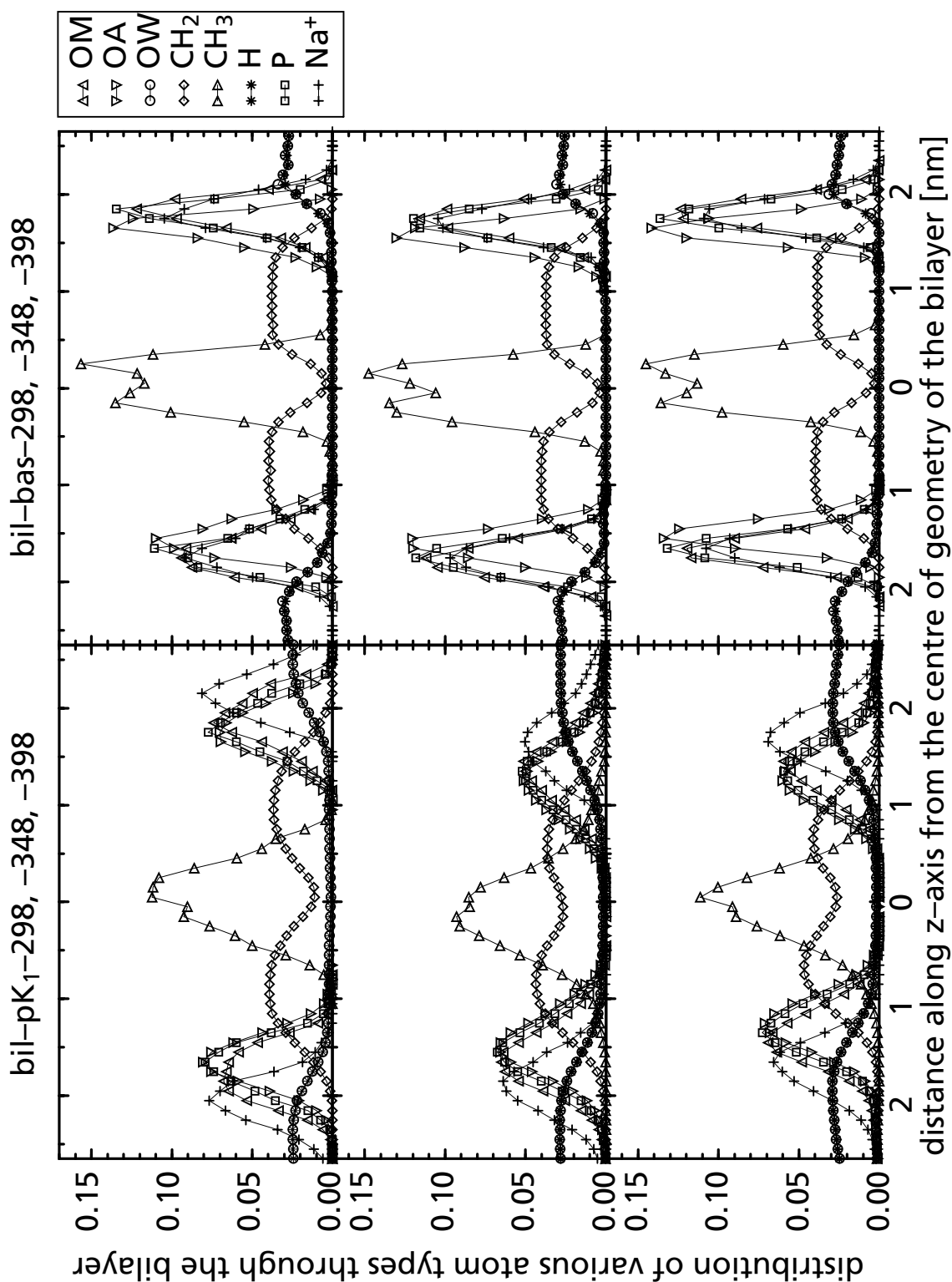


**Figure 3.6** Distribution of atom types across bilayer membranes.

The average distribution of different GROMOS96 atom types is compared (OM: double-bonded oxygen; OA: hydroxyl or ester oxygen; OW: water oxygen). The distributions have been normalised.

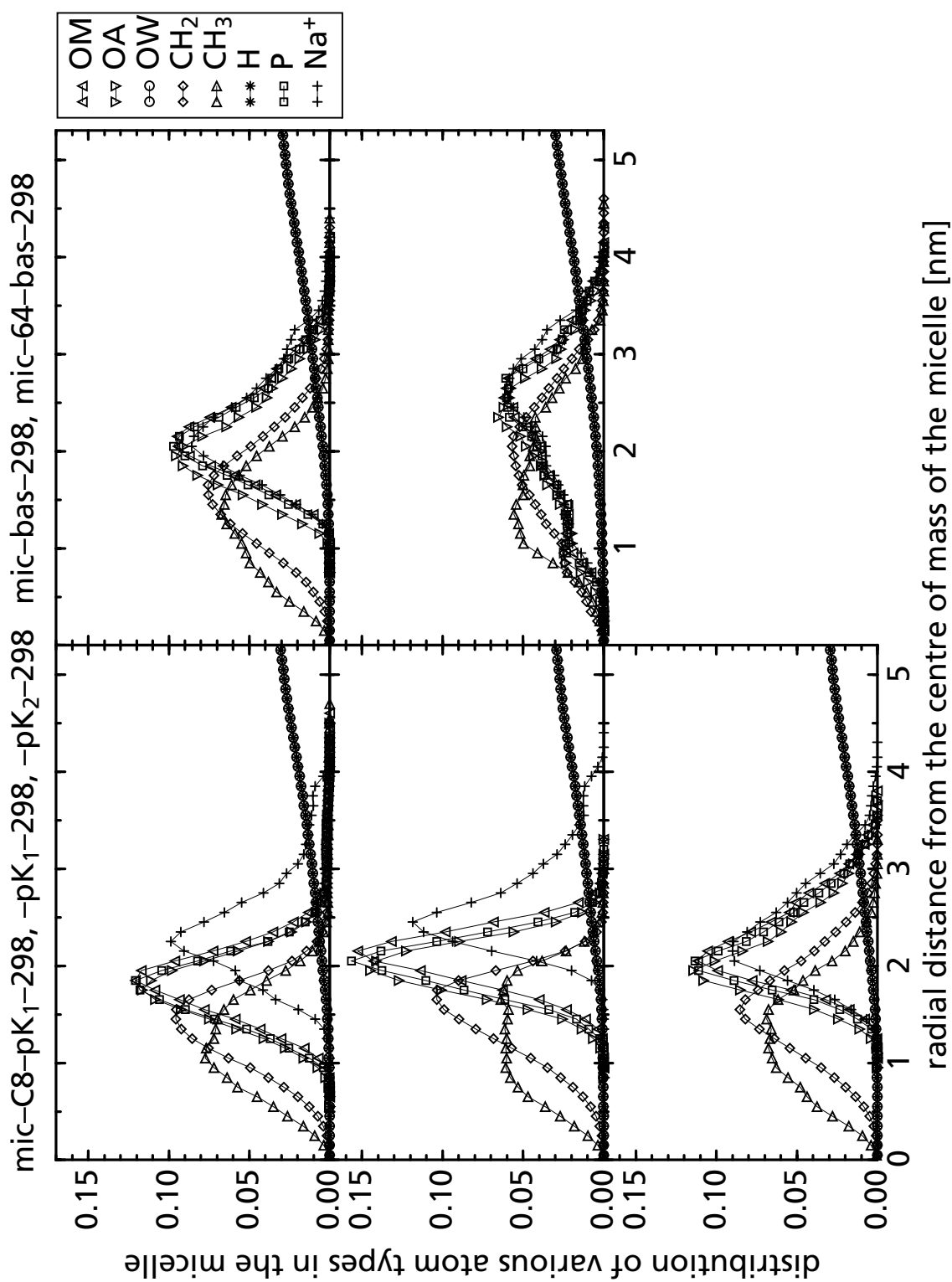


**Figure 3.7** Radial distribution of atom types from the centre of the micelles. The average distribution of different GROMOS96 atom types is compared (see caption of Figure 3.6).

### Distribution of atom types: radial distribution for micelles

Micelles very often adopt a spherical (spherical micelles) or cylindrical (rod-like micelles) geometry. Radial distributions for the different atom types are shown in Figure 3.7. The micelles simulated at acidic pH ( $pK_1$ ) differ mainly in size, the head-group peaks of P, OM, and OA atom types for mic-C8- $pK_1$ -298 appear at a lower distance than for mic- $pK_1$ -298. The spread of the lipids through the computational box is wider in the former: for mic-C8- $pK_1$ -298 a  $CH_3$  united atom is present at a maximum distance of 4.5 nm from the centre of the micelle, whereas for mic- $pK_1$ -298 this value is 3.3 nm. Both micellar structures at high pH (mic-bas-298, mic-64-bas-298) which only differ in the number of lipids and counterions, show different distributions. For 64 lipids there is a considerable overlap between ions ( $Na^+$ ) and head group atoms (P, OM, OA) and tail atoms ( $CH_2$ ,  $CH_3$ ). The sharper distributions for the large aggregates of 90 lipids at high pH (mic-bas-298) is much more comparable with the lipid aggregate of 90 lipids at neutral  $pH=pK_2=7$  (mic- $pK_2$ -298). Common to all micellar distributions is the appearance of tail end atom types ( $CH_3$ ) up to close to the head group (P, OM, OA) atom types, illustrating that lipids in micelles are able to expose their tails to the micellar surface. In three micellar systems (mic-C8- $pK_1$ -298, mic-bas-298, mic-64-bas-298) we found lipid tail traces up to 4.5 nm. Experiments that provide the aggregation numbers for *n*-octyl-phosphate ( $43 \pm 5$  lipids, [94]) and *n*-dodecylphosphate (90 lipids, [76]) leave room for variation in the number of lipids in an aggregate. The number of lipids in the aggregate also varies in the simulation. Single lipids diffuse into the solvent and back into the micelle (mic-64-bas-298 and mic-bas-298) and the shorter tail lipid aggregate (mic-C8- $pK_1$ -298) loses several aggregate members.

### Diffusion coefficients

From the atom mean-square displacement, the diffusion coefficients for lipids (P atoms) and counterions ( $Na^+$  atoms) were estimated (Figure 3.8). The results are displayed in Table 3.4. Sodium counterions move faster than the lipids (phosphorus head-group atoms). For lipid diffusion we estimate  $2 \times 10^{-6} \text{ cm}^2 \text{ s}^{-1}$  for bilayer membranes of *n*-dodecylphosphoric acid and -phosphate (bil- $pK_1$ -298), a value that increases with temperature. Not unexpected, both counterion and lipid diffusion decreases with decreasing acidity. Sodium ions are – according to Figure 3.7 – less surface bound at acidic micelles and this may ex-



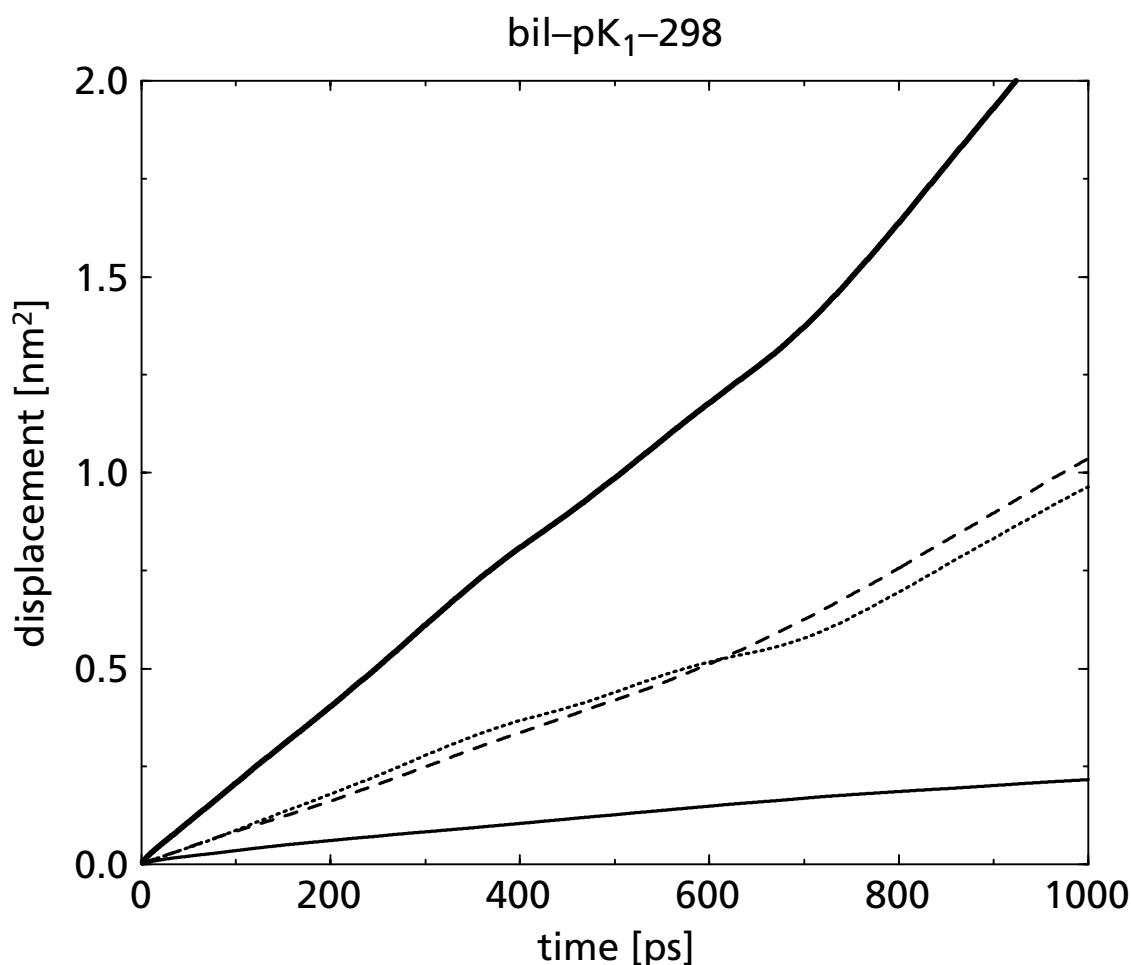


**Figure 3.8** Example of data calculated to estimate the diffusion coefficient. Measurements have been taken over 3 ns from a trajectory of the *n*-dodecylphosphate bilayer at  $pK_1$  and at 298 K which has been elongated from 3 to 6 ns. Of these only the first nanosecond for the sodium counterions is shown. The lower thin line corresponds to the mean-square displacement orthogonal to the lipid bilayer membrane plane ( $z$  direction), whereas the parallel dashed and dotted lines represent the displacement in the orthogonal  $x$  and  $y$  directions lateral in the bilayer membrane plane. The thick black line represents the 3-dimensional displacement. Its slope leads to a value of  $D = 3.3 \times 10^{-6} \text{ cm}^2 \text{ s}^{-1}$  (see Table 3.5, for bil- $pK_1$ -298).

plain the faster diffusion in comparison with the basic micelles or the acidic bilayer. Within the lipid bilayer at room temperature lipids laterally diffuse faster than within micelles. In micellar aggregates at high pH (mic-bas-298) a factor of two difference between large (90) and small (64) aggregation numbers with  $1 \times 10^{-6} \text{ cm}^2 \text{ s}^{-1}$  and  $2 \times 10^{-6} \text{ cm}^2 \text{ s}^{-1}$  was found. The essential contribution to lipid diffusion in micelles might be the micelle rotation and diffusion and not the

movement of the strongly interacting lipids themselves, since lipid diffusion of the larger micelle mic-bas-298 is slower than for the smaller micelle mic-64-bas-298. In general, experimentally determined diffusion coefficients for lipids in membranes are in the range of  $10^{-8}$  to  $10^{-6}$   $\text{cm}^2\text{s}^{-1}$  (e.g. [92]).

**Table 3.4** Diffusion coefficients  $10^{-6} \times [\text{cm}^2\text{s}^{-1}]$  from mean square displacement of atoms. The diffusion of phosphorus atoms is taken for the lipid diffusion within (lateral) or out of the membrane (bulk diffusion).

<i>bilayer simulations</i>	<i>bil-pK<sub>1</sub>-298</i>	<i>bil-pK<sub>1</sub>-348</i>	<i>bil-pK<sub>1</sub>-398</i>	<i>bil-bas-298</i>	<i>bil-bas-348</i>	<i>bil-bas-398</i>
Na <sup>+</sup> -ions	3.3	9.0	14.2	1.6	3.0	4.6
P bulk	2.1	3.6	5.3	1.1	2.0	2.8
P lateral	2.6	4.6	6.9	1.1	1.5	3.9
<i>micelle simulations</i>	<i>mic-C8-pK<sub>1</sub>-298</i>	<i>mic-pK<sub>1</sub>-298</i>	<i>mic-pK<sub>2</sub>-298</i>	<i>mic-bas-298</i>	<i>mic-64-bas-298</i>	
Na <sup>+</sup> -ions	8.7	7.7	4.3	2.1	4.2	
P bulk	1.9	1.2	2.5	1.0	2.2	

### Torsion angle dynamics

The internal dynamics of the lipid chains can be analysed in terms of torsion angle transitions between potential energy minima. The three potential energy wells of the  $\square\text{-CH}_2\text{-CH}_2\text{-}\square$  torsion angle potential energy term in the force field are used to define the transitions. The transitions for every torsion angle along the lipid chains were counted and averaged over the number of molecules.

With increasing temperature the frequency of transitions increases for both bilayer systems, bil-pK<sub>1</sub>-298, -348, -398 and bil-bas-298, -348, -398. The increase is, however, more pronounced for the acidic bilayer system. In the case of the different micelles, at high pH (mic-bas-298, mic-64-bas-298) or at neutral pH (mic-pK<sub>2</sub>-298), there is no difference in frequency of torsion angle transitions. The acidic micellar systems (mic-pK<sub>1</sub>-298 and mic-C8-pK<sub>1</sub>-298) show barely faster transitions.

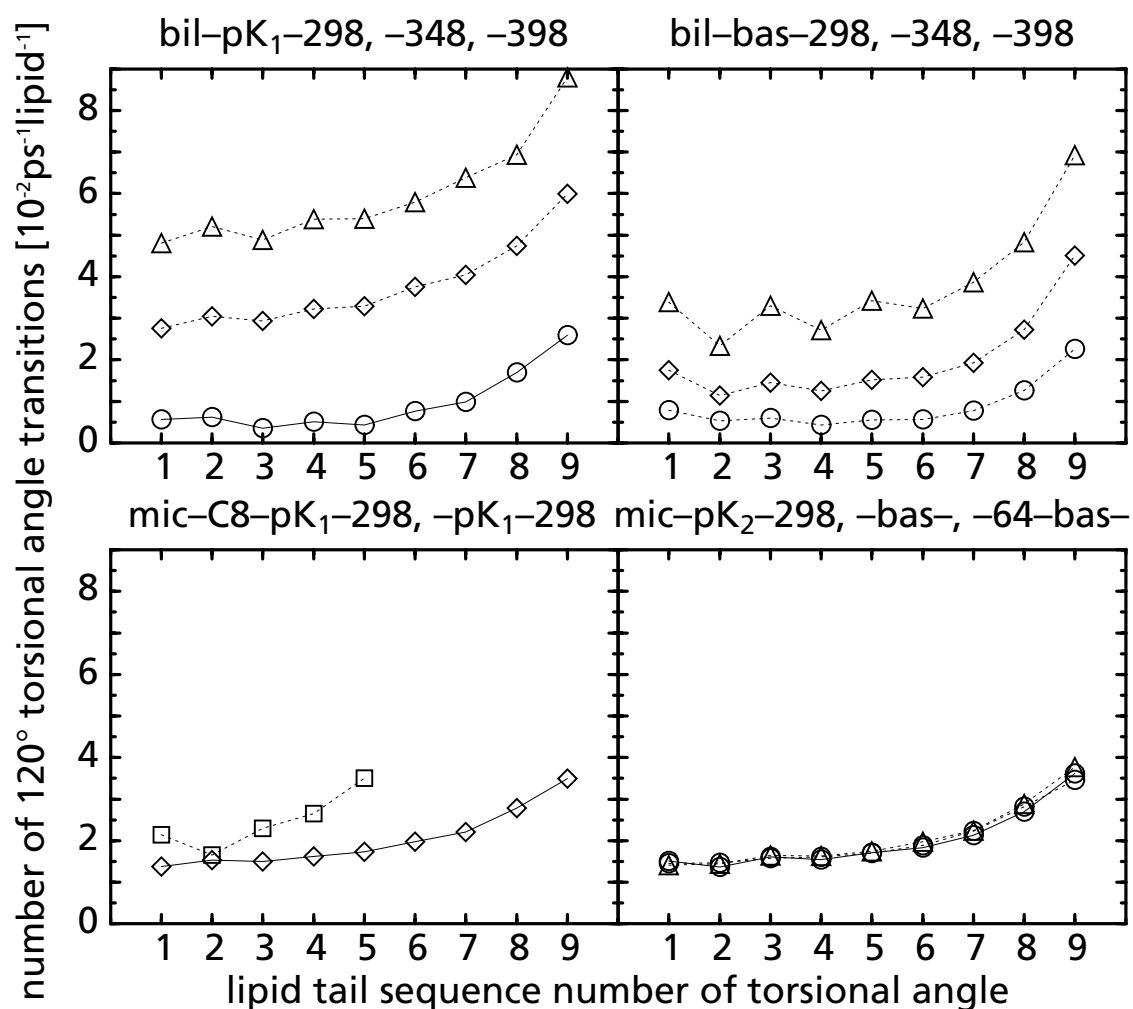


**Figure 3.9** Number of transitions between the three wells of the torsion angle per 100 ps as function of torsion angle sequence number along the lipid chains.

Upper left: pK<sub>1</sub>-bilayer, 3 temperatures, bil-pK<sub>1</sub>-298 (○), bil-pK<sub>1</sub>-348 (◇), bil-pK<sub>1</sub>-398 (△)

Upper right: pH>11-bilayer, 3 temperatures, bil-bas-298 (○), bil-bas-348 (◇), bil-bas-398 (△)

Lower left: pK<sub>1</sub>-micelles at 298 K, mic-C8-pK<sub>1</sub>-298 (□), mic-pK<sub>1</sub>-298 (◇)

Lower right: pK<sub>2</sub>- and pH>11-micelles at 298 K, mic-pK<sub>2</sub>-298 (△), mic-bas-298 with 90 lipids (○, solid line), mic-64-bas-298 with 64 lipids (○, dotted line)

## 3.5 Conclusions

The membrane and micellar aggregates of *n*-dodecylphosphoric acid and *n*-dodecylphosphate as set at the beginning of the simulations do not lose their integrity over a simulation time of 3 to 8 ns. Indeed, the head group area that was roughly estimated to be 0.21 nm<sup>2</sup> for *n*-dodecylphosphate bilayers (Eq. 3.1) was calculated to be 0.20 nm<sup>2</sup> in the simulation. A micelle of aggregation number 90 (mic-90-bas-298) seems to be more stable than a smaller one of aggregation number 64 (mic-64-bas-298), since the latter shows more diffusive character and tends to lose lipids more easily. This is in agreement with experiment.

The experimentally determined phase transition temperature  $T_m$  is about 276 K for the bilayer membrane system [14], which our simulation contradicts. At  $pK_1=2$  and room temperature (298 K) the bilayer membrane looks as in a so-called “gel phase” below the phase transition temperature (Figure 3.3) but melts when heated up. The liquefaction of the micelle is observed through more transitions of torsion angles when the pH is lowered to  $pK_2$  or  $pK_1$ . We assume this liquefaction to be indicative for a structural transition on the longer time scale. On the other hand a bilayer structure of *n*-dodecylphosphate that is simulated at high pH shows a ripple phase structure at room temperature (Figure 3.3), but does not lose its integrity after transition towards a liquid crystalline phase when the temperature is raised. We see partial dissolution of a 90-member micellar aggregate of shorter lipids of *n*-octylphosphate. All these observations from molecular dynamics simulations show that the force field set 43A2 strikes the balance between experimentally and energetically favoured and unfavoured structures in most cases.

The bilayer structure at low pH shows the profile of *trans* torsion angles along lipid tails one could expect for a stable bilayer system and melts upon heating. A similar proportion of *trans* torsion angles along lipid tails we find for the high pH micelles, but not for other micelles. In agreement with experiments it is concluded that high pH energetically favours micelles of *n*-dodecylphosphates over bilayer membranes.

The simulations allow for predictions that cannot be verified, since measurements are not available:

- We would expect the NMR  $-S_{CD}$  order parameter of  $n$ -dodecylphosphate bilayers at the plateau region to be close to  $0.215 \pm 0.01$ . For the tail methyl-group at the end of the lipid chain the value would decrease to below 0.10.

- Lipid-lipid hydrogen bonds seem to stabilise the bilayer, and their lifetimes cover a broad range with an average value of 9 ps.

- If water molecules are hydrogen bonded to  $n$ -dodecylphosphate bilayers they are bound longer than at micellar surfaces, for about 13 ps compared to 5 ps on average, whereas water-water hydrogen bonds do live much shorter: 1.5 ps.

- We expect sodium counterion diffusion to be around  $D = 3 \times 10^{-6} \text{ cm}^2 \text{ s}^{-1}$ , lipid diffusion within bilayers or micelles around  $2 \times 10^{-6} \text{ cm}^2 \text{ s}^{-1}$ . Lipids may diffuse faster within bilayers than in micelles, since their torsional dihedral conformations in micelles display a chain entanglement that might hinder a faster diffusion process. For the experimental lipid aggregate number in micelles the lipids appear half as diffusive as for bilayers, but not for the smaller micelle aggregate, where diffusion was equally fast.

## 3.6 Acknowledgement

We would like to thank Prof. Dr. P. Luigi Luisi, who initiated this work, for his scientific and financial support.



# Chapter 4

---

## **An Improved GROMOS96 Force Field for Aliphatic Hydrocarbons in the Condensed Phase**

# 4. An Improved GROMOS96 Force Field for Aliphatic Hydrocarbons in the Condensed Phase

## 4.1 Abstract

Over the past four years the GROMOS96 force field has been successfully used in biomolecular simulations, e.g. in peptide folding studies and detailed protein investigations, but no applications to lipid systems have been published yet. Here we provide a detailed investigation of aliphatic liquid systems. For liquids of larger aliphatic chains, *n*-heptane and longer, the standard GROMOS96 parameter sets 43A1 and 43A2 yield a too low pressure at the experimental density. Therefore, a reparametrisation of the GROMOS96 force field regarding aliphatic carbons was initiated. The new force field parameter set 45A3 shows considerable improvements for *n*-alkanes, cyclo-, iso- and neoalkanes and other branched aliphatics. Liquid densities and heat of vaporisation are reproduced for almost all of these molecules. Excellent agreement is found with experiment for the free energy of hydration for alkanes. The GROMOS96 45A3 parameter set should therefore be suitable for application to lipid aggregates such as membranes and micelles, for mixed systems of aliphatics with or without water, for polymers and other apolar systems that may interact with different biomolecules.

## 4.2 Introduction

In classical molecular dynamics (MD) simulations the mechanical laws of physics are applied to propagate simulated particles such as atoms and molecules through space and time. Since a fully quantum-mechanical description of the interaction of larger molecules is not feasible, classical MD simulation uses a simpler level of abstraction based on chemical knowledge. Atoms are described as spherically symmetric particles, connected into molecules through covalent bonds and interacting with their non-covalently bound neighbours throu-



gh van der Waals interactions and, if the interacting particles are charged, through Coulomb type interactions. The potential energy function that describes the interaction between the particles or atoms is called a force field [80]. Although most biomolecular force fields are based on a similar functional form of the interaction function, they show considerable differences in their parametrisation and parameter values [16,22-33,35-37,93]. The GROMOS force field has been developed over many years [16,30,31,35-37,93] and, as with all other force fields [22-29,32,33], the empirical force-field parameters can only be as satisfactory as comparisons of simulated properties against experimental data demonstrate [105]. Here we exemplify that an established force field successfully used over the years in biomolecular simulations of a variety of molecules, such as peptides [106-109], proteins [110-115], sugars [116-118] and nucleotides [119,120] is not necessarily producing satisfactory results for another class of large molecules, simple aliphatic chains. Although a small set of alkanes representative of the types of aliphatic groups present in proteins (with chain length smaller than 7) has been successfully parametrised [35,93], the same force field yields a too high density (at 1 atm pressure) or negative pressure (at constant experimental density) when applied to longer alkanes (up to chain length 20). Therefore, a detailed MD investigation of *n*-alkanes and other aliphatic molecules was undertaken and is presented here together with a new set of GROMOS96 force field parameters called 45A3 that is suitable to systems with aliphatic chains of various lengths, such as alkanes, lipids and polymers. The most important experimental properties of a liquid to be reproduced in a simulation are the density (volume or pressure), the heat of vaporisation and the free energy of hydration, as a proper description of mixtures with water is essential for most biomolecular systems. These quantities should be in good agreement with experimental data at room temperature, the temperature of most of the applications of the force field. To achieve this goal one must know the influence of the different force field parameters on the quantities studied. Therefore, the dependence of these quantities upon different force-field parameters, such as van der Waals or Lennard-Jones  $C_{12}$  and  $C_6$  coefficients, non-bonded interaction cut-off length and charge-group size is investigated first. The next step is to choose a calibration set of molecules for which the force-field parameters are tuned such that in MD simulations of the condensed phase the experimental density and heat of vaporisation are reproduced. Previously, a set of 9 linear, branched and cyclic alkanes of short chain length (up to 6  $\text{CH}_n$  units) was used to this end [35]. This set was chosen with an eye to the occurrence of aliphatic fragments in proteins, sugars and nucleotides. Howe-

ver, much larger aliphatic chains are present in lipids and membranes. Therefore, the current reparametrisation of the aliphatic  $\text{CH}_n$  atom groups (including  $n=0$ ) of the GROMOS96 force field is based on a much larger set of alkanes. For  $n$ -alkanes, chain lengths up to 20 (eicosane), were considered.

In the reparametrisation of the GROMOS96 force field three sets of molecules were distinguished in regard to their properties in the condensed phase as obtained by MD simulation with the GROMOS96 force field:  $n$ -alkanes, cyclo-alkanes and branched alkanes such as iso- or neoalkanes. Most common in biomolecular simulations, e.g. of lipid membranes, will be chains consisting of  $\text{CH}_2$  and  $\text{CH}_3$  atom groups or united atoms. Consistently, in a first parametrisation step, the calibration set was composed of  $n$ -alkanes only. Compared to our previous work [35] the set of  $n$ -alkanes was expanded beyond hexane ( $\text{C}_6$ ) to eicosane ( $\text{C}_{20}$ ).

## 4.3 Methods

For the parametrisation of aliphatics, many simulations had to be carried out. Three types of species were considered:  $n$ -alkanes, cyclo-alkanes and branched alkanes (see Tables 4.2–4.4). First, liquid systems consisting of 512 individual molecules of the investigated species in a cubic box were built and equilibrated. For all systems the total number of molecules was the same which made the computational effort rather different for different molecules depending on their number of atoms and interactions. The molecular topologies were constructed using the GROMOS96 conventions and standard parameter values, see Table 4.1 [16,93].

In all simulations the GROMOS96 software [16,63] was used. A twin-range cut-off scheme with 0.8 nm and 1.4 nm cut-off radii was applied. The non-bonded interactions in the range between these radii were updated every 5th time step. The time step was 2 fs and the temperature was kept at 298.15 K using a Berendsen thermostat [21] with a coupling time of 0.1 ps. All bonds were kept constant with the SHAKE algorithm [18] using a relative geometrical tolerance of  $10^{-4}$  in the condensed phase simulations and  $10^{-8}$  in the vacuo simulations. For calculating the heat of vaporisation, two simulations had to be carried out, as described earlier [35,93]. The constant volume simulations of the lipids at the experimental density were equilibrated for at least 500 ps, when necessary up to 2 ns, until the average pressure converged. The atomic coordinates and velocities of the final system configuration were used to gene-

Table 4.1 Force field parameters for aliphatic molecules. The parameters and conventions are defined in [16]. The GROMOS96 integer atom code (IAC) describes the van der Waals parameters of the corresponding atoms. \*The value  $K_\varphi=5.92 \text{ kJmol}^{-1}$  in torsional dihedral type 17 used here is the one from parameter set 43A2 [93], which is slightly larger than the value  $5.86 \text{ kJmol}^{-1}$  of set 43A1.

<i>atom</i>	<i>description</i>	<i>IAC</i>	<i>mass</i> [a.m.u.]	
CH1	aliphatic CH <sub>1</sub> group	12	13.019	
CH2	aliphatic CH <sub>2</sub> group	13	14.029	
CH3	aliphatic CH <sub>3</sub> group	14	15.035	
CH4	methane, CH <sub>4</sub> group	15	16.043	
<i>bond</i>	<i>type code</i>	<i>b<sub>0</sub> [nm]</i>	<i>K<sub>b</sub> [kJmol<sup>-1</sup>nm<sup>-4</sup>]</i>	
CH <sub>n</sub> —CH <sub>n</sub>	26	0.153	$7.15 \times 10^6$	
<i>bond angle</i>	<i>type code</i>	<i>θ<sub>0</sub> [degree]</i>	<i>K<sub>θ</sub> [kJmol<sup>-1</sup>]</i>	
CH <sub>n</sub> —CH <sub>1</sub> —CH <sub>n</sub>	12	109.5	520	
CH <sub>n</sub> —CH <sub>2</sub> —CH <sub>n</sub>	14	111.0	530	
<i>improper dihedral</i>	<i>type code</i>	<i>ξ<sub>0</sub> [degree]</i>	<i>K<sub>ξ</sub> [kJmol<sup>-1</sup>degree<sup>2</sup>]</i>	
around CH <sub>1</sub> group	2	35.26439	0.102	
<i>torsional dihedral</i>	<i>type</i>	<i>cos(δ)</i>	<i>m<sub>n</sub></i>	<i>K<sub>φ</sub> [kJmol<sup>-1</sup>]</i>
CH <sub>n</sub> —CH <sub>n</sub> —CH <sub>n</sub> —CH <sub>n</sub>	17	+1.0	3	5.92*

rate initial positions and velocities for the gas phase simulations. Each individual molecule was translated to a grid point 50 nm apart from the other molecules. This new starting configuration representing a sample in vacuo at room temperature with no intermolecular interactions (long-range cut-off = 1.4 nm) allows for faster averaging (100 ps) of the gas phase potential energy over the 512 molecules, instead of simulating one molecule over a 512 times longer time period. The difference between the potential energies in the gas phase and the liquid phase is assumed to be directly related to the heat of vaporisation (apart from a term RT) since the vacuo system is considered to be an ideal gas. A calculation of the virial of the equilibrated liquid provides the pressure of the system. With the large number of different molecules investigated an automated procedure [121-123] for parametrisation of the coefficients against the two key properties, heat of vaporisation and pressure, was not feasible. Instead, every new parameter set was individually considered and modified, slowly progressing to a desirable degree of consistency. To test the parameters found with this procedure, simulations at constant pressure [21] were additionally carried out to compare the average density against experimental values. The reference pressure was set to the experimental pressure, the pressure coupling time was set to

0.5 ps, and a value for the compressibility  $\kappa_T$  was used as determined from separate constant volume simulations as follows. For each molecule, two constant volume simulations of the liquid were carried out at volumes smaller ( $V_1$ ) and larger ( $V_2$ ) than the experimental volume  $V$ . These provide the difference in pressures ( $p_1$  and  $p_2$ ) observed upon the change of volume, which yields the isothermal compressibility  $\kappa_T$  through equation 4.1.

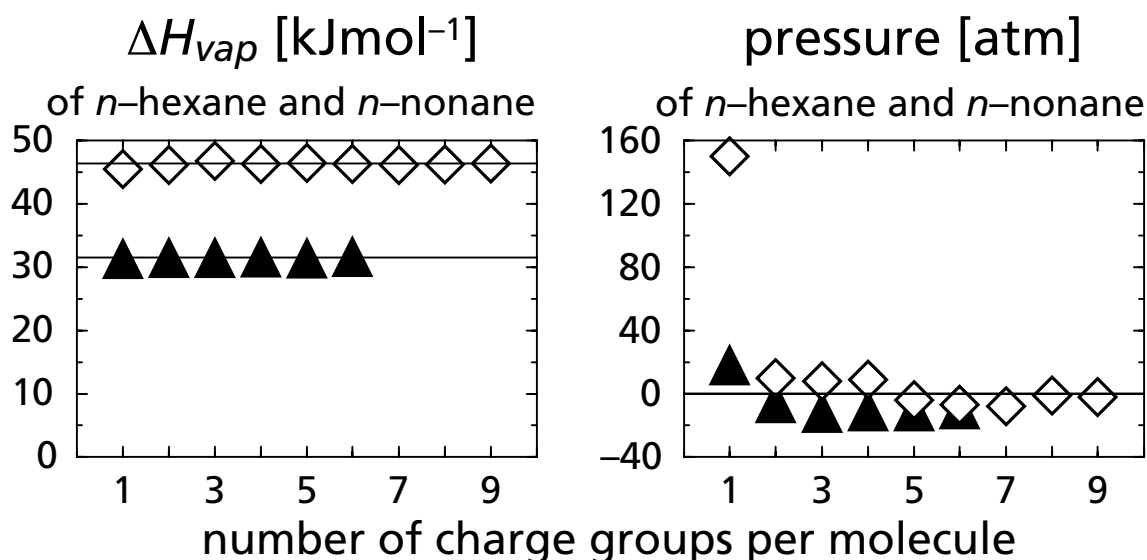
$$\kappa_T = \frac{V_1 - V_2}{V(p_2 - p_1)} \quad \text{Eq. 4.1}$$

Correct reproduction of the free energies of solvation of molecules or their aggregates in water is crucial for any accurate model description of biomolecular systems. The calculation of the free energy of hydration of molecules by MD simulation is straightforward, e.g. by using the thermodynamic integration method [124,125]. A solute molecule that is interacting with the solvent molecules is in state A. When its non-bonded interactions with the solvent molecules are switched off, it is in state B. A thermodynamic coupling parameter  $\lambda$  is used to smoothly change state A ( $\lambda=0$ ) into state B ( $\lambda=1$ ); and/or vice versa. Individual MD simulations are carried out at a number of  $\lambda$  values in the range [0,1] and the average of the derivative of the Hamiltonian with respect to  $\lambda$ ,  $\langle \partial H / \partial \lambda \rangle_\lambda$  is calculated for each  $\lambda$  value. The free energy of hydration is then obtained by numerically integrating these averages from  $\lambda=1$  to  $\lambda=0$  [126].

The solute-water systems for the thermodynamic integration calculations were set up as follows. A single aliphatic molecule was introduced into a truncated octahedron box with water (minimum solute to solvent distance of 0.23 nm) such that the solute to wall distance was at least 1.6 nm, or 1.75 nm if the solute molecule conformation had several kinks. This rather large solute to box wall distance will allow the solute to expand without interacting with its own periodic image, when periodic boundary conditions are applied. The number of water molecules in the box was always over a thousand. The simple point charge (SPC) water model was used [20]. The solute-water configuration was energy minimised under periodic boundary conditions using the steepest descent method. Subsequently, the system was equilibrated for 200 ps of MD at room temperature. A reaction-field contribution originating from interactions beyond the long-range (1.4 nm) cut-off distance was added to the forces [127]. A value of 66.6 was used for the dielectric permittivity  $\epsilon_{\text{RF}}$  of the continuum outside the cut-off sphere, as recently estimated for the SPC model

[128]. After equilibration, a 1 ns slow growth simulation [125] was performed as a means to obtain starting configurations and velocities for the simulations at fixed  $\lambda$  values for thermodynamic integration. Initial thermodynamic-integration free-energy values were obtained by numerical integration of  $\langle \partial H / \partial \lambda \rangle_\lambda$  using 21 equally spaced  $\lambda$  values between 0 and 1 (inclusive). Where the curvature of the integrand was large, additional  $\lambda$  values were used. The simulation time was chosen in accordance to the rate of convergence of  $\langle \partial H / \partial \lambda \rangle_\lambda$ . Typically, 25  $\lambda$  values were used with equilibration periods of 50 ps and averaging periods of 150 ps, in some cases extended to 350 or even 950 ps. A soft-core  $\lambda$ -dependent interaction function was used to evaluate the solute-solvent van der Waals interactions in the slow growth and thermodynamic integration simulations, with a parameter  $\alpha_{LJ}$  of 0.5 [35,63]. Plots of the convergence of the free energy values as function of the number of  $\lambda$  points and the extent of sampling (not shown) suggest that the uncertainty in the numbers shown in Table 4.5 (column 45A3) is in all cases below 0.5 kJ/mol.

## 4.4 Results and Discussion



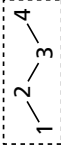
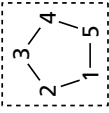
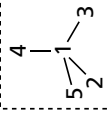
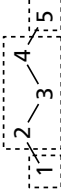
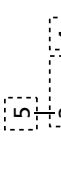
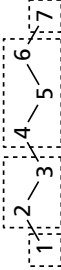
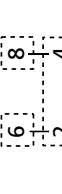


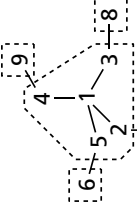
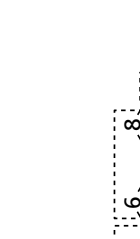


**Figure 4.1** Heat of vaporisation and pressure as function of the number of charge groups used. Simulated heat of vaporisation and pressure in equilibrated liquid simulations (1 ns of 512 molecules) at constant volume and temperature for *n*-hexane (▲) and *n*-nonane (◇) as function of the number of charge groups defined for each molecule. The solid horizontal lines represent the experimental values.

The GROMOS force field makes use of the concept of charge groups. The atoms that belong to a charge group are chosen such that their partial atomic charges add up to zero (or to a multiple of  $\pm e$ ). In the GROMOS non-bonded interaction subroutines the atom-atom non-bonded interactions are calculated for atom pairs within a charge group, and for atom pairs between charge groups. Considering two different charge groups, either all or none of the atom pairs for which one atom belongs to one charge group and the other atom belongs to the other charge group are contributing to the non-bonded force. This implies that the charge groups should be approximately spherical and that if the largest charge groups in the system are of diameter  $d$ , the non-bonded cut-off radius  $R_c$  must be chosen much larger than  $d$ , in order to avoid omission of atom pairs from neighbouring charge groups in the calculation of the non-bonded forces. If charge groups in alkanes are too big, i.e. if the number of charge groups per alkane molecule is too small, the missing non-bonded interactions will be reflected in a too high pressure, since attractive van der Waals forces are then neglected. This is illustrated in Figure 4.1 for MD simulations of liquid *n*-hexane ( $\blacktriangle$ ) and liquid *n*-nonane ( $\blacklozenge$ ). In Figure 4.2 the recommended charge group definitions for alkane molecules modelled using the GROMOS force field are displayed. A charge group contains at most five atoms which are separated (except for *n*-butane) by at most two bonds. This charge group definition yields accurate results when used in conjunction with a 1.4 nm cut-off di-

**Figure 4.2** Examples of charge-group definition for a set of uncharged aliphatic molecules. Definition of charge group boundaries (dashed lines) as used in the simulations using the GROMOS force field. The examples of united-atom aliphatic hydrocarbon structures have been ordered according to the following set of rules:

- 1) If the total number of united atoms in a molecule is less or equal to 4, use one charge group for the whole molecule.
- 2) If the total number of united atoms in a molecule or a molecule fragment is equal to 5, use
  - A) if the maximal width of the molecule corresponds to the span of one bond-angle, one charge group.
  - B) else follow rule 3) accordingly.
- 3) For molecules not subject to rules 1) and 2A), e.g. with more than 5 united atoms do take all  $\text{CH}_3$  united atoms into single charge groups. The remaining structure should be judged using rule 2), before the remaining fragments are divided into segments of 2 atoms per charge group and 3 atoms per charge group.

1	2A	2B	3
 01  001  0001	 00001  00001	 10011  10111	 1010011  1001111  0101001  0101010  000011111  101010011011

The united atoms of each structure have been numbered and the charge-group codes (0 or 1) of the corresponding GROMOS96-topology building blocks are displayed below each structure.

stance for non-bonded interactions. We note that the use of charge groups is computationally efficient even for a model in which atoms bear zero partial charge, since neighbour searching is faster for charge groups than for atoms, as long as there are charge groups containing more than one atom.

The performance of the GROMOS96 force field parameter sets 43A1 [16,35] and 43A2 [93] with respect to MD simulation of single chain alkanes of length 2 to 20 in the condensed phase is shown in Figure 3A. The original GROMOS96 parameter set 43A1 ( $\times$ ) reproduces the experimental heat of vaporisation of liquid *n*-alkanes ( $\circ$ ) up till a chain length of about 14, and yields excellent agreement for *n*-alkanes of length 3 to 7. The more recent parameter set 43A2 (+) yields good agreement up till a chain length of 20. However, both parameter sets fail to reproduce the correct pressure in constant volume simulations at the experimental density of the liquids. This observation forced us to reconsider the van der Waals parameters for the CH<sub>2</sub> and CH<sub>3</sub> united atoms in the GROMOS force field. These atoms are abundant in systems composed of lipids and their parameters will affect the simulated density and energy of membranes. A reparametrisation of the CH<sub>2</sub> and CH<sub>3</sub> van der Waals parameters for the whole set of *n*-alkanes led to a satisfactory result, as is shown in Figure 3B. The new set of parameters is called 45A3. A detailed look at constant volume and constant pressure simulation results obtained with parameter set 45A3 is offered in Table 4.2. Three things are important to mention. First, for the smallest molecule, ethane, the united atom model used could not be parametrised to reproduce the density and heat of vaporisation at the same time. Ethane always did evaporate after a finite simulation period at constant pressure conditions, and CH<sub>3</sub> van der Waals parameters that reproduce both the experimental density and enthalpy could not be found. Second, in molecular dynamics simulation the pressure is more sensitive than the density to changes in force field parameters, i.e. a parametrisation based on a fitting to the experimental pressure in constant volume simulations is more precise than one based on fitting to the experimental density in constant pressure simulations. In practice, if in a constant volume simulation the pressure deviates less than 100 atm from the experimental value (usually 1 atm), the corresponding constant pressure simulation will closely reproduce the experimental density or volume. With this approach perfect agreement in volume could be achieved with errors below 0.5% for most of the *n*-alkanes investigated. Third, at constant volume a slight increase of pressure with chain length is noticeable going from *n*-hexane to *n*-heptadecane after which the pressure slightly decreases again. This may reflect the experimental observation that *n*-heptadecane should be liquid at



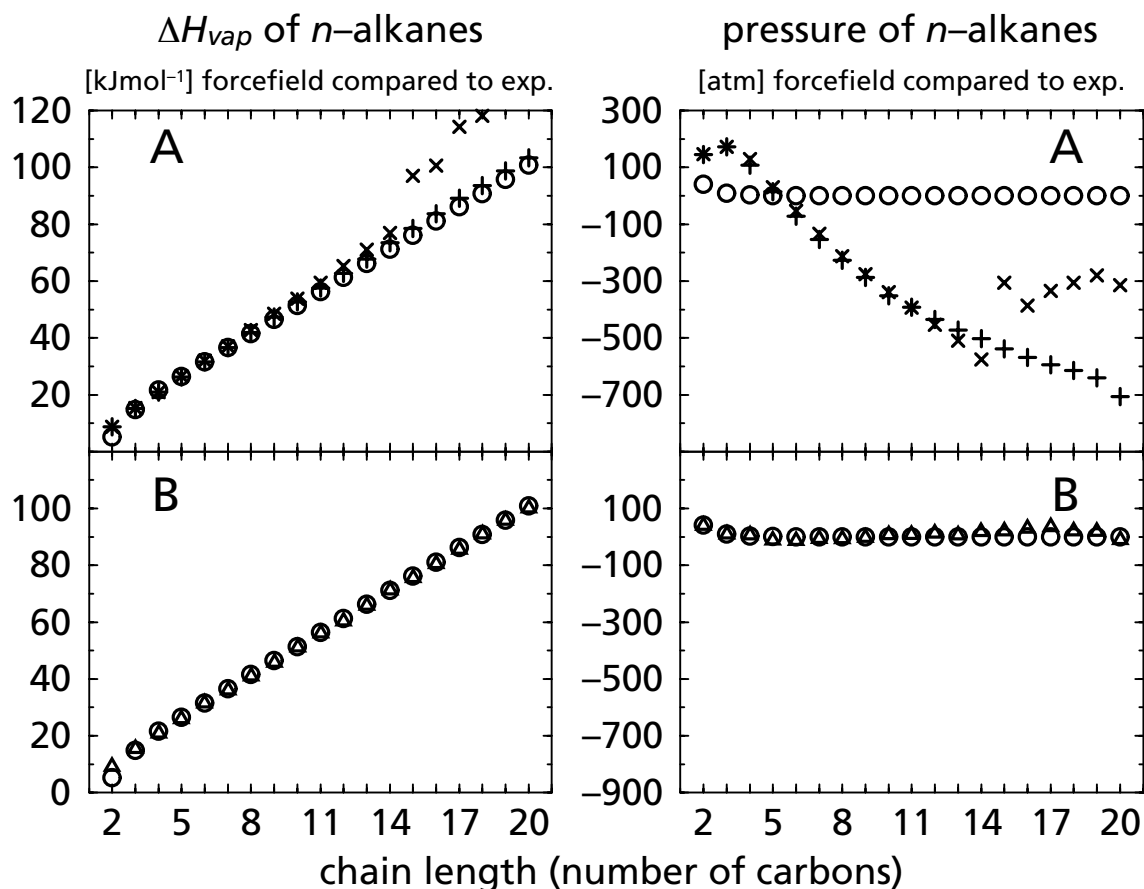


**Figure 4.3A** Liquid key properties for *n*-alkanes using GROMOS96 liquid force-fields 43A1 and 43A2. GROMOS96 force-fields 43A1 (×) and 43A2 (+) have been tested for a series of *n*-alkanes (ethane to eicosane). Whereas the heat of vaporisation is close to experimental values (○) for both force-fields – with a slight improvement of 43A2 over 43A1 – the pressure in a constant volume simulation drastically drops below zero beyond a chain length of 6 (*n*-hexane). The jump in simulated values obtained using force field set 43A1 occurs beyond chain length 14 where these alkane structures crystallised after equilibration.

**Figure 4.3B** Results for the new set 45A3 (△). The van der Waals parameters CH<sub>2</sub> and CH<sub>3</sub> united atoms have been successfully reparametrised to reproduce heat of vaporisation and pressure at constant volume at room temperature.

**Table 4.2** *n*-alkanes: a comparison of simulated and experimental data. For the first 19 *n*-alkane chains experimental and simulated liquid properties are given. Columns four and six show the results from constant volume simulations with which the parametrisation was undertaken. The third column shows experimental heat of vaporisation to which simulated results in the fourth column can be compared. Corresponding experimental and simulated pressures are given in columns five and six. Columns seven through nine compare experiments with constant pressure simulations. Column seven contains the calculated heat of vaporisation at constant pressure to compare with columns three and four. The obtained density is reflected in columns eight and nine which contain the experimental and simulated volumes. All experimental data in columns three, five and eight was taken from [38]. For some molecules the experimental isothermal compressibility taken from CRC Handbook of Chemistry and Physics is given in column ten. Isothermal compressibility from simulations is shown in the last column. Except for the smaller *n*-alkanes indicated with two asterisks, these values have directly been used for the pressure coupling simulations. In the case of the smaller *n*-alkanes an increase of the pressure coupling time  $\tau_p$  to 5 ps instead of 0.5 ps was necessary to keep the volume constant. However in the case of ethane (one asterisk), the liquid evaporated into the larger volume of 291.37 nm<sup>3</sup> after about 100 ps.

<i>n</i> -alkane name	number of C-atoms	$H_{vap}$		pressure		$H_{vap}$	volume		isothermal compressibility	
		exp kJmol <sup>-1</sup>	NVT kJmol <sup>-1</sup>	exp atm	NVT atm	NPT kJmol <sup>-1</sup>	exp nm <sup>3</sup>	NPT nm <sup>3</sup>	exp 10 <sup>-2</sup> × (kJmol <sup>-1</sup> nm <sup>-3</sup> ) <sup>-1</sup>	NVT
ethane	2	5.16	9.50	41.08	41	14.88*	81.16*	82.25		41.770**
propane	3	14.79	15.79	9.48	9	15.89	76.05	75.99		1.130**
butane	4	21.62	21.19	2.43	8	21.16	86.24	86.38		0.523**
pentane	5	26.43	26.18	0.68	-7	26.27	98.78	98.48	0.362	0.359
hexane	6	31.55	31.60	0.20	-10	31.67	111.89	111.58	0.277	0.282
heptane	7	36.55	36.40	0.06	-4	36.44	125.38	125.25		0.241
octane	8	41.49	41.28	0.02	-4	41.31	139.02	138.92	0.213	0.212
nonane	9	46.44	46.16	0.00	0	46.20	152.77	152.70	0.195	0.192
decane	10	51.37	51.52	0.00	10	51.48	166.53	166.68	0.182	0.182
undecane	11	56.33	56.31	0.00	11	56.30	180.44	180.51	0.171	0.169
dodecane	12	61.29	60.69	0.00	14	60.64	194.34	194.49	0.164	0.154
tridecane	13	66.23	66.18	0.00	10	66.14	208.25	208.47	0.157	0.142
tetradecane	14	71.17	71.43	0.00	19	71.33	222.17	222.58	0.151	0.148
pentadecane	15	76.15	75.97	0	22	75.70	236.11	236.75	0.146	0.144
hexadecane	16	81.09	80.84	0	32	80.72	250.06	250.61	0.142	0.142
heptadecane	17	86.19	86.03	0	38	85.75	263.94	264.66		0.134
octadecane	18	90.79	91.26	0	22	90.52	277.73	278.81		0.128
nonadecane	19	95.81	96.15	0	22	95.78	291.83	292.69		0.132
eicosane	20	100.83	100.42	0	-6	99.05	307.08	306.88		0.142

**Table 4.3** Cyclic alkanes: a comparison between simulated and experimental data. Analogously to Table 4.2, experimental and simulated properties are given for a series of cycloalkanes in the liquid phase.

cycloalkane name	number of C-atoms	$H_{vap}$		pressure		$H_{vap}$	volume		isothermal compressibility	
		exp kJmol <sup>-1</sup>	NVT kJmol <sup>-1</sup>	exp atm	NVT atm	NPT kJmol <sup>-1</sup>	exp nm <sup>3</sup>	NPT nm <sup>3</sup>	exp 10 <sup>-2</sup> × (kJmol <sup>-1</sup> nm <sup>-3</sup> ) <sup>-1</sup>	NVT
cyclobutane	4	23.64	21.71	1.57	816	19.38	69.24	78.33	0.181	
cyclopentane	5	28.53	27.72	0.42	36	26.56	80.47	84.24	0.221 <sup>a</sup>	0.158
cyclohexane	6	33.05	33.25	0.13	-0	33.42	92.45	91.74	0.196	0.182
cycloheptane	7	38.53	38.65	0.03	+2	38.63	103.50	103.52	0.153 <sup>a</sup>	0.150
cyclooctane	8	43.35	44.13	0.01	-25	44.21	114.67	114.45	0.133 <sup>a</sup>	0.134

<sup>a</sup> experimental values taken at T=293 K.

room temperature (melting point 295 K) whereas *n*-octadecane should be still solid (melting point 301 K). In the literature another united atom model was found that was mainly used for C<sub>44</sub> chains [129]. The CH<sub>2</sub> and CH<sub>3</sub> parameters of our new GROMOS96 45A3 parameter set are closer to the values used in [129] for polymer melts ( $\sigma=0.4$  nm for both,  $\varepsilon=0.389$  kJmol<sup>-1</sup> for CH<sub>2</sub> and  $\varepsilon=0.947$  kJmol<sup>-1</sup> for CH<sub>3</sub> united atoms, compare to Table 4.6) than to the older 43A1 or 43A2 parameter values. The same is true when comparing the old and new GROMOS96 values to those ( $\sigma=0.395$  nm and  $\varepsilon=0.382$  kJmol<sup>-1</sup> for CH<sub>2</sub> and  $\sigma=0.375$  nm and  $\varepsilon=0.815$  kJmol<sup>-1</sup> for CH<sub>3</sub>) derived in [130] for *n*-alkane phase equilibria.

The next step was to investigate cycloalkanes in a series from cyclobutane to cyclooctane using the new CH<sub>2</sub> parameters. The pressure at constant volume increased to about 1000 atm for all cycloalkanes. This meant that either CH<sub>2</sub> parameters had to be compromised to fit experimental data for *n*-alkanes and cycloalkanes thereby losing the excellent agreement for the more relevant *n*-alkanes, or a new CH<sub>2</sub> united atom type for cycloalkanes had to be introduced, as had already been done earlier for CH groups in aromatic rings [16,35]. The latter option was chosen and an atom type 44 named CH2r (r for ring) was introduced in the GROMOS96 force field. Table 4.3 shows some properties of cycloalkanes obtained with the optimised parameter set 45A3. Our aim was to achieve good agreement with experiment primarily for cyclohexane, the most common species and widely used as organic solvent [131-133]. It was possible to keep the pressure and volume close to the experimental values for cyclohexane and larger rings, but not for the smaller ones. The geometry of smaller rings is unfavorable for the dihedral angle potentials (type 17) and bond-angle bending potentials (type 14) used (Table 4.1). Thus, relative to the

experimental values, in the simulations at constant pressure the densities of cyclopentane and cyclobutane were off by 5% and 12%, respectively, and the heats of vaporisation were off by 3% and 8% respectively. The 45A3 parameter set will be applicable to most mixed systems of linear and cyclic alkanes.

The next step was to consider branched alkanes, e.g. isoalkanes and neoalkanes which contain two other (united) atom types,  $\text{CH}_1$ , and  $\text{CH}_0$ . The latter has been introduced as a new atom type 45, since the bare carbon with atom type 11 was initially designed for use in planar groups, e.g. carbonyl and aromatic groups, and not for tetrahedral carbons. Table 4.4 shows species by their name and the atom types involved, together with simulated and experimental properties. Some of the selected species are of more relevance regarding their occurrence as structural elements in biomolecular systems than others. In such systems methylated branches occur as in isoalkanes. 4-Propylnonane and 6-methylundecane have larger branches and were chosen as test molecules because they have been used as actual lipid tails in experiments [75] and because they combine the  $\text{CH}_1$  centre with shorter and longer chains. The species isobutane, isopentane, 6-methylundecane and 4-propylnonane which show increasing interactions of the  $\text{CH}_1$  central atom with  $\text{CH}_2$  instead of  $\text{CH}_3$ , show properties in close agreement to the experimental data. The series isobutane, 2,3-dimethylbutane, 2,3,4-trimethylpentane, 2,3(R),4(S),5-tetramethylhexane covers the interaction between  $\text{CH}_1$  and  $\text{CH}_3$  united atoms. It is noticeable how the pressure is reduced towards longer chains. It was impossible to find a parameter set that does not show this trend without having bad side effects on interactions of other atoms ( $\text{CH}_2$ ,  $\text{CH}_0$ ) with  $\text{CH}_1$  atoms. It is known from experiment that tetramethylhexane should not solidify at room temperature. It does not in our simulations either, but the observed drop in pressure with increasing chain length indicates that this process might have started. However, experimental results given in [38] for tetramethylhexane do not mention that it consists of a racemic mixture of two diastereomers. Three independent simulations were performed in order to check whether the RS and the RR compounds are different in their properties or if the racemic mixture (1:1 in a first approximation since no synthesis description indicative of a particular distribution was found) gives results closer to the experimental properties with the chosen parameter set. After a long equilibration of 1.5 ns, differences in the liquid properties are negligible and this might explain why none of the experimental reports mentions stereospecificity. Combinations of a tetrahedral carbon and  $\text{CH}_3$  groups occur in the series neopentane, tetramethylbutane and hexamethylpentane. Here, again, the smaller molecules fit the experimental properties much

**Table 4.4** Branched alkanes: a comparison of simulated and experimental data. Various species of different branched alkanes have been selected to obtain different combinations of united atoms. The second column indicates these combinations as number of hydrogens attached to the carbon of the (united) atom whereas the third column provides the size of the molecule in terms of the number of carbon atoms. The following columns are again analogous to those of Tables 4.2 and 4.3 shifted by one column.

branched alkane	C-atoms	$H_{\text{vap}}$			pressure			$H_{\text{vap}}$			volume			isotherm. compressibility	
		exp	NVT	exp	exp	NVT	NPT	exp	NVT	NPT	exp	NVT	exp	NVT	exp
name		kJmol <sup>-1</sup>	kJmol <sup>-1</sup>	atm	atm	atm	kJmol <sup>-1</sup>	atm	atm	kJmol <sup>-1</sup>	nm <sup>3</sup>	nm <sup>3</sup>	nm <sup>3</sup>	10 <sup>-2</sup> [kJmol <sup>-1</sup> nm <sup>-3</sup> ] <sup>-1</sup>	10 <sup>-2</sup> [kJmol <sup>-1</sup> nm <sup>-3</sup> ] <sup>-1</sup>
isobutane	CH1/3	4	19.23	3.48	91	18.95	89.69	92.24						0.597	
isopentane	CH1/2/3	5	24.85	0.92	35	24.81	99.91	100.57						0.381	
neopentane	CH0/3	5	21.84	1.71	-20	21.71	104.84	102.20						0.553	
2,3-dimethylbutane	CH1/3	6	29.12	0.31	93	28.75	111.52	113.31						0.270	
2,2,3-trimethylbutane	CH0/1/3	7	32.05	0.13	-91	32.34	124.26	121.96						0.395	
2,3,4-trimethylpentane	CH1/3	8	37.75	0.04	14	39.03	135.96	135.96						0.217	
2,2,3,3-tetramethylbutane	CH0/3	8	42.90	0.03	179	40.60	118.19	119.36						0.095	
3,3-diethylpentane	CH0/2	9	42.4	0.01	-142	44.07	145.41	142.94						0.229	
2,3(R),4(S),5-tetramethylhexane	CH1/3	10	46.9	0.01	-191	48.40	162.25	158.95						0.179	
2,3(R),4(R),5-tetramethylhexane	CH1/3	10	46.9	0.01	-191	48.65	162.25	158.34						0.194	
1:1 racemic mixture of above	CH1/3	10	46.9	0.01	-186	48.70	162.25	158.68						0.203	
2,2,3,3,4,4-hexamethylpentane	CH0/3	11	53.9	0.00	-380	50.36	164.70	157.85						0.207	
4-propylnonane	CH1/2/3	12	58.8	0.00	-13	59.36	192.61	192.41						0.164	
6-methylundecane	CH1/2/3	12	59.4	0.00	3	59.86	193.47	193.66						0.168	

\*experimental values taken at T=293 K.

more easily than the larger one. Hexamethylpentane is a solid at room temperature, it melts at 64-66 °C [134], which is reflected in the large negative pressure in the constant volume simulation. A fully methylated chain is rare in nature and therefore of less relevance in biomolecular simulations. Further investigations might consider parameters of dihedral angle torsional potentials involving  $\text{CH}_1$  and  $\text{CH}_0$  tetrahedral carbon atoms to improve the properties of this series, in the same way as the change from the GROMOS96 43A1 parameter set to the 43A2 parameter set involved a, substantial, improvement for dihedral potentials of n-alkane chains. Finally, a combination of the  $\text{CH}_0$  car-

Table 4.5 Free energies of hydration for various alkanes with new and old force field. Three sections of aliphatic hydrocarbons contain a selection of the molecules presented in Tables 4.2, 4.3 and 4.4, so *n*-alkanes, cycloalkanes and some branched alkanes. Their names are presented in the first and their number of carbons in the second column. Free energies of hydration have been measured (or calculated) by Cabani et al. [138] (column 3) and Ben-Naim and Marcus [139] (column 4) for which an average up to one decimal precision is given in column 5. Free energies of hydration obtained using the original GROMOS96 force field 43A1 published in [35] are presented in column 6 and the values for the force field 45A3 are presented in column 7.

aliphatic compounds	C-atoms	<i>free energies of hydration [kJmol<sup>-1</sup>]</i>			43A1	45A3
		[138]	[139]	aver.		
methane	1	8.37	8.08	8.2	8.0	6.2
ethane	2	7.66	7.40	7.5	9.2	7.4
propane	3	8.18	8.26	8.2	9.0	8.6
butane	4	8.70	8.99	8.8	7.7	8.7
pentane	5	9.76	9.78	9.8	–	10.2
hexane	6	10.40	10.68	10.5	–	11.5
heptane	7	10.96	10.99	11.0	–	11.8
octane	8	12.10	12.08	12.1	–	13.0
nonane	9	12.58*	12.76*	12.7*	–	12.6
—						
cyclobutane	4	4.06*	–	4.1*	–	6.8
cyclopentane	5	5.02	5.06	5.0	–	5.1
cyclohexane	6	5.14	5.18	5.2	–	2.9
cycloheptane	7	3.33	3.36	3.3	–	4.4
cyclooctane	8	3.58	3.51	3.5	–	5.1
—						
isobutane	4	9.70	9.55	9.6	10.4	10.3
isopentane	5	9.97	9.97	10.0	–	11.4
neopentane	5	10.46	11.22	10.8	–	9.9

\*estimate from experimental fits of [138], resp. [139].

bon with CH<sub>2</sub> and CH<sub>1</sub> united atoms was tested by considering 3,3-diethylpentane and 2,2,3-trimethylbutane, respectively. Surprisingly, while tetramethylbutane is a solid at room temperature, the related 2,2,3-trimethylbutane is liquid. Indeed, we see this feature confirmed in our simulations with the new force field parameters. The CH<sub>1</sub> parameters of our new GROMOS96 45A3 parameter set are closer to the values derived in [130] for isobutane phase equilibria ( $\sigma=0.465$  nm and  $\varepsilon=0.0831$  kJmol<sup>-1</sup>) than to the older 43A1 or 43A2 parameter values.

After the 45A3 parameter set had been obtained it still had to prove its applicability to mixed water/solute systems. Therefore, free energies of hydration were calculated for a number of selected compounds as described in the methods section. GROMOS96 uses different van der Waals C<sub>12</sub> parameters for the oxygen atom types OW of SPC water depending on whether it interacts with an apolar or a polar (hydrogen bond donor or acceptor) atom. Thus, in a mixed alkane-water system the C<sub>12</sub><sup>1/2</sup>(1) of OW is used for interactions with CH<sub>n</sub> atoms and the C<sub>12</sub><sup>1/2</sup>(2) is used for water-water interactions. Because of the changes introduced in the van der Waals parameters of the aliphatic groups, the C<sub>12</sub><sup>1/2</sup>(1) of OW had to be reparametrised (Table 4.6) in order to reproduce the experimental free energies of hydration of the set of test alkanes. Interestingly, the new value of the C<sub>12</sub><sup>1/2</sup>(1) parameter of OW is equal to its C<sub>12</sub><sup>1/2</sup>(2) value (Table 4.6), which improves the transferability of the model. The new force field 45A3 reproduces not only the free energies of hydration of *n*-alkanes excellently, but also that of other cyclic or branched species (Table 4.5). Specifically, the somewhat more moderate performance for cycloalkanes may be explained with the many energetically different conformations adopted by these molecules in experiment, which are not sampled sufficiently by one solute molecule in water within finite simulation time. It can be assumed that the general and good agreement with experiment will provide manifold advantages for studying mixed systems of apolar substances with water, micellar or other lipid aggregates in water, or inverted micelles in apolar solvents.

**Figure 4.6** Changes in GROMOS96 force-field parameters for aliphatic hydrocarbons. GROMOS96 force field parameters are presented for water oxygen (OW) and aliphatic hydrocarbon united atoms ( $\text{CH}_n$ ) from left to right. The standard  $C_6$ ,  $C_{12}$  and special third neighbour (1-4)  $CS_6$ ,  $CS_{12}$  parameters are used within GROMOS96 parameter files and presented in the first five sections. Parameters  $C_6^{1/2}$  in  $[\text{kJmol}^{-1}\text{nm}^6]^{1/2}$ ,  $C_{12}^{1/2}$  in  $10^{-3} \times [\text{kJmol}^{-1}\text{nm}^{12}]^{1/2}$  for all sets 43A1 to 45A3. Additionally the corresponding  $\varepsilon$  and  $\sigma$  parameters for the same Lennard-Jones potentials are given in the last two sections for convenient comparison with other force fields.  $\varepsilon$  and  $\sigma$  values are converted from  $C_{12}^{1/2}(1)$  and  $C_6^{1/2}$  and given in  $[\text{kJmol}^{-1}]$  and  $[\text{nm}]$ , respectively.

Every section consists of three rows providing values of the GROMOS96 force fields used. Set A1 is the original set 43A1 provided since 1996 [16,35]. Set A2 (43A2) was published in [93] and contained improved dihedral angle energy potentials and 1-4 van der Waals parameters for liquid *n*-alkanes, whereas set A3 (45A3) is the one presented here considering a larger set of aliphatic hydrocarbons for parametrisation against liquid properties.

		<i>water</i>	<i>aliphatic hydrocarbon chains</i>			<i>methane</i>	<i>aliphatic rings</i>	<i>tetrahedral aliphatic C</i>
TYPE		OW	CH1	CH2	CH3	CH4	CH2r	CH0
IAC		4	12	13	14	15	44	45
parameters $C_6^{1/2}$ in $[\text{kJmol}^{-1}\text{nm}^6]^{1/2}$ , $C_{12}^{1/2}$ in $10^{-3} \times [\text{kJmol}^{-1}\text{nm}^{12}]^{1/2}$ for all sets 43A1 to 45A3								
$C_6^{1/2}$	43A1	0.05116	0.06148	0.08429	0.09958	0.1148	-	-
	43A2	0.05116	0.06148	0.08429	0.09958	0.1148	-	-
	45A3	0.05116	0.07790	0.08642	0.09805	0.1148	0.08564	0.04896
$C_{12}(1)^{1/2}$	43A1	1.544	3.373	5.077	5.794	5.862	-	-
	43A2	1.544	3.373	5.077	5.794	5.862	-	-
	45A3	1.623	9.850	5.828	5.162	5.862	5.297	14.330
$C_{12}(2)^{1/2}$	43A1	1.623	3.373	5.077	5.794	5.862	-	-
	43A2	1.623	3.373	5.077	5.794	5.862	-	-
	45A3	1.623	9.850	5.828	5.162	5.862	5.297	14.330
$CS_6$	43A1	0.05116	0.05396	0.06873	0.08278	0.1148	-	-
	43A2	0.05116	0.05396	0.06873	0.08278	0.1148	-	-
	45A3	0.05116	0.05396	0.06873	0.08278	0.1148	0.06873	0.04838
$CS_{12}$	43A1	1.544	1.933	2.667	3.473	5.862	-	-
	43A2	1.544	1.933	2.17760	2.45582	5.862	-	-
	45A3	1.623	1.933	2.17760	2.45582	5.862	2.178	1.837
$\sigma$ and $\varepsilon$ values are converted from $C_{12}(1)^{1/2}$ and given in $[\text{kJmol}^{-1}]$ , respective $[\text{nm}]$								
$\varepsilon$	43A1	0.7184	0.3139	0.4896	0.7323	1.2636	-	-
	43A2	0.7184	0.3139	0.4896	0.7323	1.2636	-	-
	45A3	0.6502	0.09489	0.4105	0.8672	1.2636	0.4793	0.006995
$\sigma$	43A1	0.3113	0.3800	0.3920	0.3875	0.3710	-	-
	43A2	0.3113	0.3800	0.3920	0.3875	0.3710	-	-
	45A3	0.3166	0.5019	0.4070	0.3748	0.3710	0.3955	0.6639



## 4.5 Conclusions

Since GROMOS96 was developed, several suggestions for changes to the force field have been made [135-137]. All of them affect only small molecules or have little impact on biomolecular simulations of peptides and proteins. The changes suggested here are more dramatic since they consider all (hydro)carbon (united) atoms present in the forcefield of GROMOS96 except the aromatic CH united atom CR1 (atom type 16) that was used for benzene and other aromatic rings. The changes in the GROMOS96 force field introduced with the parameter set 45A3 will affect every molecule containing aliphatic atoms (types 11 through 14). The differences between parameter sets 45A3, 43A2 [93] and 43A1 [16] are summarized in Table 4.6. The CH<sub>2</sub> and CH<sub>3</sub> united atom parameters were optimised for liquid *n*-alkanes and kept fixed throughout the rest of the parametrisation procedure. A new CH<sub>2</sub> atom type, CH2r, had to be introduced in order to reproduce the experimental data for cycloalkanes. A CH<sub>2</sub> united atom that would be appropriate for simulation of both *n*-alkanes and cycloalkanes could not be modelled. Finally branched alkanes led to new CH<sub>1</sub> parameters and to a new CH<sub>0</sub> atom type (aliphatic bare carbon), which were used in combination with the previously derived CH<sub>2</sub> and CH<sub>3</sub> parameters.

Most force field development for classical molecular dynamics is nowadays either based on ab initio quantum-mechanical calculations or on experimental properties of the molecules investigated, or on a combination of both. The task of parametrisation of a force field is very time consuming, not because the systems investigated are large but because the number of systems that have to be investigated is large. A larger calibration set of molecules (or pure systems) and their corresponding properties, to which the chosen parameters are fitted, will always lead to a more general force field than a smaller calibration set. The well balanced GROMOS96 force field parameter set 43A1, which produces results fine for a variety of biomolecules, did fail for long (more than 6 carbons) *n*-alkanes. It is, therefore, recommended to include at least one or a few long-chain species in the calibration set.

With this philosophy in mind, it was shown that the new 45A3 parameter set perfectly fits *n*-alkane species longer than propane. A limitation of the force field lies in the very small *n*-alkanes and cycloalkanes. The essential features of these molecules are not captured in a united atom-model and harmonic bond-angle bending potentials may be insufficient to describe e.g. the ring puckering of cyclopentane. Properties of larger cycloalkanes are reproduced very well with

the new GROMOS96 atom CH2r (type 44), especially those of cyclohexane. Properties of smaller branched aliphatics or larger aliphatics with few branches are also reproduced well. Only for highly methylated longer chains it seems difficult to come close to experimental densities and energies.

Finally it has been shown that after a parametrisation of the van der Waals  $C_{12}^{1/2}(1)$  oxygen (OW) parameter of the SPC water model for interactions with non-polar atoms, the experimental free energies of hydration of alkanes are reproduced within the limits of accuracy of the thermodynamic integration method.

## 4.6 Acknowledgement

We would like to thank Peter Tieleman for testing lipid bilayer systems with the improved parameter set GROMOS96 43A2. It was his criticism that led us further investigate *n*-alkanes and other aliphatics.

## Chapter 5

---

**The GROMOS96 45A3 force field is benchmarked by using DPPC, Dipalmitoylphosphatidylcholine**

# 5. The GROMOS96 45A3 force field is benchmarked by using DPPC, Dipalmitoylphosphatidylcholine

## 5.1 Introduction

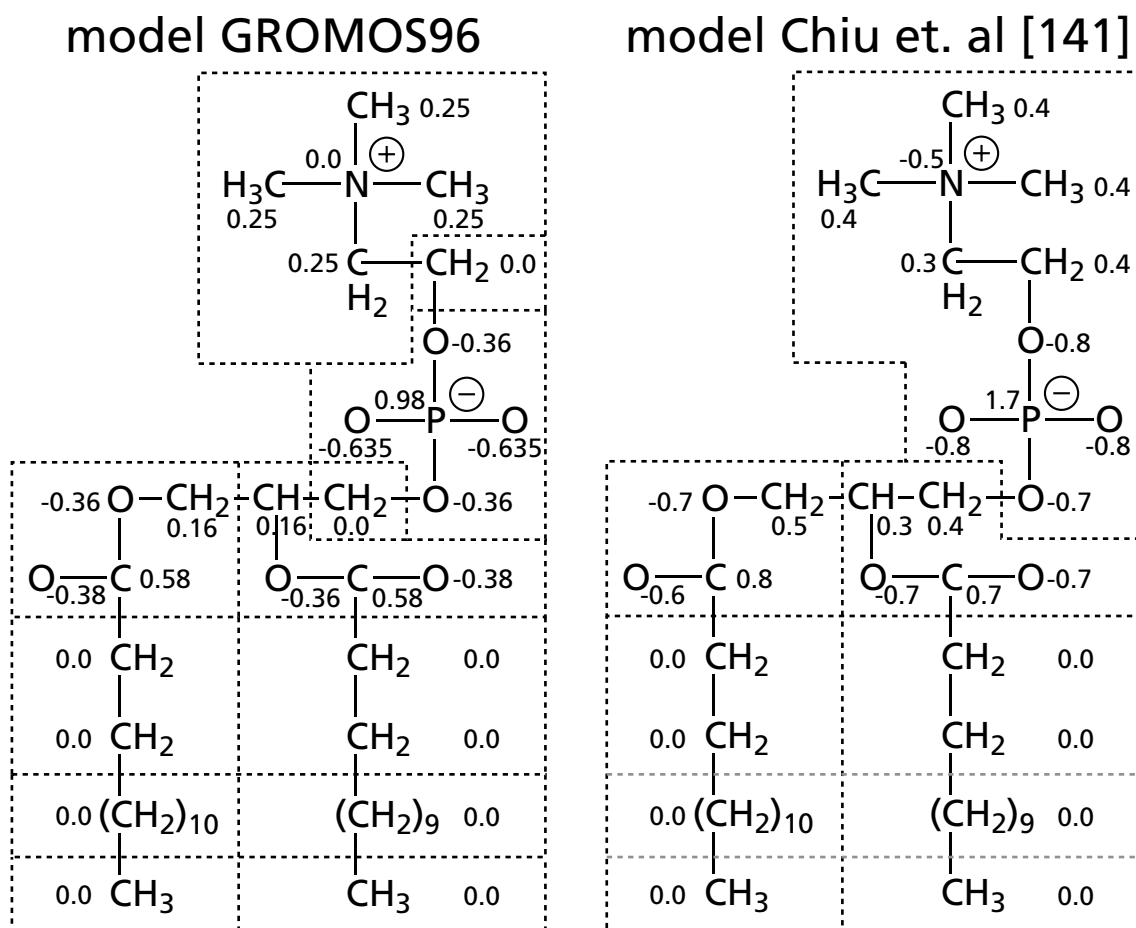
To test the new GROMOS96 force-field parameter set 45A3 derived in Chapter 4, a well characterised system of a dipalmitoylphosphatidylcholine (DPPC) bilayer was chosen. It had been equilibrated before and was initially simulated by Tieleman and Berendsen [88]. They used a force field that was based on the earlier GROMOS87 [37] force field and included a set of different modifications which altogether yielded reliable results which compared well to experimental data. For this system the simulated atomic positions were available. First the system was minimised using the condensed phase force field 45A3 and then simulated at 325 K for more than 3 ns. The carbonyl carbons were treated equal to the new tetrahedral aliphatic carbon (atom type 45), since it was not evident from GROMOS96 building blocks that the bare carbon parameters (type 11) should not be used in a tetrahedral context or vice versa.

Unexpectedly, using GROMOS96 partial charges together with the common twin-range cut-off of 0.8/1.4 nm and the condensed phase force field 45A3, the bilayer system did not equilibrate within 3.5 ns. It shrunk substantially in its area per lipid head group from initially 0.646 nm<sup>2</sup> to about 0.49 nm<sup>2</sup> during that period. One could estimate from looking at the end conformation that the system would transform into a gel phase.

These findings are not in agreement with experiment – where a transition temperature of 315 K has been measured between the gel and liquid phase of DPPC [140]. Since the force field derived in Chapter 4 should achieve a well balanced density for the lipid tails, the definition of head group parameters was investigated further. A number of differences between the model used by Tieleman and Berendsen [88] and our model were evident. A distinction between the types of differences seems appropriate: differences in the topology and parameters of the head group on one hand, and then the methodological procedure for the actual MD simulation on the other hand.

In Figure 5.1 the topological differences are introduced in detail. Simulation differences are shown in the adjacent Table 5.1.

Figure 5.1 Topological differences in two setups of the same DPPC-molecules



Apart from the force field, charge group definitions chosen for the head group of phosphatidylcholine were different. Indeed, the whole phosphate-choline group has been divided in three groups in the model that is according to GROMOS96 conventions, where Tieleman et al. have used one bigger charge group for it. Ab-initio derived charges from Chiu et al. [141] have been used in their earlier simulation, whereas the partial charges of GROMOS96 are smaller in comparison.

**Table 5.1** Different simulation set-up for DPPC.

Tieleman applied a large twin range cut-off of 1.0/2.0 nm, since the charge-group size chosen for the lipid head group might be too big to accommodate a smaller cut-off or would lead to undesirable fluctuations. Besides that, no reaction field correction was applied, since it might be neglected with the larger cut-off. The time for the pressure coupling constant was chosen double the length of what with GROMOS96 is commonly applied and the centre of mass motion was removed in every simulation step.

<i>parameter</i>	<i>GROMOS96</i>	<i>Tieleman et al. [88]</i>
cut-off	0.8/1.4	1.0/2.0
reaction field $\epsilon$	54.0	1.0 (none)
pressure coupling $\tau_p$	0.5 ps	1.0 ps
period of COM motion removal	50000 steps	1 step

## 5.2 Methods

It was obvious that a different definition of partial charges may have an influence on how well the head groups pack within the membrane. In Table 5.2 the different alterations are shown that were made to the topological and simulation conditions to stepwise approach the setup that was used before by Tieleman and Berendsen [88] for the same system. Parameter set 45A3 was used for all of these systems since it performed so well for long alkane chains (Chapter 4).

**Table 5.2** Various simulation set-ups for the DPPC bilayer to study changes made between GROMOS96 and Tieleman and Berendsen [88]

<i>parameters</i>	<i>GROMOS96 (A)</i>	<i>(B)</i>	<i>(C)</i>	<i>(D)</i>	<i>Tieleman (E)</i>	<i>(F)</i>
<i>topology</i>						
charge groups	split	unified	unified	unified	unified	unified
charges	GROMOS96	GROMOS96	GROMOS96	GROMOS96	Chiu et al.	Chiu et al.
<i>simulation</i>						
cut-off	0.8/1.4	0.8/1.4	1.0/2.0	1.0/2.0	1.0/2.0	1.0/2.0
reaction field $\epsilon$	54.0	54.0	54.0	1.0 (none)	1.0	54.0
pressure coupling $\tau_p$	0.5 ps	0.5 ps	0.5 ps	1.0 ps	1.0 ps	1.0 ps
COM motion removal	50000 steps	50000 steps	50000 steps	500 steps	1 step	1 step

Results of these simulations could have been analysed in manyfold ways, but first it is important to observe the system size for measuring the area per lipid head group. If this property cannot satisfy the experimental range of about  $0.62 \pm 0.05 \text{ nm}^2$  for the area occupied per lipid molecule [142], then it is much more likely that a phase transition will occur.

With the different setups chosen in Table 5.2, simulations have been running for at least 300 ps, a time period which is long enough to study the biggest effects which are discussed briefly in the results section.

Since the recent parametrisations for GROMOS96 have been using the 0.8/1.4 nm twin range cut-off (Chapter 4) with success and the influence of larger cut-offs on calculation time is substantial, another investigation was to follow by *selecting* the charges of Chiu et al. [141] as defined in Figure 5.1, while splitting the head charge-group into two charge groups (counting one methyl to the choline and one methyl to the phosphate group) to accommodate the smaller cut-off. This model (similar to A, but with Chiu charges) was then used to reconsider the carbonyl van der Waals parameters, since the atom type 45 introduced for tetrahedral aliphatic carbons has a much larger  $\sigma$  value than the original carbonyl atom type 11.

## 5.3 Results and Discussion

Different membrane systems (A) to (F) described in Table 5.2 starting from the same system configuration, have been simulated over various periods, but at least for 300 ps. Figure 5.2 shows, how the area per lipid head group is reduced for all but one of the systems. Indeed some of them immediately drop to values lower than the experimentally observed range for the  $L_\alpha$  phase indicated by borderlines.

If the model (A) using GROMOS96 standard building blocks and charges is compared to the two models (E and F) using the charges from Chiu et al. [141], the difference in equilibration is obvious. The higher charges seem to lead to a stronger repulsion between lipid head-groups within a layer.

Can we explain the effect of subtle changes made to the system? Model (B) has rejoined the minus e and plus e charged head-group charge-groups for the phosphate and choline to one single and neutral charge group. Nothing else was altered. The structural change is unfavourable, leading to an area per lipid of  $0.598 \text{ nm}^2$  within 500 ps, but has to be considered as unrealistic as the char-

## DPPC bilayer model test systems

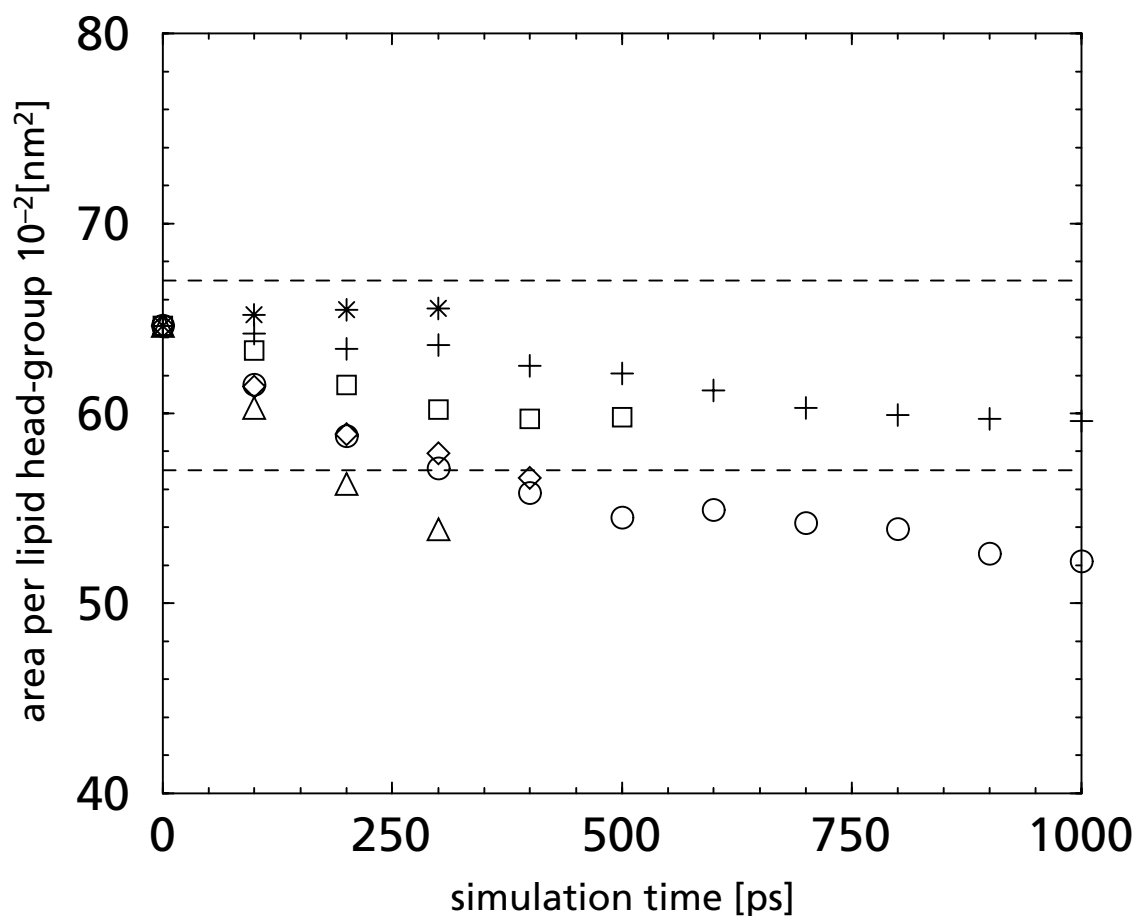


**Figure 5.2** Models A to F (Table 5.2) are indicated by (A) circles, (B) squares, (C) diamonds, (D) triangles, (E) crosses and (F) stars. The area per head group decreases for all systems but model F.

ge-group cut-off combination is. Model (C) corrects for this relation using the larger cut-off 1.0/2.0 nm as in all the models closer to model (E). This change cannot satisfy the experimental structure, as it is transforming towards a gel phase. Switching of the reaction field and correcting more often for the centre of mass motion, seems to make things worse (model D). The setup most similar to the one Tieleman et al. used according to his thesis and personal communications, seemed to work much better, at least there was no obvious loss in fluidity of the membrane, instead the surface became more rough. Still one had to ask whether a reaction field correction was not recommendable, and there-



fore model (F) was setup additionally. It yields indeed a value for the area per head group that stays within the experimental range and the fluidity of the lipid tails is maintained as it should be at that temperature of 325 K for this system.

Since a model using the larger partial charges seemed most promising, the GROMOS96 cut-off scheme (0.8/1.4 nm) was combined with a split head charge-group model as described in the methods section, including a reaction field force. It was evident from longer simulations, that only small changes of several percent reduction (i.e. 6%) of the partial charges used in this model would have a large effect on the bilayer structure concerning the area per lipid head group (data not shown). Therefore the partial charges as they were described in literature [141] were kept and the effect of varying the carbonyl carbon van der Waals parameters, that were not subject of the investigation of chapter 4 (atom type 11) was considered. Switching from the GROMOS96 force field 45A3 atom type 45 to atom type 11 for the carbonyl carbon makes a large difference in the area per lipid head group from about 0.66 nm<sup>2</sup> to 0.61 nm<sup>2</sup> as is evident from Figure 5.3. Whereas use of atom type 45 is leading to a too loose structure, use of atom type 11 of set 45A3 leads to a too narrow spacing between lipids. In both cases the membrane structure is still liquid crystalline. From literature [143, 144], it was estimated that the ideal (experimental) head group area for our model would be at 0.638 to 0.64 nm<sup>2</sup> per lipid (DPPC) at the simulation temperature of 325 K. Therefore the geometric mean of the previous atom types 11 and 45 for bare carbons was chosen as the new atom type 11. This led to a value of about 0.615 nm<sup>2</sup>. As an alternative the geometric mean of atom type 45 (CH0) van der Waals parameters (introduced in set 45A3) and atom type 12, CH1 (of set 45A3) was used. This then led to an area per lipid head group of 0.625 nm<sup>2</sup>, which is closer to the experimental estimate and within both experimental and simulation errors. This new parameter set will be used throughout several simulations to test its properties and will be published as GROMOS96 force field parameter set 45A4, since atom type 45 parameters now have been revised to the geometric mean of the former atom type 45 (45A3) parameters and atom type 12 (45A3 and 45A4) parameters. Although 4 ns (between 6 and 10 ns) is certainly enough to equilibrate, fluctuations in the area per lipid head group ranged from 0.61 to 0.645 nm<sup>2</sup>. Despite these fluctuations, the membrane is expected to maintain its liquid crystalline structure and this was inferred by calculating the  $-S_{CD}$  NMR order parameter as shown in Figure 5.4. Indeed the NMR order parameter calculated for both

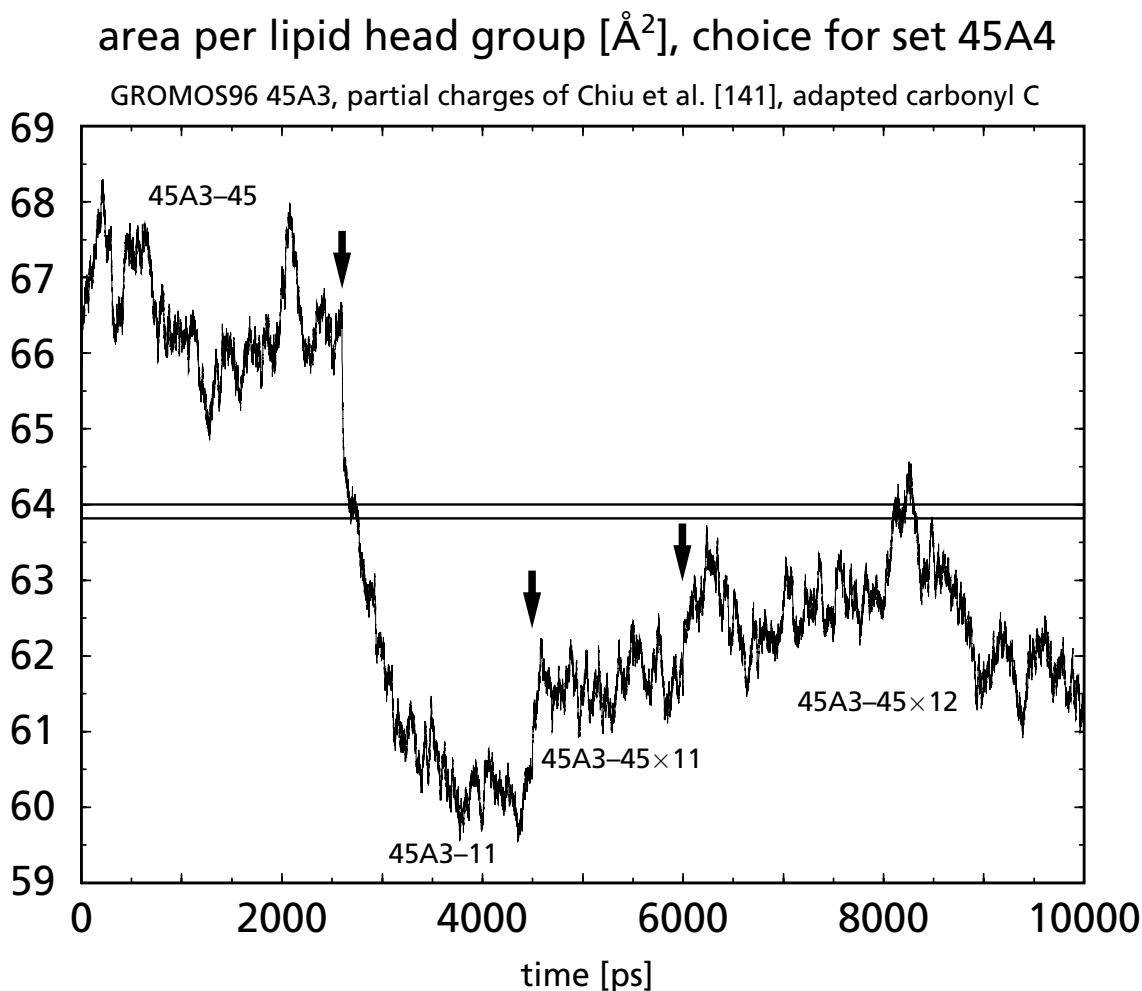


**Figure 5.3** The carbonyl carbon parameters used in the GROMOS96 force field 45A3 (atom type 11) have been unchanged since about twenty years. Therefore as a newer combination for DPPC the parameter set of atom type 45 (tetrahedral aliphatic carbon) was used first instead of the old atom type 11 in combination with all the other hydrocarbon parameters that were changed recently in 45A3. The structure was equilibrated after about one nanosecond and at 2.6 ns the carbonyl parameters were changed to the values of atom type 11. The smaller van der Waals radii relaxed the bilayer membrane structure to a smaller area per lipid head group of about  $0.605 \text{ nm}^2$  within 1.5 ns. At 4.5 ns, the carbonyl parameter values were switched to the geometric mean of the former two. Equilibration was quick and at 6 ns another switch of the carbonyl van der Waals parameters was done to the geometric mean of 45A3 atom type 12 (CH1) and 45A3 type 45. This again increases sigma but still avoids loss of possible hydrogen bonding to the carbonyl bound oxygen that may result from a too large sigma value of the carbonyl carbon. This combination therefore was chosen for the force field set 45A4 and will be further tested for its application to mixed biomolecular systems. Two lines indicate the target values for the area per lipid head group for our system of DPPC at 325 K. It has been derived from recent experimental data of [143, 144].

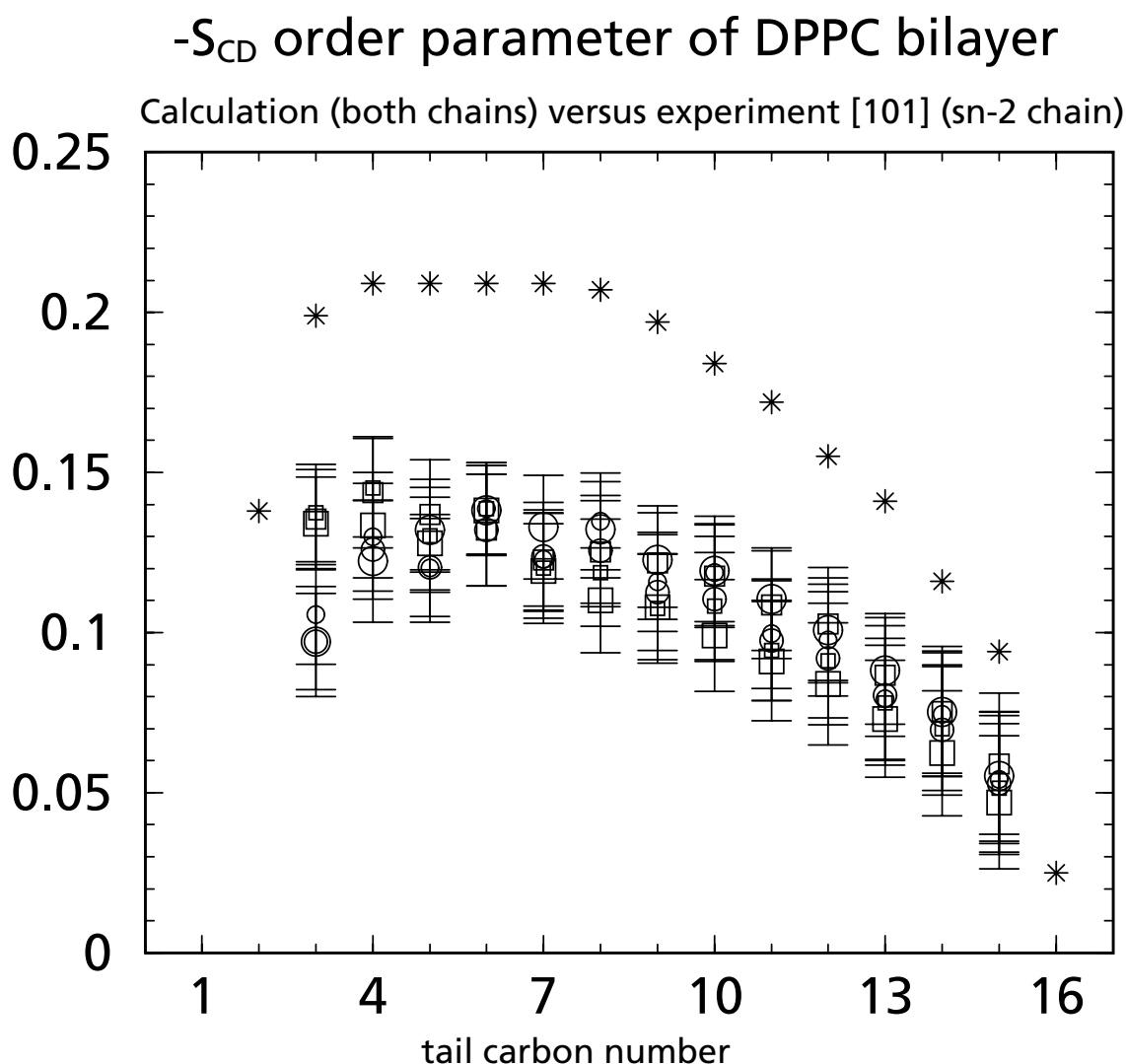


**Figure 5.4**  $-S_{CD}$  NMR order parameter calculation for DPPC and comparison to experiment [101]. Experimental values are for the sn-2 chain only and indicated by stars. Calculated values are taken from the trajectory shown in Figure 5.3 from 7 to 10 ns in parts of 1 ns each. The sn-1 chain is indicated by squares, sn-2 chain by circles. The smaller symbols are calculated of data from 7-8 ns, the medium from 8-9 ns and the larger from 9-10 ns. Error bars correspond to the mean square deviation of the average over all lipids during 1 ns.

chains is lower and therefore shows more disorder than what was found in experiment for the sn-2 chain of DPPC [101]. The fluctuations of the area per lipid head group seen in Figure 5.3 is not reflected in the values of the order parameters from the same trajectory.

## 5.4 Conclusions

The topological information of partial charges or lipid head groups might be of much more importance than expected. The balance between the well parametrised unpolar lipid tails and the charged head groups is now achievable with the current force field and protocols. To get a good model description for larger lipid molecules such as DPPC, Smondyrev and Berkowitz have pointed out that many considerations are relevant [145]. On the other hand a detailed parametrisation of every single bond-angle and dihedral within the lipid as they did seems not to be mandatory since a liquid crystal phase was also obtained using our generalised force field 45A3 together with charges of Chiu et. al. [142], a larger cut-off and reaction field correction, or, even with smaller cut-off and an accommodated charge group size and updated lipid carbonyl parameters. A recent overview of the various issues different researchers have addressed as targets and problems concerning simulations of lipid bilayers can be found in [146].

Twofold investigations should help to analyse these important findings: One is to understand the influence of the presence of countercharges by studying lipids of different total charge with counterions against neutral ones without ions as have been used here. A system with counterions gave reasonable results, as we have seen in Chapter 3 by using less pronounced partial charges. Another task is to make sure that the heteroatoms that use GROMOS96 reduced charges can satisfy the density in combination with the van der Waals parameters used or, if the van der Waals parameters are not questionable, whether the charges have to be chosen closer to the ones in vacuo if used within lipid systems. One could imagine the influence of the water to be small, since only about 6 to 11 water molecules are accommodated by one lipid.

The new parameter set 45A4 derived finally, seems promising for use in mixed systems, since it combines the well established hydrocarbon tail parameters and a new charge group and carbonyl van der Waals parameter selection for DPPC. Expectations regarding its use with proteins are such that results should at least improve. Besides all nice expectations it should not be forgotten, that DPPC is just one of a whole range of different lipids and it will not always be easy to define an appropriate parameter set, if there is not already an established charge set available.

---

Although the area per lipid head group is now close to experiment the calculated order parameter shows more disorder than expected from experiment. This last finding needs further investigation about the influence of the chosen lipid head group and simulation parameters on this property. It might still be necessary to choose an independent charge set from the predefined ones of Figure 5.1. It is not in the format of this thesis that these further investigations can be undertaken and the author would like to express his feeling, that whoever follows the paths of this work can only get closer to an even better solution.



# References

---

## Cumulative References

# Cumulative References

- [1] S. J. Singer and G. L. Nicolson, "The fluid mosaic model of the structure of cell membranes", *Science*, 175, 720–731 (1972).
- [2] J. N. Israelachvili, D. J. Mitchell and B. W. Ninham, "Theory of self-assembly of lipid bilayers and vesicles", *Biochim. Biophys. Acta*, 470, 185–201 (1977).
- [3] C. Tanford, "The hydrophilic effect: formation of micelles and biological membranes", John Wiley and Sons, New York, 1980.
- [4] J. N. Israelachvili, "Intermolecular & surface forces", Israelachvili Jacob, eds. 2nd edition, Academic Press, London, 1991, 17, pp 370–382.
- [5] D. M. Small, "The physical chemistry of lipids, from alkanes to phospholipids", 1st edition, Plenum Press, New York, 1986.
- [6] P. Bucher, A. Fischer, P. L. Luisi and P. Walde, "Giant vesicles as biochemical compartments: the use of microinjection techniques", *Langmuir*, 14, 2712–2721 (1998).
- [7] M. Langner and T. E. Kral, "Liposome-based drug delivery systems", *Pol. J. Pharmacol.*, 51, 211–222 (1999).
- [8] R. Kuboi, M. Yoshimoto, P. Walde and P. L. Luisi, "Refolding of carbonic anhydrase assisted by 1-palmitoyl-2-oleoyl-sn-glycero-3-phosphocholine liposomes", *Biotech. Progress*, 13, 828–836 (1997).
- [9] M. Blocher, D. J. Liu and P. L. Luisi, "Liposome-assisted selective polycondensation of alpha-amino acids and peptides: The case of charged liposomes", *Macromol.*, 33, 5787–5796 (2000).
- [10] G. Ourisson and Y. Nakatani, "The terpenoid theory of the origin of cellular life: the evolution of terpenoids to cholesterol", *Chem. Biol.*, 1, 11–23 (1994).
- [11] D. W. Deamer, "The first living systems: a bioenergetic perspective", *Microbiol. & Mol. Biol. Rev.*, 61, 239–261 (1997).
- [12] P. L. Luisi, P. Walde and T. Oberholzer, "Lipid vesicles as possible intermediates in the origin of life", *Curr. Op. Coll. Int. Sci.*, 4, 33–39 (1999).
- [13] K. Morigaki, S. Dallavalle, P. Walde, S. Colonna and P. L. Luisi, "Autopoietic self-reproduction of chiral fatty acid vesicles", *J. Am. Chem. Soc.*, 119, 292–301 (1997).
- [14] P. Walde, M. Wessicken, U. Rädler, N. Berclaz, K. Conde-Frieboes and P. L. Luisi, "Preparation and characterization of vesicles from mono-*n*-alkyl phosphates and phosphonates", *J. Phys. Chem. B*, 101, 7390–7397 (1997).
- [15] D. Berti, P. Baglioni, G. Barsacchi-Bo and P. L. Luisi, "Base complementarity and nucleoside recognition in phosphatidyl nucleoside vesicles", *J. Phys. Chem. B*, 102, 303–308 (1998).



- [16] W. F. van Gunsteren, S. R. Billeter, A. A. Eising, P. H. Hünenberger, P. Krüger, A. E. Mark, W. R. P. Scott and I. G. Tironi, "Biomolecular Simulation, The GROMOS96 Manual and User Guide", vdf Hochschulverlag AG an der ETH Zürich and BIOMOS b.v., Zürich, Groningen, 1996.
- [17] M. P. Allen and D. J. Tildesley, "Computer simulation of liquids", Oxford University Press: New York, 1987.
- [18] J. P. Ryckaert, G. Ciccotti and H. J. C. Berendsen, "Numerical integration of the cartesian equations of motion of a system with constraints: Molecular dynamics of *n*-alkanes", *J. Comput. Phys.*, 23, 327–341 (1977).
- [19] H. J. C. Berendsen, "Treatment of long-range forces in Molecular Dynamics", In: "Molecular Dynamics and Protein Structure", J. Hermans, eds. Polycrystal Book Service, P.O. Box 27, Western Springs, Ill. 60558 USA, 1985, pp 18–22.
- [20] H. J. C. Berendsen, J. P. M. Postma, W. F. van Gunsteren and J. Hermans, "Interaction models for water in relation to protein hydration", In: "Intermolecular forces", ed. B. Pullmann, Reidel: Dordrecht, 331–342 (1981).
- [21] H. J. C. Berendsen, J. P. M. Postma, W. F. van Gunsteren, A. DiNola and J. R. Haak, "Molecular dynamics with coupling to an external bath", *J. Chem. Phys.*, 81, 3684–3690 (1984).
- [22] M. Levitt, "Energy refinement of hen-egg white lysozyme", *J. Mol. Biol.*, 82, 393–420 (1974).
- [23] M. Levitt, M. Hirshberg, R. Sharon and V. Daggett, "Potential energy function and parameters for simulations of the molecular dynamics of proteins and nucleic acids in solution", *Comp. Phys. Com.*, 91, 215–231 (1995).
- [24] A. T. Hagler, E. Huler and S. Lifson, "Energy functions for peptides and proteins. 1. derivation of a consistent force field including the hydrogen bond from amide crystals", *J. Am. Chem. Soc.*, 96, 5319–5327 (1974).
- [25] P. Dauber-Osguthorpe, V. A. Roberts, D. J. Osguthorpe, J. Wolff, M. Genest and A. T. Hagler, "Structure and energetics of ligand binding to proteins: *E. coli* dihydrofolate reductase-trimethoprim, a drug-receptor system", *PROTEINS: Structure, Function and Genetics*, 4, 31–47 (1988).
- [26] B. R. Brooks, R. E. Bruccoleri, B. D. Olafson, D. J. States, S. Swaminathan and M. Karplus, "CHARMM: A program for macromolecular energy minimization and dynamics calculations", *J. Comp. Chem.*, 4, 187–217 (1983).
- [27] Jr. MacKerell, A. D. Bashford, M. Bellott, Jr. Dunbrack, J. D. Evanseck, M. J. Field, S. Fischer, J. Gao, H. Guo, S. Ha, D. Joseph-McCarthy, L. Kuchnir, K. Kuczera, F. T. K. Lau, C. Mattos, S. Micknick, T. Ngo, D. T. Nguyen, B. Prodhom, W. E. Reiher III, B. Roux, M. Schlenkrich, J. C. Smith, R. Stote, J. Straub, M. Watanabe, J. Wiorkiewicz-Kuczera, D. Yin and M. Karplus, "All-atom empirical potential for molecular modeling and dynamics studies of proteins", *J. Phys. Chem. B*, 102, 3586–3616 (1998).

- [28] S. J. Weiner, P. A. Kollman, D. A. Case, U. C. Singh, C. Ghio, G. Alagona, S. Jr. Profeta and P. Weiner, "A new force field for molecular mechanical simulation of nucleic acids and proteins", *J. Am. Chem. Soc.*, 106, 765–784 (1984).
- [29] W. D. Cornell, P. Cieplak, C. I. Bayly, I. R. Gould, K. M. Jr. Merz, D. M. Ferguson, D. C. Spellmeyer, T. Fox, J. W. Caldwell and P. A. Kollman, "A second generation force field for the simulation of proteins, nucleic acids and organic molecules", *J. Am. Chem. Soc.*, 117, 5179–5197 (1995).
- [30] J. Hermans, H. J. C. Berendsen, W. F. van Gunsteren and J. P. M. Postma, "A consistent empirical potential for water-protein interactions", *Biopolymers*, 23, 1513–1518 (1984).
- [31] E. Egberts, S. J. Marrink and H. J. C. Berendsen, "Molecular dynamics simulation of a phospholipid membrane", *Eur. Biophys. J.*, 22, 423–436 (1994).
- [32] W. L. Jorgensen and J. Tirado-Rives, "The OPLS potential functions for proteins. Energy minimization for crystals of cyclic peptides and crambin", *J. Am. Chem. Soc.*, 110, 1657–1666 (1988).
- [33] W. L. Jorgensen, D. S. Maxwell and J. Tirado-Rives, "Development and testing of the OPLS all-atom force field on conformational energetics and properties of organic liquids", *J. Am. Chem. Soc.*, 118, 11225–11236 (1996).
- [34] I. Chandrasekhar, "Parameter development for molecular dynamics simulation of lipids, in *Biomembrane Structure & Function*", The State of the Art, Adenine Press, Albany New York, 1992.
- [35] X. Daura, A. E. Mark and W. F. van Gunsteren, "Parametrization of aliphatic CH<sub>n</sub> united atoms of GROMOS96 force field", *J. Comp. Chem.*, 19, 535–547 (1998).
- [36] W. F. van Gunsteren, X. Daura and A. E. Mark, "The GROMOS force field", *Encyclopaedia of Comp. Chem.*, 2, 1211–1216 (1998).
- [37] W. F. van Gunsteren and H. J. C. Berendsen, "Groningen Molecular Simulation (GROMOS), Library Manual", BIOMOS b.v., Groningen, 1987.
- [38] "TRC Thermodynamic Tables-Hydrocarbons", Texas A & M University System, College Station, TX.
- [39] G. J. Sasz, N. Sheppard and D. H. Rank, "Spectroscopic studies of rotational isomerism. I. Liquid butane and the assignment of the normal modes of vibration", *J. Chem. Phys.*, 16, 704–711 (1948).
- [40] N. Sheppard and G. J. Sasz, "Spectroscopic studies of rotational isomerism. III. The normal paraffins in the liquid and solid states", *J. Chem. Phys.*, 17, 86–92 (1949).
- [41] P. J. Flory, "Statistical mechanics of chain molecules", Wiley-Interscience: New York, 1969.
- [42] A. L. Verma, W. F. Murphy and H. J. Bernstein, "Rotational isomerism. XI. Raman spectra of butane, 2-methylbutane and 2,3-dimethylbutane", *J. Chem. Phys.*, 60, 1540–1544 (1974).

- [43] W. F. Bradford, S. Fitzwater and L. S. Bartell, "Molecular structure of *n*-butane: calculation of vibrational shrinkages and an electron diffraction reinvestigation", *J. Mol. Struct.*, 38, 185–194 (1977).
- [44] J. R. Durig and D. A. C. Compton, "Analysis of torsional spectra of molecules with two internal  $C_{3v}$  Rotors. 12<sup>1a</sup>. low frequency vibrational spectra, methyl torsional function, and internal rotation of *n*-butane", *J. Phys. Chem.*, 83, 265–268 (1979).
- [45] L. Colombo and G. Zerbi, "Enthalpy difference of rotational isomers in liquid butane and pentane from infrared spectra", *J. Chem. Phys.*, 73, 2013–2014 (1980).
- [46] S. Kint, J. R. Scherer and R. G. Snyder, "Raman spectra of liquid *n*-alkanes. III. Energy difference between trans and gauche *n*-butane", *J. Chem. Phys.*, 73, 2599–2602 (1980).
- [47] D. A. C. Compton, S. Montero and W. F. Murphy, "Low-frequency Raman spectrum and asymmetric potential function for internal rotation of gaseous *n*-butane", *J. Chem. Phys.*, 84, 3587–3591 (1980).
- [48] M. Räsänen and V. E. Bondybey, "Rotamerization of normal-butane in solid neon – example of a mode specific chemical-reaction", *J. Chem. Phys.*, 82, 4718–4719 (1985).
- [49] W. Hüttner, W. Majer and H. Kästle, "Ground-state rotational spectrum and spectroscopic parameters of the gauche butane conformer", *Mol. Phys.*, 67, 131–140 (1989).
- [50] R. G. Snyder and Y. Kim, "Conformation and low-frequency isotropic Raman-spectra of the liquid *n*-alkanes  $C_4$ - $C_9$ ", *J. Phys. Chem.*, 95, 602–610 (1991).
- [51] J. R. Durig, A. Wang, W. Beshir and T. S. Little, "Barrier to asymmetric internal rotation, conformational stability, vibrational spectra and assignments, and ab initio calculations of *n*-butane- $d_0$ ,  $d_5$  and  $d_{10}$ ", *J. Raman Spectrosc.*, 11, 683–704 (1991).
- [52] W. F. Murphy, J. M. Fernandez-Sanchez and K. Raghavachari, "Harmonic force-field and Raman-scattering intensity parameters of normal-butane", *J. Phys. Chem.*, 95, 1124–1139 (1991).
- [53] R. F. Frey, M. Cao, S. Q. Newton and L. Schäfer, "Electron correlation-effects in aliphatic nonbonded interactions – comparison of *n*-alkane MP2 and HF geometries", *J. Mol. Struct. (Theochem)*, 285, 99–113 (1993).
- [54] W. A. Herrebout, B. van der Veken, A. Wang and J. R. Durig, "Enthalpy difference between conformers of *n*-butane and the potential function governing conformational interchange", *J. Phys. Chem.*, 99, 578–585 (1995).
- [55] D. S. Maxwell, J. Tirado-Rives and W. L. Jorgensen, "A comprehensive study of the rotational energy profiles of organic-systems by ab-initio MO theory, forming a basis for peptide torsional parameters", *J. Comp. Chem.*, 16, 984–1010 (1995).

- [56] G. D. Smith and R. L. Jaffe, "Quantum chemistry study of conformational energies and rotational energy barriers of *n*-alkanes", *J. Phys. Chem.*, 100, 18718–18724 (1996).
- [57] N. L. Allinger, J. T. Fermann, W. D. Allen and H. F. Schaefer III, "The torsional conformations of butane: definitive energetics from ab initio methods", *J. Chem. Phys.*, 106, 5143–5150 (1997).
- [58] S. Mizushima and H. Okazaki, "Equilibrium ratio of rotational isomers of *n*-pentane: with special reference to its difference from that of 1,2-dichloroethane", *J. Am. Chem. Soc.*, 71, 3411–3412 (1949).
- [59] I. Harada, H. Takeuchi, M. Sakakibara, H. Matsuura and T. Shimanouchi, "Vibration spectra and rotational isomerism of chain molecules. II. Butane, pentane, hexane, pentane-d<sub>12</sub>, and hexane-d<sub>14</sub>", *Bull. Chem. Soc. Jpn.*, 50, 102–110 (1977).
- [60] M. Maissara, J. C. Cornut, J. Devaure and J. Lascombe, "Conformational equilibrium of pentane as a function of temperature and pressure", *Spectrosc. Int. J.*, 2, 104–119 (1983).
- [61] I. Kanesaka, R. G. Snyder and H. L. Strauss, "Experimental-determination of the trans-gauche energy difference of gaseous *n*-pentane and diethyl-ether", *J. Chem. Phys.*, 84, 395–397 (1986).
- [62] J. R. Scherer and R. G. Snyder, "Raman spectra of liquid *n*-alkanes. II. Longitudinal acoustic modes and the gauche-trans energy difference", *J. Phys. Chem.*, 72, 5798–5808 (1980).
- [63] W. R. P. Scott, P. H. Hünenberger, I. G. Tironi, A. E. Mark, S. R. Billeter, J. Fennen, A. E. Torda, T. Huber, P. Krüger and W. F. van Gunsteren, "The GROMOS biomolecular simulation program package", *J. Phys. Chem. A*, 103, 3596–3607 (1999).
- [64] R. A. Bonham and L. S. Bartell, "The molecular structure and rotational isomerisation of *n*-butane", *J. Am. Chem. Soc.*, 81, 3491–3496 (1959).
- [65] G. Kaminski, E. M. Duffy, T. Matsui and W. L. Jorgensen, "Free energies of hydration and pure liquid properties of hydrocarbons from the OPLS all-atom model", *J. Phys. Chem.*, 98, 13077–13082 (1994).
- [66] W. L. Jorgensen, J. D. Madura and C. J. Swenson, "Optimized intermolecular potential functions for liquid hydrocarbons", *J. Am. Chem. Soc.*, 106, 6638–6646 (1984).
- [67] W. L. Jorgensen, "BOSS", Version 4.0, Yale University: New Haven, CT, 1998.
- [68] G. Ourisson and Y. Nakatani, "The terpenoid theory of the origin of cellular life: the evolution of terpenoids to cholesterol", *Chem. Biol.*, 2, 631–631 (1995).
- [69] P. L. Luisi, "About various definitions of life", *Orig. Life & Evol. Biosph.*, 28, 613–622 (1998).

- [70] J. M. Boggs, "Lipid intermolecular hydrogen-bonding – Influence on structural organisation and membrane-function", *Biochim. Biophys. Acta*, 906, 353–404 (1987).
- [71] P. Walde, R. Wick, M. Fresta, A. Mangone and P. L. Luisi, "Autopoietic self-reproduction of fatty-acid vesicles", *J. Am. Chem. Soc.*, 116, 11649–11654 (1994).
- [72] E. Blöchliger, M. Blocher, P. Walde and P. L. Luisi, "Matrix effect in the size distribution of fatty acid vesicles", *J. Phys. Chem. B*, 102, 10383–10390 (1998).
- [73] A. Wagenaar, L. Rupert, J. F. B. N. Engberts and D. Hoekstra, "Synthesis and vesicle formation of identical-chain and mixed-chain di-*n*-alkyl phosphate amphiphiles", *J. Org. Chem.*, 54, 2638–2642 (1989).
- [74] R. T. Buwalda, A. Wagenaar and J. F. B. N. Engberts, "Synthesis and aggregation behavior of cyclic single- and double-tailed phosphate amphiphiles: A novel class of phosphate surfactants - Comparison with the aggregation behavior of sodium di-*n*-alkyl phosphates", *Liebigs Annalen-Recueil*, 8, 1745–1753 (1997).
- [75] B. J. Ravoo and J. F. B. N. Engberts, "Single-tail phosphates containing branched alkyl chains - synthesis and aggregation in water of a novel class of vesicle-forming surfactants", *Langmuir*, 10, 1735–1740 (1994).
- [76] T. Tahara, I. Satake and R. Matuura, "The micellar properties of disodium monoalkyl phosphates in aqueous solutions", *Bull. Chem. Soc. Jpn.*, 42, 1201–1205 (1969).
- [77] J. Arakawa and B. A. Pethica, "Micellization in aqueous solutions of monoalkyl phosphate salts", *J. Colloid Interface Sci.*, 75, 441–450 (1980).
- [78] S. G. Zhang and Z. C. Ouyang, "Undulation modes in bilayer membranes", *Acta Phys. Sin.*, 8, 321–325 (1999).
- [79] D. A. Brown, T. Malkin and G. K. Maliphant, "An X-ray examination of long-chain alkyl dihydrogen phosphates and dialkyl hydrogen phosphates and their sodium salts", *J. Sci. Ind. Res. India*, 14, 1584–1588 (1955).
- [80] W. F. van Gunsteren and H. J. C. Berendsen, "Computer simulation of molecular dynamics: methodology, applications and perspectives in chemistry", *Angew. Chem. Int. Ed. Engl.*, 29, 992–1023 (1990).
- [81] E. Egberts and H. J. C. Berendsen, "Molecular dynamics simulation of a smectic liquid crystal with atomic detail", *J. Chem. Phys.*, 89, 3718–3732 (1988).
- [82] P. Ahlström and H. J. C. Berendsen, "A molecular dynamics study of lecithin monolayers", *J. Phys. Chem.*, 97, 13691–13702 (1993).
- [83] M. Yoneya and H. J. C. Berendsen, "Molecular dynamics simulation of chiral nematic liquid crystals", *J. Phys. Soc. Japan*, 63, 1025–1030 (1994).
- [84] K. V. Damodaran and K. M. Merz, "A comparison of DMPC-based and DLPE-based lipid bilayers", *Biophys. J.*, 66, 1076–1087 (1994).

- [85] A. D. MacKerell, "Molecular dynamics simulation analysis of a sodium dodecyl-sulfate micelle in aqueous solution – decreased fluidity of the micelle hydrocarbon interior", *J. Phys. Chem.*, 99, 1846–1855 (1995).
- [86] D. J. Tobias and M. L. Klein, "Molecular dynamics simulation of a calcium carbonate calcium sulfonate reverse micelle", *J. Chem. Phys.*, 100, 6637–6648 (1996).
- [87] M. J. Callaway, D. J. Tildesley and N. Quirke, "Molecular dynamics simulation of a Langmuir-Blodgett patch", *Mol. Sim.*, 18, 277–301 (1996).
- [88] P. Tieleman and H. J. C. Berendsen, "Molecular dynamic simulations of a fully hydrated dipalmitoylphosphatidylcholine bilayer with different macroscopic boundary conditions and parameters", *J. Chem. Phys.*, 105, 4871–4880 (1996).
- [89] D. P. Tieleman, S. J. Marrink and H. J. C. Berendsen, "A computer perspective of membranes: molecular dynamics studies of lipid bilayer systems", *Biochim. Biophys. Acta*, 1331, 235–270 (1997).
- [90] R. G. Larson, "Simulations of self-assembly", *Curr. Op. Coll. Int. Sci.*, 2, 361–364 (1997).
- [91] H. Kuhn and H. Rehage, "Solvation and counterion-distribution of sodium octanoate micelles studied by molecular dynamics simulations", *Ber. Buns. Ges. Phys. Chem. Chem. Phys.*, 101, 1493–1500 (1997).
- [92] U. Essmann and M. L. Berkowitz, "Dynamical properties of phospholipid bilayers from computer simulation", *Biophys. J.*, 76, 2081–2089 (1999).
- [93] L. D. Schuler and W. F. van Gunsteren, "On the choice of dihedral angle potential energy functions for *n*-alkanes", *Mol. Sim.*, 25, 301–319 (2000).
- [94] Y. Chevalier and C. Chachaty, "NMR investigation of the micellar properties of monoalkylphosphates", *J. Coll. & Polym. Sci.*, 262, 489–496 (1984).
- [95] A. E. Bailey, T. P. Hilditch, H. E. Longenecker and K. S. Markley, "Melting and solidification of fats", Bailey A. E., Hilditch T. P., Longenecker H. E., Marley K. S., eds. Wiley Interscience, New York, 1950, pp 117–179.
- [96] J. D. Turner and E. C. Lingafelter, "The X-ray crystallography of the *n*-aliphatic amides", *Acta Crystallogr.*, 4, 104– (1955).
- [97] E. von Sydow, "The normal fatty acids in solid state. A crystal structure investigation.", *Ark. Kemi*, 9, 231–231 (1956).
- [98] D. K. Schwartz, M. L. Schlossman and P. S. Pershan, "Reentrant appearance of phases in a relaxed Langmuir monolayer of tetracosanoic acid as determined by X-ray-scattering", *J. Chem. Phys.*, 96, 2356–2370 (1992).
- [99] K. P. Bell and S. A. Rice, "A molecular-dynamics study of the structure of a long-chain amphiphile monolayer adsorbed on ice <sup>1</sup>H", *J. Chem. Phys.*, 99, 4160–4167 (1993).
- [100] F. MacRitchie, "Chemistry at Interfaces", 1st edition, Academic Press, San Diego, 1990.

- [101] J. Douliez, A. Léonard and E. J. Dufourc, "Restatement of order parameters in biomembranes: calculation of C-C bond order parameters from C-D quadrupolar splittings", *Biophys. J.*, 68, 1727–1739 (1995).
- [102] J. Seelig and W. Niederberger, "Deuterium labeled lipids as structural probes in liquid crystalline bilayers.", *J. Am. Chem. Soc.*, 96, 2069–2072 (1974).
- [103] J. M. Pope, L. W. Walker and D. Dubro, "On the ordering of *n*-alkane and *n*-alcohol solutes in phospholipid bilayer model membrane systems", *Chem. Phys. Lipids*, 35, 259–277 (1984).
- [104] O. Söderman, G. Carlström, U. Olsson and T. C. Wong, "Nuclear magnetic resonance relaxation in micelles", *J Chem Soc Faraday Trans*, 84, 4475–4486 (1988).
- [105] W. F. van Gunsteren and A. E. Mark, "Validation of molecular dynamics simulation", *J. Chem. Phys.*, 108, 6109–6116 (1998).
- [106] X. Daura, K. Gademann, B. Jaun, D. Seebach, W. F. van Gunsteren and A. E. Mark, "Peptide Folding: When Simulation Meets Experiment", *Angew. Chem. Int. Ed. Engl.*, 38, 236–240 (1999).
- [107] C. Peter, X. Daura and W. F. van Gunsteren, "Peptides of aminoxy acids: a molecular dynamics study of conformational equilibria under various conditions", *J. Am. Chem. Soc.*, 122, 7461–7466 (2000).
- [108] W. F. van Gunsteren, R. Bürigi, C. Peter and X. Daura, "The key to solving the protein folding problem lies in an accurate description of the denatured state", *Angew. Chem. Int. Ed.*, in press (2001).
- [109] A. M. J. J. Bonvin and W. F. van Gunsteren, " $\beta$ -hairpin Stability and Folding: Molecular Dynamics Studies of the First  $\beta$ -Hairpin of Tendamistat", *J. Mol. Biol.*, 296, 255–268 (2000).
- [110] W. F. van Gunsteren, H. J. C. Berendsen, J. Hermans, W. G. J. Hol and J. P. M. Postma, "Computer simulation of the dynamics of hydrated protein crystals and its comparison with X-ray data", *Proc. Natl. Acad. Sci. USA*, 80, 4315–4319 (1983).
- [111] H. J. C. Berendsen, W. F. van Gunsteren, H. R. J. Zwinderman and R. G. Geurtsen, "Simulations of proteins in water", *Ann. New York Acad. Sci.*, 482, 269–285 (1986).
- [112] P. E. Smith, R. C. van Schaik, T. Szyperski, K. Wüthrich and W. F. van Gunsteren, "Internal mobility of the Basic Pancreatic Trypsin Inhibitor in solution: a comparison of NMR spin relaxation measurements and molecular dynamics simulations", *J. Mol. Biol.*, 246, 356–365 (1995).
- [113] L. J. Smith, A. E. Mark, C. M. Dobson and W. F. van Gunsteren, "Comparison of MD simulations and NMR experiments for hen lysozyme: analysis of local fluctuations, cooperative motions and global changes", *Biochem.*, 34, 10918–10931 (1995).

- [114] R. M. Brunne, K. D. Berndt, P. Güntert, K. Wüthrich and W. F. van Gunsteren, "Structure and internal dynamics of the Bovine Pancreatic Trypsin Inhibitor in aqueous solution from long-time molecular dynamics simulations", *Proteins*, 23, 49–62 (1995).
- [115] U. Stocker and W. F. van Gunsteren, "Molecular Dynamics Simulation of Hen Egg White Lysozyme: A Test of the GROMOS96 Force Field Against Nuclear Magnetic Resonance Data", *Proteins*, 40, 145–153 (2000).
- [116] J. E. H. Koehler, W. Saenger and W. F. van Gunsteren, "Molecular dynamics simulation of crystalline  $\beta$ -cyclodextrin dodecahydrate at 293 K and 120 K", *Eur. Biophys. J.*, 15, 211–224 (1987).
- [117] J. E. H. Koehler, W. Saenger and W. F. van Gunsteren, "The flip-flop hydrogen bonding phenomenon: molecular dynamics simulation of crystalline  $\beta$ -cyclodextrin", *Eur. Biophys. J.*, 16, 153–168 (1988).
- [118] A. E. Mark, S. P. van Helden, P. E. Smith, L. H. M. Janssen and W. F. van Gunsteren, "Convergence properties of free energy calculations: Alpha-cyclodextrin complexes as a case study", *J. Am. Chem. Soc.*, 116, 6293–6302 (1994).
- [119] W. F. van Gunsteren, H. J. C. Berendsen, R. G. Geurtsen and H. R. J. Zwinderman, "A molecular dynamics computer simulation of an eight-base-pair DNA fragment in aqueous solution: comparison with experimental two-dimensional NMR data", *Ann. New York Acad. Sci.*, 482, 287–303 (1986).
- [120] A. M. J. J. Bonvin, M. Sunnerhagen, G. Otting and W. F. van Gunsteren, "Water Molecules in DNA Recognition II: A Molecular Dynamics View of the Structure and Hydration of the trp Operator", *J. Mol. Biol.*, 282, 859–873 (1998).
- [121] S. L. Njo, W. F. van Gunsteren and F. Müller-Plathe, "Determination of force field parameters for molecular simulation by molecular simulation: an application of the weak-coupling method", *J. Chem. Phys.*, 102, 6199–6207 (1995).
- [122] F. Müller-Plathe, H. Liu and W. F. van Gunsteren, "Conceptual hierarchies in polymer electrolyte simulations – from quantum chemistry to molecular dynamics", *Comput. Polymer Science*, 5, 89–98 (1995).
- [123] R. Faller, H. Schmitz, O. Biermann and F. Müller-Plathe, "Automatic parametrization of force-fields for liquids by simplex optimization", *J. Comp. Chem.*, 20, 1009–1017 (1999).
- [124] T. P. Straatsma and H. J. C. Berendsen, "Free energy of ionic hydration: Analysis of a thermodynamic integration technique to evaluate free energy differences by molecular dynamics simulations", *J. Chem. Phys.*, 89, 5876–5886 (1988).



- [125] W. F. van Gunsteren, "Computation of free energy in practice: choice of approximations and accuracy limiting factors", In: "Computer simulation of biomolecular systems, theoretical and experimental applications", W. F. van Gunsteren, P. K. Weiner, A. J. Wilkinson eds., eds. Escom Science Publishers, Leiden, The Netherlands, 1993, pp 315–348.
- [126] X. Daura, P. H. Hünenberger, A. E. Mark, E. Querol, F. X. Avilés and W. F. van Gunsteren, "Free energies of transfer of Trp analogs from Chloroform to water: Comparison of theory and experiment and the importance of adequate treatment of electrostatics and internal interactions", *J. Am. Chem. Soc.*, 118, 6285–6294 (1996).
- [127] I. G. Tironi, R. Sperb, P. E. Smith and W. F. van Gunsteren, "A generalized reaction field method for molecular dynamics simulations", *J. Chem. Phys.*, 102, 5451–5459 (1995).
- [128] A. Glättli, "Derivation of an improved SPC model for liquid water", Diploma thesis at the Institute of Physical Chemistry, ETH Zürich (2000).
- [129] W. Paul, D. Y. Yoon and G. D. Smith, "An optimized united atom model for simulations of polymethylene melts.", *J. Chem. Phys.*, 103, 1702–1709 (1995).
- [130] C. D. Wick, M. G. Martin and J. I. Siepmann, "Transferable potentials for phase equilibria. 4. United-atom description of linear and branched alkenes and alkylbenzenes", *J. Phys. Chem. B*, 104, 8008–8016 (2000).
- [131] H. Tamura, M. Yoshida, K. Kusakabe, C. Young-Mo, R. Miura, M. Kubo, K. Teraishi, A. Chatterjee and A. Miyamoto, "Molecular dynamics simulation of friction of hydrocarbon thin films", *Langmuir*, 15, 7816–7821 (1999).
- [132] H. Schmitz, R. Faller and F. Müller-Plathe, "Molecular mobility in cyclic hydrocarbons: A simulation study", *J. Phys. Chem. B*, 103, 9731–9737 (1999).
- [133] W. S. Price and O. Soderman, "Self-diffusion coefficients of some hydrocarbons in water: Measurements and scaling relations", *J. Phys. Chem. A*, 104, 5892–5894 (2000).
- [134] L. Fitjer, H. J. Scheuermann, U. Klages, D. Wehle, D. S. Stephenson and G. Binsch, "Sterically crowded cycloalkanes, 3: 4,4,8,8,12,12-Hexamethyltrispiro[2.1.2.1.2.1]dodecane and 4,4,8,8,9,9,10,10-Octamethyldispiro[2.1.2.3]decane – Two per(cyclo)alkylated cyclohexanes adopting twistboat conformation", *Chem. Ber.*, 119, 1144–1161 (1986).
- [135] F. Müller-Plathe, "An All-atom Force Field for Liquid Ethanol - Properties of Ethanol-Water Mixtures", *Mol. Sim.*, 18, 133–143 (1996).
- [136] R. Walser, A. E. Mark, W. F. van Gunsteren, M. Lauterbach and G. Wipff, "The effect of force-field parameters on properties of liquids: Parametrization of a simple three-site model for methanol", *J. Chem. Phys.*, 112, 10450–10459 (2000).
- [137] D. Juchli, "Amine Hydration: A Challenge to United Atom Force Fields", Diploma thesis at the Institute of Physical Chemistry, ETH Zürich, (2000).

- [138] S. Cabani, P. Gianni, V. Mollica and L. Lepori, "Group contributions to the thermodynamic properties of non-ionic organic solutes in dilute aqueous solution", *J. Solut. Chem.*, 10, 563–595 (1981).
- [139] A. Ben-Naim and Y. Marcus, "Solvation thermodynamics of nonionic solutes", *J. Chem. Phys.*, 81, 2016–2027 (1984).
- [140] M. J. D. Janiak, M. Small and G. G. Shipley, "Nature of the thermal pretransition of synthetic phospholipids: dimyristoyl- and dipalmitoyllecithin", *Biochem.*, 15, 4575–4580 (1976).
- [141] S. W. Chiu, M. Clark, V. Balaji, S. Subramaniam, H. L. Scott and E. Jakobsson, "Incorporation of surface-tension into molecular-dynamics simulation of an interface – A fluid-phase lipid bilayer-membrane", *Biophys. J.*, 69, 1230–1245 (1995).
- [142] R. L. Thurmond, S. W. Dodd and M. F. Brown, "Area/lipid of bilayers from NMR", *Biophys. J.*, 59, 108–113 (1991).
- [143] J. F. Nagle and S. Tristram-Nagle, "Structure of lipid bilayers", *Biochim. et Biophys. Acta – Reviews on Biomembranes*, 1469, 159-195 (2000).
- [144] H. I. Petrache, S. W. Dodd and M. F. Brown, "Area per lipid and acyl length distributions in fluid phosphatidylcholines determined by  $^2\text{H}$  NMR spectroscopy", *Biophys. J.*, 79, 3172-3192 (2000).
- [145] A. M. Smondyrev and M. L. Berkowitz, "United atom force field for phospholipid membranes: Constant pressure molecular dynamics simulation of dipalmitoylphosphatidylcholine/water system", *J. Comp. Chem.*, 20, 531–545 (1999).
- [146] S. E. Feller, "Molecular dynamics simulations of lipid bilayers", *Curr. Op. Coll. Int. Sci.*, 5, 217–223 (2000).

# Curriculum Vitae

## Personal Information

Name	Lukas Daniel Schuler
Date of birth	6th of June, 1969
Place of birth	Männedorf, Kanton Zurich, Switzerland
Citizenship	Schwyz, Kanton Schwyz, Switzerland

## Education

Primary and Secondary School in Hombrechtikon, Kanton Zurich, Switzerland	1976–1985
A Level School, <i>Matura Typus C</i> Kantonsschule Zürcher Oberland in Wetzikon ZH Kanton Zurich, Switzerland	1985–1989
Diploma as Natural Scientist Swiss Federal Institute of Technology (ETH Zürich) Zurich, Switzerland	1990–1995
Diploma as Chemistry Teacher, <i>Höheres Lehramt</i> Swiss Federal Institute of Technology (ETH Zürich) Zurich, Switzerland	1995–1996
Ph. D. Thesis at the Institute of Physical Chemistry Swiss Federal Institute of Technology (ETH Zürich) Zurich, Switzerland	1996–2000

## Work Experience

Express Delivery Service	PTT	1986–1990
Information Technology Co-Worker	Ascom–Zellcom AG	1989–1990
Database Development	ETH Zürich	1994–1996
Co-Authoring Astronomy Software	astroNovum software	1990–1997
Layout and Graphics	Metex AG	1990–1996

# The Final Point



This picture has been reprinted with kind permission from the artist himself, therefore, many thanks go to Ralf Alex Fichtner.